Using cell size to represent phytoplankton diversity in studies of nitrogen dynamics in the southern Benguela

Josephine Ffion Atkins

A thesis presented in fulfillment of the requirement for the degree of

Doctor of Philosophy

Faculty of Science, Department of Oceanography

University of Cape Town

South Africa

February, 2017

“We shape our self to fit this world, and by the world are shaped again”

David Whyte

Declaration

I hereby declare that this thesis is my own work and effort, both in concept and execution, with normal guidance and assistance from my supervisors. A few comments are needed on the data used in this thesis:

- Data for Chapter 2 ("Can effective diameter (D_{eff}) capture the nitrogen utilisation by high biomass blooms at upwelling/downwelling timescales") were given to me by the Department of Agriculture, Forestry and Fisheries (DAFF). The sampling methods described are those carried out by Trevor Probyn (^{15}N uptake), Grant Pitcher (phytoplankton community composition, chlorophyll *a* and primary productivity) and Andre du Randt (CTD profiles). The Coulter Counter data used were collected by Stewart Bernard. Wind data were supplied by the South African Weather Service (SAWS). A paper was published by Fawcett et al. (2007) focusing on wind forcing on phytoplankton succession using data from 2005, but there is little overlap in the focus of the published paper and Chapter 2 here. The scripts used to illustrate the winds are an adaptation of those used in Fawcett et al (2007), given to me by Jenny Veitch of the Department of Oceanography, University of Cape Town. My role in Chapter 2 was to re-analyse the data in order to predict nitrogen uptake from a satellite-derived bulk property, D_{eff}.

- Data used in Chapter 3 ("An investigation into the use of effective diameter to represent the nitrogen dynamics in diatom-dominated assemblages: The case of Saldanha Bay, South Africa.") were collected in collaboration with Trevor Probyn and Grant Pitcher of DAFF. I was involved in the collection of *in situ* samples and deploying *in situ* uptake incuba-

tions, laboratory determinations of nutrients and preparation of ^{15}N experiments, Coulter Counter derived particle size distributions and I assisted in determinations of chlorophyll a concentrations. Enumeration of samples for phytoplankton community composition was carried out by Lisa Mansfield (DAFF) and Grant Pitcher.

- Data used in Chapter 4 ("Estimating nitrogen uptake from ambient concentrations and cell size") come from Chapters 2 and 3. Advice on approach for model development was given to me by Coleen Moloney, who also consistently verified the equations and methods used.

I, Josephine Ffion Atkins, hereby declare that the work on which this thesis is based is my original work (except where indicated otherwise) and that neither the whole work nor any part of it has been, is being, or is to be submitted for another degree in this or any other university. I authorise the University to reproduce for the purpose of research either the whole or any portion of the contents in any manner whatsoever.

Signed by candidate

Signature Removed

Josephine Ffion Atkins

Cape Town, February 2017

Acknowledgments

For academic support and guidance, I am indebted to my supervisors Coleen Moloney, Stewart Bernard and Eric Machu. I am grateful for the guidance and feedback they have given me throughout the progression and wrapping up of this thesis. I feel privileged to have been able to learn from Coleen's example in thought process and rigorous attention to detail. I would also like to thank the anonymous examiners of this thesis for their thorough examination and thought provoking comments.

For data from Lamberts Bay, I thank Trevor Probyn and Grant Pitcher from the Department of Agriculture Forestry and Fisheries (DAFF). I have thoroughly enjoyed working with them and I am grateful for their extensive guidance during field work in Saldanha Bay. Their collective feedback has been invaluable to my academic development and I warmly acknowledge their contributions to this thesis. Trevor's guidance has been a big highlight during this PhD journey.

For assistance and humour in the field, I gratefully acknowledge Andre du Randt, Lisa Mansfield and Marie Smith.

For funding, I thank the Ma-Re institute, the Council for Scientific and Industrial Research (CSIR) and the National Research Foundation (NRF) for their collective financial support. And thank you, both Emlyn Balarin and Gilly Smith, for orchestrating where all the funding came from.

I particularly thank fellow students/graduates Sarah Nicholson, Ceinwen Smith, Maya Pfaff, Hayley Evers-King, Emily McGregor and Otto Whitehead for enjoying the small things with me. Josh Weeber, you've been such a rock. Thank you!

Finally, I wish to thank my family near and far for their love, support and understanding throughout it all. I dedicate this thesis to my parents, Stephen and Cerys Atkins, for always

encouraging my adventures into the natural world. Thank you.

Contents

Abstract

Phytoplankton are a key component in the functioning of marine ecosystems and play a central role in the cycling of nitrogen and other elements. Metrics that can adequately represent the biogeochemical processes associated with phytoplankton diversity are needed in order to make use of remote sensing and modeling platforms. A single-value size proxy, effective diameter (D_{eff}), represents the mean volume to surface area ratio across the nano and micro plankton size fraction (2-200μm) in the southern Benguela, but has yet to be tested regarding its biogeochemical relevance. Cell size imposes overarching constraints on phytoplankton metabolism; there are therefore strong grounds for evaluating the usefulness of the metric (D_{eff}) in studies of nitrogen dynamics in diverse, natural assemblages. Three case studies were used to explore the nitrogen dynamics in naturally occurring assemblages and to evaluate the relationships between D_{eff} and the uptake of the different sources of nitrogen. Two of the case studies comprised high biomass, harmful algal blooms observed off Lamberts Bay during an upwelling/downwelling cycle. The third case study used bi-monthly sampling over a full year in Saldanha Bay. The Lamberts Bay case studies involved blooms occasionally dominated by HAB-forming species: a mixotrophic ciliate, *Myrionecta rubra,* and a dinoflagellate, *Prorocentrum triestinum*. The nitrogen uptake rates followed the well observed pattern of high nitrate uptake by large cells and regenerated nitrogen uptake by small cells. *Myrionecta rubra* had a wide range of nitrate (NO_3^-) uptake rates (0.02-0.3 μmol N L^{-1} h^{-1}). *Prorocentrum triestinum* showed slower rates of NO_3^- uptake (0.01-0.2 μmol N L^{-1} h^{-1}) and dominated in low NO_3^-, stratified conditions. Diatoms were the most efficient utilisers of NO_3^- and total nitrogen in these cases. The effective diameter was significantly related to the uptake rates of ammonium (NH_4^+) (r=-0.54, p<0.005) and urea (r=-0.59, p<0.005), but not NO_3^- (r=0.27, p=0.11). This was at-

tributed to some instances of bi-modality in observed size distributions as well as potentially specialist nutrient uptake strategies employed by diatoms. The year-round data from Saldanha Bay indicated the system was diatom-dominated and was used to assess how well D_{eff} could represent the nitrogen uptake strategies employed by the diverse diatom assemblages. The Saldanha Bay system has NO_3^- limited surface waters during summer, and light-limited bottom waters during winter. No significant relationship was found between D_{eff} and the mass-specific uptake rates of the different nitrogen species in this data set. This was attributed to the complex shapes of the size distributions and the comparatively low biomass observed. Uptake kinetic experiments revealed high variability for maximum uptake rates (V_{max}) and half saturation values (K_s) for both NO_3^- and NH_4^+. For NO_3^-: V_{max} ranged 0.007-0.17 μmol N L^{-1} h^{-1}, and K_s ranged between 0.2-42.5 μmol N L^{-1}. For NH_4^+ V_{max} was observed between 0.02-2.7 μmol N L^{-1} h^{-1}; and K_s values ranged 0.1-14.02 μmol N L^{-1}. Variability was observed in association with the availability of the ambient sources of nitrogen, but some variation was accounted for by the presence of different diatom species. From these three case studies it was concluded that the single-value size proxy was an adequate metric to quantify the uptake of regenerated nitrogen in scenarios of high biomass algal blooms. Such blooms are a pervasive feature in the southern Benguela Ecosystem. For lower biomass blooms, however, D_{eff} did not adequately represent the nutrient dynamics of diverse diatom-dominated assemblages. The variable shape of the size spectrum is an important factor in determining the rates of nutrient uptake and, in cases of bi- or multi-modality, this information could be lost when represented by a single descriptor such as D_{eff}. It was subsequently hypothesised that size spectra could be used to accurately represent the nitrogen dynamics in diverse phytoplankton assemblages. This was tested by comparing the observed uptake rates of the three case studies to estimated uptake rates based on size spectra. Observed particle size distributions were used to estimate the uptake of NO_3^- and NH_4^+, based on theoretical relationships to calculate size-dependent values of V_{max} and K_s. Michaelis-Menten models were applied to measured ambient nutrient concentrations and particle size distributions, generating size-integrated estimates of NO_3^-, NH_4^+ and total N uptake rates. The variability in the estimated uptake rates was similar to that of the measured values.

It was thus concluded that the representation of phytoplankton diversity by size spectra allowed modification of model parameters, such that improved estimates of uptake rates of NO_3^- and NH_4^+ could be obtained for a dynamic eutrophic environment.

Chapter 1

Phytoplankton, nitrogen and the southern Benguela upwelling system

Autotrophic phytoplankton are a large and diverse group of unicellular organisms, representing less than 1% of global photosynthetic biomass, but accounting for almost 50% of global primary production (Field et al., 1998). There are at least 25,000 species, spanning eight major phyla (Falkowski et al., 2004) and nine orders of magnitude in cell size (Sieburth et al., 1978; Finkel et al., 2010). The diversity of phytoplankton communities plays a major role in ecosystem function and productivity (Ptacnik et al., 2008; Vallina et al., 2014), resilience and stability (McCann, 2000; Vallina and Le Quéré, 2011) and biogeochemistry (Azam and Malfatti, 2007). Understanding ecosystem function in relation to species composition and diversity is an exciting area of research in both terrestrial and marine ecology. In recognition of the importance of phytoplankton diversity, significant advances have been made in differentiating between the various phytoplankton communities both from empirical observation, including remote sensing, and modeling methods.

Satellite-derived algal products now exist that can define phytoplankton biomass by functional group (e.g. Brown and Podestá, 1997; Sathyendranath et al., 2004), dominant size class (e.g. Ciotti et al., 2002; Ciotti and Bricaud, 2006; Uitz et al., 2006; Evers-King et al., 2014) or particle size distributions (Kostadinov et al., 2010). Equally, various forms of biogeochemical models exist that use functional group (e.g. Le Quéré et al., 2005; Dutkiewicz et al., 2009) or

cell size (e.g. Moloney et al., 1991; Baird and Suthers, 2007; Banas, 2011; Ward et al., 2012) or both (e.g. Le Quéré et al., 2005; Aumont et al., 2015) to parameterise varying degrees of phytoplankton diversity. Built on our current, empirical understanding of the relationships between community structure and biogeochemical processes, many questions remain regarding the variability in these empirical relationships at several temporal and spatial scales. The ecological relevance of each metric used to represent diverse algal assemblages needs thorough evaluation in relation to the biogeochemical processes in question, especially at the regional/local scale. The primary focus of this research is to establish to what degree simplified size descriptors can represent the functional diversity of algal assemblages and to investigate the minimum information requirements to adequately represent the principle biogeochemical signals. The size structure of an assemblage is one of the primary means of representing diverse microbial communities (Moloney et al., 1991), where the metabolism of a cell is often assumed to be scaled to size (Chisholm, 1992). However, physiological adaptations and plasticity can often weaken the relationships between cell size and phytoplankton metabolism and there is thus a need to explore these relationships further, most notably in assemblages measured in a natural context (Litchman et al., 2015). The southern Benguela is considered a useful, natural laboratory for such an endeavour owing to very strong signals from large shifts in phytoplankton population composition at high biomass. Culture experiments have been instrumental in providing a wealth of knowledge on the variation in physiological mechanisms under controlled conditions, but they lack coherence to realistic environmental gradients and biological interactions. This thesis aimed to test whether representing phytoplankton diversity via cell size and simple size proxies captures the nitrogen dynamics observed in diverse, natural assemblages.

Phytoplankton diversity

Understanding phytoplankton community structure, dynamics and its effect on large scale biogeochemistry has increasingly become a topical area of current research (see Litchman et al., 2015). Community structure is traditionally characterised by taxonomic distinction, or species

richness (number of species), but it has been recognised that nomenclatural approaches to ecology can be cumbersome owing to the branching nature of diversity (Lawton, 1999). Moreover, it is the functions performed by communities, i.e. functional diversity (Tilman, 2001), that are required for quantifying biogeochemical cycles. Functional diversity refers to the components of an ecosystem that influence its stability, productivity, resource dynamics and how it operates (Tilman, 2001). It is further noted that resource dynamics, or nutrient balance, are measured by the rates of supply and loss of resources and the efficiency with which organisms use limiting resources. In diverse communities, each species will have morphological or physiological traits that influence species abundance and ultimately ecosystem function. To reduce complexity, Chapin (1997) suggested to focus on the traits with the greatest effect on the functioning of an ecosystem, which 1) control acquisition, use and availability of limiting resources, 2) modify food-web structure and 3) affect occurrence and magnitude of disturbances.

A trait is an element of an organism's phenotype and, in phytoplankton, a trait would be cell size, body mass or stoichiometric ratio (Litchman et al., 2012). In turn, a functional trait is defined as a measurable property of an organism that strongly influences its fitness or performance (McGill et al., 2006). In phytoplankton, functional traits would include light and nutrient acquisition (Aksnes and Egge, 1991), reproductive strategy (Litchman and Klausmeier, 2008), competition for resources (Tilman et al., 1982; Hibbing et al., 2010) and strategies of predation avoidance (Kiørboe, 2008). Cell size is often observed to be strongly correlated with different functional traits and has been coined a 'master trait' (Litchman et al., 2007) that governs, to some degree, the functional traits of phytoplankton (Fig. 1.1). The degree of influence is subject to variability and thus requires deeper investigation into locale-specific relationships in natural phytoplankton assemblages in relation to the potential effects of other influential factors.

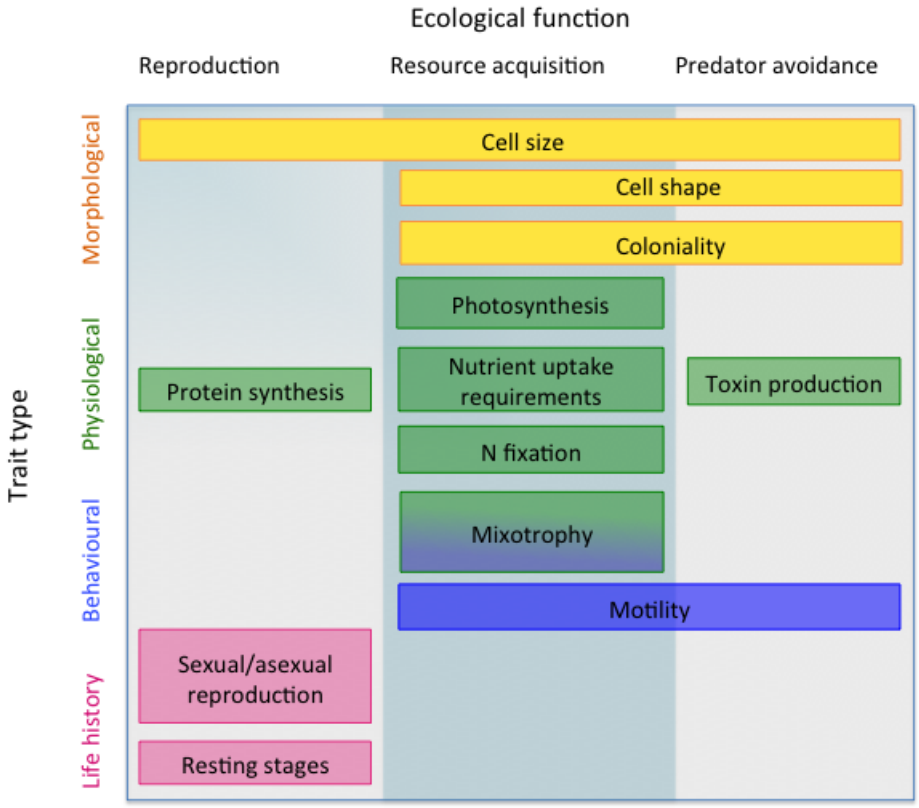

Figure 1.1: Typology of phytoplankton functional traits. Taken from Litchman and Klausmeier (2008).

Phytoplankton community structure

Community structure and diversity are controlled by bottom-up and top-down mechanisms (Tilman et al., 1982). Bottom-up controlling factors are related to resource limitation (water chemistry, light, turbulence, temperature) and top-down controlling factors are related to biological controls such as the physiological characteristics of a species, competition or predation. The relative strengths of abiotic (bottom-up) and biotic (top-down) controls on natural communities are scale dependent (Levin, 1992; Hunt and McKinnell, 2006) and can vary by location (e.g. Matson, 1992; Hunter and Price, 2012).

Phytoplankton functional groups, functional types and guilds are all terms used in the literature when describing phytoplankton communities in an ecological and biogeochemical context. Functional groups are traditionally defined by morphology or phylogenetic class, e.g. diatoms,

dinoflagellates, coccolithophores, and have been the foundation of phytoplankton ecology and studies of community succession. Earlier studies into phytoplankton succession found a distinction in habitat preference by phytoplankton, based on an *r* versus *K* selection gradient (Margalef et al., 1979). *r*-selection occurs in unstable environments and there is little advantage in adaptations that permit successful competition, and *K*-selection predominates in stable environments where the ability to compete for limited resources is crucial. A seminal conceptual model (Margalef et al., 1979) defined two groups (diatoms and dinoflagellates) according to their preference for physical disturbance and nutrient supply (Fig. 1.2). Diatoms are defined as *r*-selected; able to withstand high turbulence levels and requiring high nutrient concentrations. Dinoflagellates are considered to be *K*-selected; employing turbulence-avoidance strategies and requiring reduced nutrients. There are other important groups not considered in this conceptual model (e.g. coccolithophorids, *Phaeocystis* spp.), which also does not consider the effects of grazing. Regardless, this model has been seminal in phytoplankton ecology and spurred further conceptual models of light dependency in phytoplankton succession (e.g. Reynolds, 1989) and models of harmful algal blooms (Smayda and Reynolds, 2001).

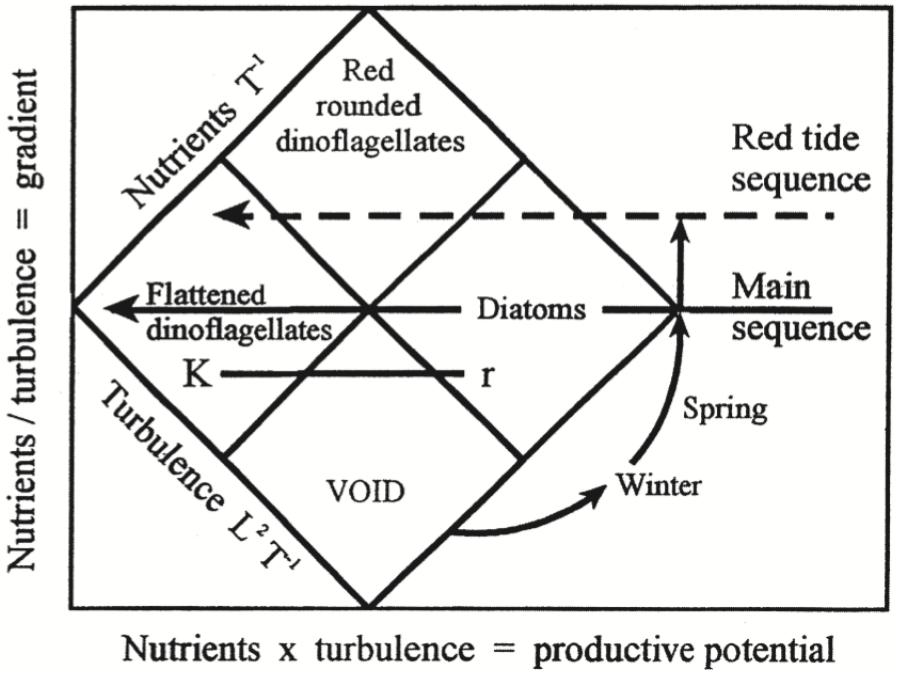

Figure 1.2: Margalef's Mandala showing the gradients of turbulence and nutrient supply favouring diatoms and dinoflagellates . Taken from (Margalef et al., 1979)

Phytoplankton Functional Types (PFTs) are defined as groups of organisms with an explicit biogeochemical role, determined by a distinct set of physiological traits and environmental requirements (Le Quéré et al., 2005). This classification is irrespective of taxonomic affiliation and comes from a biogeochemical perspective e.g. N_2 fixers, calcifiers, DMS-producers and silicifiers, and has become a more common classification in the modeling and remote sensing literature. Defining functional types requires a sound understanding of how a diversity of cells take up and assimilate nutrients under different conditions and their roles in the ecosystem. In keeping with terrestrial advances in studies of community ecology (McGill et al., 2006; Westoby and Wright, 2006), functional diversity and physiological trait-based approaches in phytoplankton dynamics (e.g. Litchman and Klausmeier, 2008; Smith et al., 2015) are increasingly being used to represent the diversity of phytoplankton and their function in the marine environment (e.g. Armstrong, 2006; Bruggeman and Kooijman, 2007; Pahlow et al., 2008; Merico et al., 2009; Follows and Dutkiewicz, 2011; Ward et al., 2012; Levy et al., 2015).

Platforms of study

The marine modeling community is faced with the task of choosing the appropriate representation of diverse plankton communities that can reflect the biogeochemical and ecological processes in response to climate change (Follows and Dutkiewicz, 2011; Prowe et al., 2014). Biogeochemical models have evolved from the simple nutrient-phytoplankton-zooplankton-detritus (NPZD) models (e.g. Steele, 1954; Fasham et al., 1990) to differentiate the phytoplankton compartment into functional groups (e.g. Moore et al., 2002; Gregg et al., 2003; Follows et al., 2007), different size fractions (e.g. Moloney and Field, 1989; Baird and Suthers, 2007; Banas, 2011; Ward et al., 2012) or a combination of both (Le Quéré et al., 2005; Aumont et al., 2015). By extrapolating laboratory and *in situ* observations of the environmental gradients that select for different phytoplankton, our conceptual understanding of global primary productivity and phytoplankton dynamics has greatly improved in recent years from functional group modeling approaches. Such an understanding does not come without certain challenges and uncertainty however, and it has been noted that simply increasing the resolution of phytoplankton

groups/types in biogeochemical models will not necessarily lead to more accurate understanding/predictions of ecosystem function (Anderson, 2005; Nair et al., 2008; Thingstad et al., 2010; Follows and Dutkiewicz, 2011). As resolution increases, so do the number of parameters and their associated uncertainties, which currently cannot be constrained within the available cultured or *in situ* observations (Ward et al., 2010). It was also suggested by Ward et al. (2010) that more information on the PFT distributions and their response to biotic and abiotic factors is needed to improve models. Culture experiments are able to quantify the response of cultured phytoplankton to isolated and controlled environmental variables, but they lack coherence to realistic environmental dynamics and interactions within the system. Equally, the relationships used to parameterise global models are often extrapolated for circumstances very different from their origin, highlighting the need for continued research into empirical relationships that are specific to a local context.

Remote sensing provides invaluable archives of routine, global and synoptic information on the distributions of phytoplankton communities and many studies rely on satellite information for comparison with outputs from models (e.g. Anderson, 2005; Doney et al., 2009). Measurements from satellites can capture variability which *in situ* studies cannot due to their limited temporal and spatial sampling scales (Joint and Groom, 2000). Both cell size and pigment composition affect spectral characteristics of phytoplankton absorption (Sathyendranath et al., 1987) and this has allowed the development of a variety of algorithms beyond gross biomass proxies, such as chlorophyll a (Chl-*a*) concentrations (McClain, 2009), to provide some limited functional type descriptors. As in many biogeochemical models, ocean color satellite data can potentially be used to differentiate between PFTs (Alvain et al., 2005, 2008; Raitsos et al., 2008), phytoplankton size classes (Ciotti and Bricaud, 2006; Uitz et al., 2006; Hirata et al., 2008; Brewin et al., 2011) or particle size distributions (Kostadinov et al., 2009, 2010).

There are several methods in current use to derive phytoplankton community structure on a global basis from spectral-based and abundance-based approaches (Brewin et al., 2011), with several other approaches used regionally (Bernard et al., 2009; Evers-King et al., 2014). Global-type spectral approaches are typically based on relationships between pigment data

derived from High Pressure Liquid Chromatography (HPLC) and spectral characteristics of Chl-*a*-normalised water-leaving radiance (Alvain et al., 2012). Spectral characteristics of the reflectance signal can be attributed to certain groups; e.g. *Phaeocystis*, diatoms, *Prochlorococcus*, or nano phytoplankton (e.g. Alvain et al., 2005; 2008). Further, variations in the spectral shape can be defined either by dominant size class using absorption signals (Ciotti and Bricaud, 2006; Mouw and Yoder, 2005) or by particle size distributions using backscattering signals (Kostadinov, 2009; 2010). Alternatively, abundance-based methods assume a change in size structure with a change in Chl-*a* concentrations (Uitz et al., 2006; Brewin et al., 2010; Hirata et al., 2011), based on empirical observed relationships between cell size and assemblage biomass (as indexed by Chl-*a*). Such approaches appear to perform adequately for certain large scale ecologically-driven community shifts (e.g. the North Atlantic spring bloom as observed by Alvain et al., 2008). However in diverse assemblages of multiple size classes or PFTs, it becomes more difficult to differentiate between them (Brewin et al., 2011). Such approaches are unsuitable for application to coastal/productive waters such as the southern Benguela, as they only address a limited range in biomass (Bernard et al., 2009).

There is uncertainty and unquantified errors in deriving PFTs, size classes or distributions from each algorithm, opening up exciting avenues of research into validation and improving the accuracy of the products available from satellite data. The choice of metric to represent the community largely depends on its application and the processes in question. Phytoplankton community dynamics are well known to have distinct characteristics between basins (Barton et al., 2010, 2013), with latitude (Ward, 2015) and between open ocean and coastal areas (Acevedo-Trejos et al., 2015). There is thus a need to assess the metrics that are used to represent the diverse assemblages in a regional/local context, and parameterisations that are constrained by and evaluated for realistic scenarios at a local scale. There are several traits, or dimensions of diversity (Dutkiewicz et al., 2016), that could be used as a currency to test how well the available metrics fare in representing the functional diversity of algal assemblages, e.g. biogeochemical function, accessory pigments, thermal niche, predation protection/avoidance, chain/colony formation or mixotrophy (e.g. Follows et al., 2007; Dutkiewicz et al., 2009). This

thesis focuses on cell size and nutrient uptake, as they are often measured *in situ,* with a comparatively sound understanding of the variability in their relationship and their individual dynamics.

Nutrient uptake and Growth

Two separate empirical equations are considered here that are used to define nutrient-limited growth rate, μ. One expresses μ as a function of S, the external nutrient concentration $(\mathrm{Monod}, 1949)$:

$$\mu = \mu_{max} \frac{S}{K_\mu + S} \tag{1.1}$$

where μ is a specific growth rate, μ_{max} is the maximum specific growth rate and K_μ is the half saturation constant for growth. This assumes that growth rate and uptake rate (V) are coupled (Dugdale, 1967). However, it has been recognised that μ_{max} and maximum uptake rate (V_{max}) are not always balanced in natural, non-steady state conditions (Sommer, 1985). This is evidenced by "luxury uptake" (Sommer, 1984), where growth exceeds uptake rates under nutrient limitation (i.e. nutrient storage during fluctuating nutrient supply); and "surge uptake" in nutrient starved cells (Glibert and Goldman, 1981; Collos et al., 1997), where relative uptake rates can far exceed growth rates. Droop (1973) hypothesised that growth rate was a function of intracellular rather than external nutrient concentrations. The Droop formulation for phytoplankton growth expresses μ as a function of internal concentration, the amount of nutrient per cell or cellular quota (Q)

$$\mu = \mu_\infty \frac{Q - K_Q}{Q} \tag{1.2}$$

where μ_∞ is specific growth rate when cell quota (Q) is infinite and K_Q is the Q under which μ=0. Q (N cell^{-1}), the cellular quota, is defined as the cellular nutrient to carbon ratio, calculated from the relationship between cellular nutrient uptake rate normalised to cell carbon and the cell division rate (Sunda et al., 2009).

These two equations constitute some major differences in ecosystem models which use either Monod or Droop equations to express population growth rates. Monod has been the traditional formulation as parameter values are widely available in the literature and it is less computationally expensive than Droop. Some global models (e.g. Aumont et al., 2015), originally Monod, have now incorporated an internal quota model for certain nutrients, such as iron in the case of PISCES (Aumont et al., 2015). Monod and Droop formulations have often yielded different predictions of nutrient concentrations, C:N ratios and phytoplankton dynamics (Sunda et al., 2009).

In systems with highly variable nutrient supply, the ability of a cell to store nitrogen (Eppley and Rogers, 1970; Collos and Slawyk, 1976) is critical to sustain phytoplankton growth rates (Dortch, 1982). The ability of diatoms to store nitrate (Dortch et al., 1984) is one explanation for their proliferation in upwelling areas where nitrate supplies are highly fluctuating. Droop formulations are more complex than Monod, where mass balances for internal nutrient pools are driven by available nutrient concentrations in the water column and internal nutrient concentrations, as well as uptake and growth rates that vary with these concentrations (Cerucci et al., 2010).

Nutrient uptake rates are expressed as Michaelis-Menten kinetics:

$$V = \frac{V_{max} * S}{K_s + S} \tag{1.3}$$

where V_{max} is the maximum nutrient uptake rate, *S* is the substrate concentration at the cell surface and K_s is the half-saturation constant for nutrient uptake. V_{max} will give an indication of high/low competitive advantage at relative high/low concentrations. Species with low half saturation constants are able to efficiently take up nutrients at low substrate concentrations. As these two parameters are essential to estimating nutrient dependent growth rates, much research has focused on defining species/group level values.

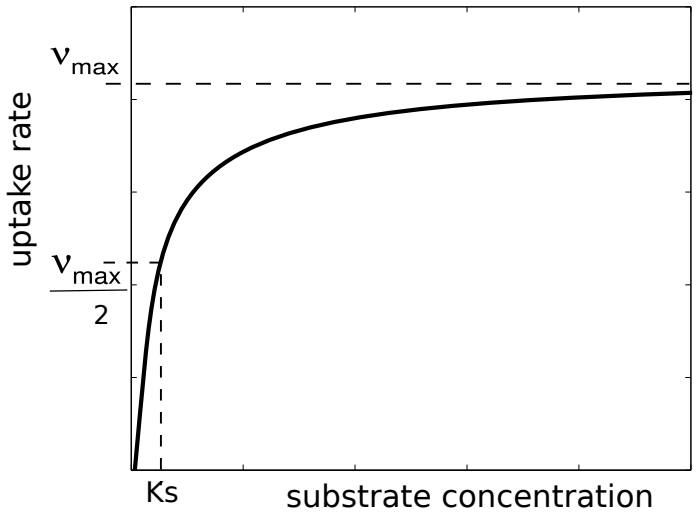

Figure 1.3: Michaelis-Menten hyperbola as described in Eq. 3 where V_{max} is the maximum uptake rate at increasing substrate concentration, and K_s is the substrate concentration at which half the V_{max} is achieved.

The influence of allometry

The relationship between body mass/size and metabolic rate is known as allometry and is widely used in many facets of terrestrial (e.g. West et al., 1997; Brown et al., 2004) and marine ecology (e.g. Chisholm, 1992; Litchman and Klausmeier, 2008; Edwards et al., 2012). It is well observed that phytoplankton cell size influences nutrient acquisition (Probyn, 1985; Stolte and Riegman, 1995; Litchman et al., 2007) and other metabolic rates (Chisholm, 1992; Kiørboe, 1993, Brown et al., 2004) which influence food web structure (Moloney and Field, 1989; Laws et al., 2000; Finkel et al., 2007), and biogeochemical cycling (Laws et al., 2000). The general allometric equation is as follows:

$$R = aM^b \tag{1.4}$$

where R can be one of many metabolic rates, M is body mass, a the rate coefficient which varies depending on different major groups of organisms (i.e. homeotherms, heterotherms or unicells), and b is a relatively constant size-scaling parameter. Moloney and Field (1989) noted considerable debate regarding the range of values for b, and so based on data from literature,

body masses, log transformed rate processes and regression estimates, they proposed a value of -0.25. Taxonomic differences (Moloney and Field, 1989; Cermeño et al., 2006), phenotypic and physiological plasticity (Brown et al., 2004) and environmental conditions such as temperatures, irradiance and nutrient concentrations influence the size scaling slopes and intercept of this equation. A recent study (Lindemann et al., 2016) of the affinities for nutrients suggested that the slopes may also vary between small and large cells. This was attributed to the costs incurred by small cells investing energy into nutrient transporter sites on the cell well.

Chisholm (1992) reviewed the relationship between size/respiration and size/growth rate. In terms of respiration, the relationship was inconclusive owing to a paucity of data, with arguments for a -0.25 scaling exponent (Banse, 1975) or a very weak relationship (Falkowski and Owens, 1978). For growth rates, the intricacies between and within phylogenetic morphotypes (i.e. diatoms and dinoflagellates) complicate the application of the simple allometric equation mentioned above. Chisholm (1992) noted that diatoms grow three times faster than dinoflagellates of equal size and even the maximum growth rate (μ_{max}) of a given species within diatoms can vary by a factor of two (Platt, 1985). The size dependence of growth rates in phytoplankton as a group, according to Chisholm (1992) is weak. Tang (1995) found the scaling exponent is not affected by taxonomic affiliation, but that mean growth rates do differ between certain divisions. Nevertheless the influence of cell size on nutrient uptake rates is stronger than other metabolic rates owing to first principles of surface area to volume ratios (Banse, 1975).

Despite the observed variability within an allometric framework, the biogeography of dominant size classes illustrates a clear dependence of cell size distributions on nutrient availability. It is fairly well established that there is a constant background of pico-plankton (< 2μm) with the proliferation of larger cells as nutrient supply increases (Chisholm, 1992; Agawin et al., 2000; Barnes et al., 2011). This is seen between oligotrophic and eutrophic areas (Acevedo-Trejos et al., 2013) and more locally, at upwelling/downwelling timescales (Pitcher et al., 1991; Mitchell-Innes and Pitcher, 1992; Kiørboe,1993). These patterns in the biogeography of particle size distributions (PSD) are well marked in global maps derived from PSD algorithms applied to satellite ocean color (Hirata et al., 2008; Kostadinov et al., 2010; Brewin et al., 2010). Large

cell sizes are concentrated around eutrophic areas of high nutrient supply, whereas nutrient depleted, oligotrophic areas are associated with an absence of large cells (Fig. 1.4).

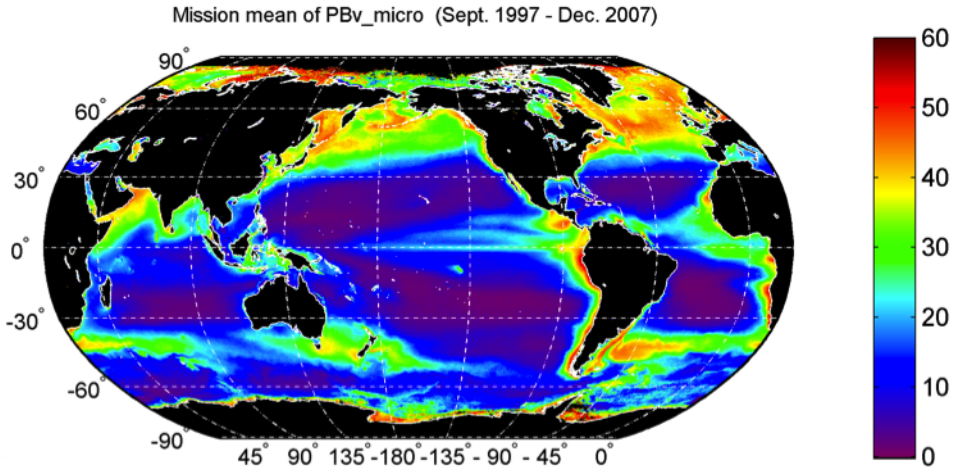

Figure 1.4: The percent volume concentration contribution of micro-plankton (20-50um) to total particle size distributions (PSD). Details of calculations in Kostadinov (2009, 2010). Micro-plankton only found in upwelling and high latitude areas, contributing <60% to total PSD. Taken from Kostadinov et al. (2010) fig. 5C

Based on allometric relationships, theoretically, the rate at which nutrients are transferred to higher trophic levels or sequestered to depth should be quantifiable by the size structure of the phytoplankton community and is a tenet explored further in chapter 4. It is clear that size has an overarching influence on metabolic rates, more specifically on uptake rates. However, there are several other important factors that may influence nutrient uptake, such as light or nutrient-limitation (MacIsaac and Dugdale, 1972), inherent taxonomic differences (Platt, 1985), physiological status and plasticity (Bonachela et al., 2011) and nutrient prehistory. Given that many studies of the size dependence of nutrient uptake come from culture experiments (with exceptions: e.g. Furnas, 1983; Riegman et al., 1998; Probyn and Painting, 1985; Probyn et al., 1990; Bury et al., 2001), there are few studies that focus on the compounding effects of all variables on nutrient uptake, in a natural system. The interdisciplinary nature of such an approach is challenging, owing to the interactions between variables at several timescales (Levin, 1992). Equally, measured rates are the sum of many influences and disentangling the effects of each influence (in a natural system) is inherently challenging. Inevitable questions arise when nutrient uptake is considered in the context of natural assemblages. At what point does allometry

become too broad to accurately quantify mechanistic processes such as nutrient uptake and transfer? And when should differences in functional group/type be taken into account? More specifically to nitrogen, can an allometric approach be effectively used for all (or any) of the different nitrogen components in a variety of phytoplankton assemblages?

V_{max} and K_s as functional traits

The ability to compete for nutrients in a given habitat, and the strategy employed by the organism/group of organisms is considered a key trait that drives species succession (Margalef et al., 1979). Relative values of V_{max} and K_s for a given nutrient are suggested to predict the competitive advantage of a species and are considered key functional traits of resource utilisation as they directly affect the organism fitness and efficiency (Litchman and Klausmeier, 2008). A low K_s implies an ability to take up nutrients at low concentrations and a high K_s indicates a requirement for high concentrations. A high V_{max} is considered a competitive advantage when nutrients are at high concentrations. Sommer (1989) classified low K_s species as 'affinity strategists' and species with a high V_{max} as 'growth strategists'. However, Healey (1980) suggested that the ratio between V_{max} and K_s, known as the affinity (α), is a better indicator of nutrient uptake efficiency:

$$\alpha = \frac{V_{max}}{K_s} \tag{1.5}$$

Small phytoplankton are more efficient at taking up nutrients at low concentrations due to their low K_s, and this is often used to explain why small cells dominate in nutrient limited conditions (Eppley et al., 1969; Aksnes and Egge, 1991; Hein et al., 1995). Large phytoplankton, on the other hand, are seen to dominate eutrophic areas of high nutrient supply (Acevedo-Trejos et al., 2013) and they are observed to have high K_s and high V_{max}. Essentially, competitive ability for nutrient uptake declines as cell size increases (Edwards et al., 2012).

An often asked question is whether V_{max} and K_s values that have predominantly come from culture experiments can be used to accurately assess phytoplankton responses in natural conditions (Harris, 1980; Sommer, 1989; Collos et al., 2005; Litchman et al., 2015). Edwards

et al. (2013) found that using lab-based traits effectively predicted the variation in community structure in response to seasonal fluctuations in the English Channel. Values of K_s and V_{max} can vary substantially within groups and are sensitive to environmental conditions.

Variations in V_{max} and K_s

Uptake parameters are often assumed constant for the phytoplankton compartments in many plankton-based models. However, it is recognised that high variance in uptake parameters is observed within and between functional groups (Litchman et al., 2007; Edwards et al., 2012), under variable nutrient concentrations (Collos et al., 2003) and variable temperatures (Aksnes and Egge, 1991; Lomas and Glibert, 1999). V_{max} and K_s are also seen to vary with cell size (Fig. 1.5), where both have a positive correlation with cell volume, although half saturation constants are observed to be less constrained by cell volume (Edwards et al., 2012).

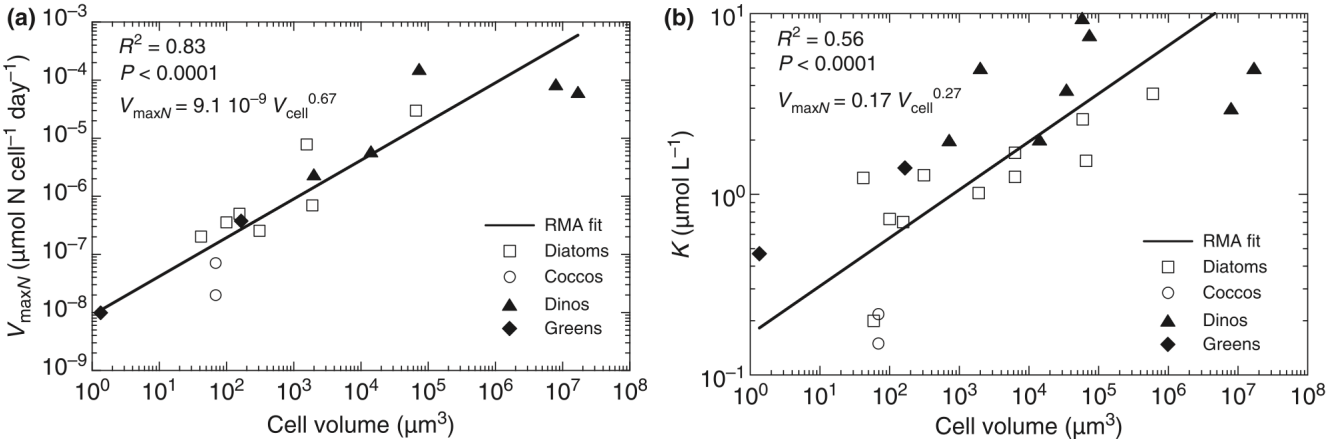

Figure 1.5: Taken from Litchman et al. (2012), the relationships between cell volume and a) V_{max} and b) K_s of nitrogen. Different groups (diatoms, coccolithophorids, dinoflagellates and green algae) are represented by different markers. Relationships are highly significant (p <0.0001) for both V_{max} and K_s.

The nutrient prehistory and physiological status of the cell have been observed to change uptake parameters. Harrison et al. (1996) observed an increase in V_{max} in nitrogen-starved batch cultures. The effect of nitrogen starvation is understood to be dependent on the nitrogen source, nutrient prehistory and duration of starvation (Collos, 1980). Furthermore, not all nutrient uptake kinetics can be described by the Michaelis-Menten equation. Several studies (Collos et al., 1992; Watt et al., 1992; Collos et al., 1997; Lomas and Glibert, 1999) observed

the non-saturating nature of uptake kinetics, where linear or bi-phasic uptake occurred. It has been suggested that non-saturating behaviour of uptake kinetics (and thus deviation from the typical Michaelis-Menten kinetics) is due to the uncoupling of growth and uptake and internal storage of nitrogen (McCarthy and Goldman, 1979; Lomas and Glibert, 1999). As previously described (eq. 1.2), nutrient uptake and growth are separated by making cellular growth dependent on the internal stores of nutrients (Droop, 1973). It is recognised however that this formulation does not account for phenotypic plasticity or physiological acclimation in response to highly fluctuating environmental conditions. Physiological acclimation can take many forms, but in the case for nutrient uptake, has been described by Smith et al. (2009) as the trade off in investing energy into the different mechanisms required for resource assimilation. Two mechanisms are at play here: 1) nutrient encounter at the cell surface by altering surface uptake sites (ion channels) or 2) internal enzymes, which assimilate nutrient ions once encountered. Several other models aim to incorporate an organisms' ability to dynamically rearrange their physiology to make most efficient use of their resources (e.g. Bruggeman and Kooijman, 2007; Litchman and Klausmeier, 2008). Flexible trait-based approaches are becoming increasingly used to model plankton ecosystems (Follows and Dutkiewicz, 2011; Smith et al., 2011) and several studies have shown that accounting for optimal intracellular resource allocation results in better agreement with laboratory (Pahlow, 2005; Wirtz and Pahlow, 2010; Pahlow et al., 2013) and *in situ* experiments (Smith et al., 2015). Scaling up from cellular processes to large scale dynamics is where the challenge lies for such modeling approaches and is an active area of research.

The role of nitrogen

Nitrogen is an important limiting resource in biological productivity and occupies a central role in the cycling of all other elements. Nitrogen is present in many forms, each of which has complex pathways and interactions with one another. Thus many uncertainties remain in the nitrogen cycle regarding the interactions between the different nitrogen forms, the environment and bi-

ological drivers. In the marine environment, phytoplankton are principal drivers in transporting available fixed nitrogen to the biotic components of the system. In turn, the relative contribution of the different nitrogen sources to the total nitrogen inventory can, to some extent, dictate the composition of phytoplankton communities (Glibert et al., 2014). Nitrogen in its oxidised form, nitrate (NO_3^-), is often associated with diatom assemblages (Collos et al 1992; 1997; Berg et al., 2003; Collos et al., 2005) and reduced nitrogen, NH_4^+, is observed in association with other taxa including cyanobacteria and dinoflagellates (Berg et al., 2003). The nitrogen source can also regulate the contribution of the different size fractions to total phytoplankton biomass, with a constant background of small cells (<10 μm in diameter) in nitrogen deplete conditions and large cell sizes (>10 μm) appearing in concert with increasing NO_3^- availability (Probyn, 1985; Chisholm, 1992). The vast diversity in phytoplankton plays a critical role in the rates at which nitrogen, and thus carbon and other elements, flows through marine ecosystems and yet, phytoplankton diversity remains a major challenge in studies that aim to realistically quantify nitrogen dynamics.

Forms of nitrogen

Dissolved inorganic nitrogen (DIN) (NH_4^+, NO_3^-, NO_2^-) is the form in which nitrogen is mostly taken up by phytoplankton. The nitrogen compound is transported across the cell wall via uptake/transporter sites, metabolised and stored in a variety of compounds, i.e. nitrate, ammonium, amino acids, proteins, DNA/RNA and pigments (Rhee, 1978). The principle source of nitrate in the ocean is nitrification, which usually occurs at depth, whereby ammonium (NH_4^+) is oxidised to nitrite (NO_2^-) and then to nitrate (NO_3^-). This is carried out by nitrifying bacteria in low oxygenated waters at depth, and in coastal areas these nitrate-rich waters are brought to the surface via vertical transport, e.g. upwelling. The major source of NH_4^+ is the transformation of organic nitrogen to ammonium via ammonification, a process usually carried out by heterotrophic bacteria. The residence times of oxidised (NO_3^-) or reduced (NH_4^+) forms of nitrogen differ substantially, with turnover rates for NH_4^+ being substantially quicker (Gruber, 2008). NH_4^+ is taken up almost as quickly as it is released, as it is considered to be the preferred

source of fixed nitrogen (McCarthy et al., 1977; Dortch, 1990). NH_4^+ is already in a reduced state and requires little energy for assimilation (Syrett, 1981; Zehr and Ward, 2002). Nitrate assimilation is energetically more expensive than NH_4^+, as it must first be reduced to NO_2^- using nitrate reductase (NR) and then further reduced to NH_4^+, using nitrite reductase enzyme (NiR). Dissolved organic nitrogen (DON) (urea, amino acids, peptides/proteins) is also an important source of nitrogen for phytoplankton (Mulholland and Lomas, 2008). Urea, the simplest DON compound, is the most commonly measured uptake of DON and requires the enzyme urease for assimilation into the cell (Mulholland and Lomas, 2008). Urea can contribute over 50% of total N uptake in some coastal systems (Glibert et al., 1991).

New production is associated with nitrate (NO_3^-) uptake and regenerated production with the uptake of ammonium (NH_4^+) and urea (Dugdale and Goering, 1967). The relative ratio of nitrate to total nitrogen uptake is known as the *f*-ratio (Eppley and Peterson, 1979) and is often used to estimate the export of nitrogen. The *f*-ratio can also be considered a measure of the distinction between physically (upwelled) and biologically (regenerated) mediated sources of nitrogen for primary productivity (Probyn, 1985). New production, indicated by high *f*-ratios, is considered to be the portion of production with the highest implications for carbon export or the flow of energy to higher trophic levels (Probyn, 1992). In upwelling systems, the transfer of energy to higher trophic levels is believed to be much more efficient when NO_3^- is the source of primary production (Hutchings, 1992; Probyn, 1992).

Pathways of nitrogen

The need to assess the relationships between cell size and nutrient uptake rates, in natural assemblages, becomes apparent when considered in the context of quantifying nitrogen flux in diverse communities of phytoplankton and its potential application to studies of the pathways of nitrogen to higher trophic levels. Based on well established size-spectrum theory (Kerr, 1974), the transfer of carbon/nitrogen to higher trophic levels follows some relation to the size distribution of plankton communities (e.g. Sheldon et al., 1972; Andersen and Beyer, 2006). In the southern Benguela, small pelagic fish such as sardine (*Sardinops sagax*) and anchovy

(*Engraulis encrasicolus*) are key species in the ecosystem, as they play an important role in mediating the transfer of energy from lower to higher trophic levels (Cury et al., 2000). The contribution of each of these species to total catches is subject to inter-annual variability and alternations between the two are suggested to be associated with environments that favour one species over another (van der Lingen et al., 2006). The shifting regimes between strong upwelling-favourable, and relaxed downwelling-favourable winds, which consequently drive the structure of plankton communities, are hypothesised to select for either sardine or anchovy (Shannon et al., 2004) (Fig. 1.6). The relevance of the different phytoplankton communities to pelagic ecosystem structure is clear, and although figure 1.6 is not purely size based, characterising the system by means of size-spectrum theory is an attractive alternative. Accurate representations of the effects of the nitrogen source on phytoplankton size structure is a good foundation for further studies into nitrogen flux in marine food-webs.

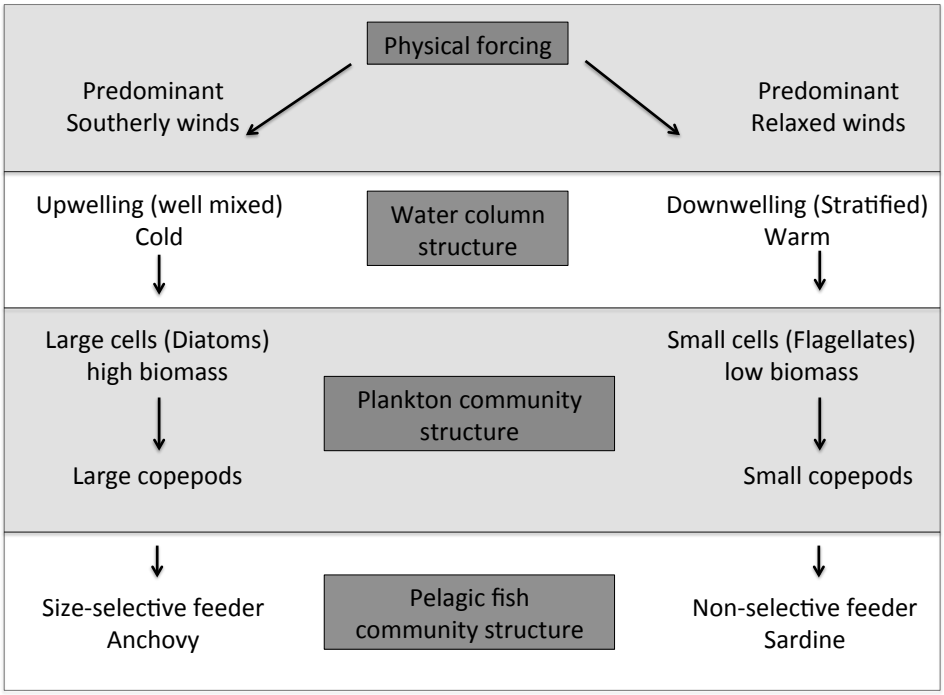

Figure 1.6: Schematic of conceptual model of physical forcing. Adapted from Van der Lingen et al. (2006)

The cellular content of nitrogen and its ratio to other essential elements such as carbon, phosphorous, silicon and iron (i.e. elemental stoichiometry), can also have consequences for grazers higher up the food chain (Lind and Jeyasingh, 2015). In a review by Glibert (2012), em-

phasis was placed on the importance of algal stoichiometry in altering food-webs. For grazers, it is the nutritional value (i.e. C:N:P ratios), rather than reproduction rate, that is key to grazer population success (Finkel et al., 2010; Glibert, 2012). It is well recognised that algal stoichiometry can vary markedly from the previously accepted Redfield ratios of 160C:16N:1P (Hecky et al., 1993; Geider and La Roche, 2002), with varying environmental conditions (nutrient limitation and nutrient saturation) and the community structure present (Glibert et al., 2013). In terms of cell size, larger cells have storage vacuoles to account for fluctuations in nutrient supply and will often have an excess of cellular concentrations of certain nutrients. In an upwelling environment it is most notably NO_3^- that will be stored and thus, in general, large cells will have a higher N:C ratio than small cells, whose nutrient requirements are much lower and can maintain growth at low nutrient concentrations. Increases in cellular vacuolation, and thus cell size, have been observed to occur in conjunction with changes in elemental stoichiometry of the substrate environment (Raven, 1997; Finkel et al., 2010). In turn, certain predators are selected for by the particular C:N:P ratios of their prey. Certain deviations from the Redfield ratio have been quantified from a species perspective (see Geider and La Roche, 2002; Michaels et al., 2001; Lind and Jeyasingh, 2015), but in terms of cell size the relationships are less well understood. Although it is recognised that C:N and N:P ratios play a significant role in the pathways of nitrogen flow by grazer and predator selection of nutrition, and quantifying the role of cell size would be a useful area of research, it is beyond the theme of the research proposed herein.

Southern Benguela Ecosystem

The Eastern Boundary Upwelling Systems (EBUS) are among the most productive of marine ecosystems (Ryther, 1969) and nitrogen is a key limiting resource of primary productivity in such systems (Dugdale, 1967; Ryther and Dunstan, 1971; Wilkerson and Dugdale, 2008). Alongshore, upwelling-favourable winds force surface waters offshore, inducing upwelling of nutrient-rich deep waters to the well-illuminated, surface coastal zone. Upwelling-favourable winds are forced predominantly by two mechanisms: Hadley cells which influence atmospheric

pressure systems over the ocean (Diaz and Bradley, 2005) and local thermodynamics of land-sea temperature contrasts (Bakun, 1990). The Intergovernmental Panel for Climate Change (IPCC) reports a likely increase in the intensity of wind-stress in upwelling systems (Bakun et al., 2015) and recent observations of EBUS generally support this notion (Sydeman et al., 2014). In the southern Benguela (Fig. 1.7), Rouault et al. (2010) found a cooling trend between 1982 and 2009 in near-shore sea surface temperatures (SST), which they attributed to an increase in upwelling-favourable winds. Several studies have assessed long term trends in Chl-*a* concentrations from *in situ* observations (Verheye, 2000; Hutchings et al., 2009) and SeaWiFS data (Demarcq et al., 2007) but no clear trend is observed. Moloney et al. (2013) noted that we still have a limited understanding of how phytoplankton community structure and primary production might respond to changes in local forcing.

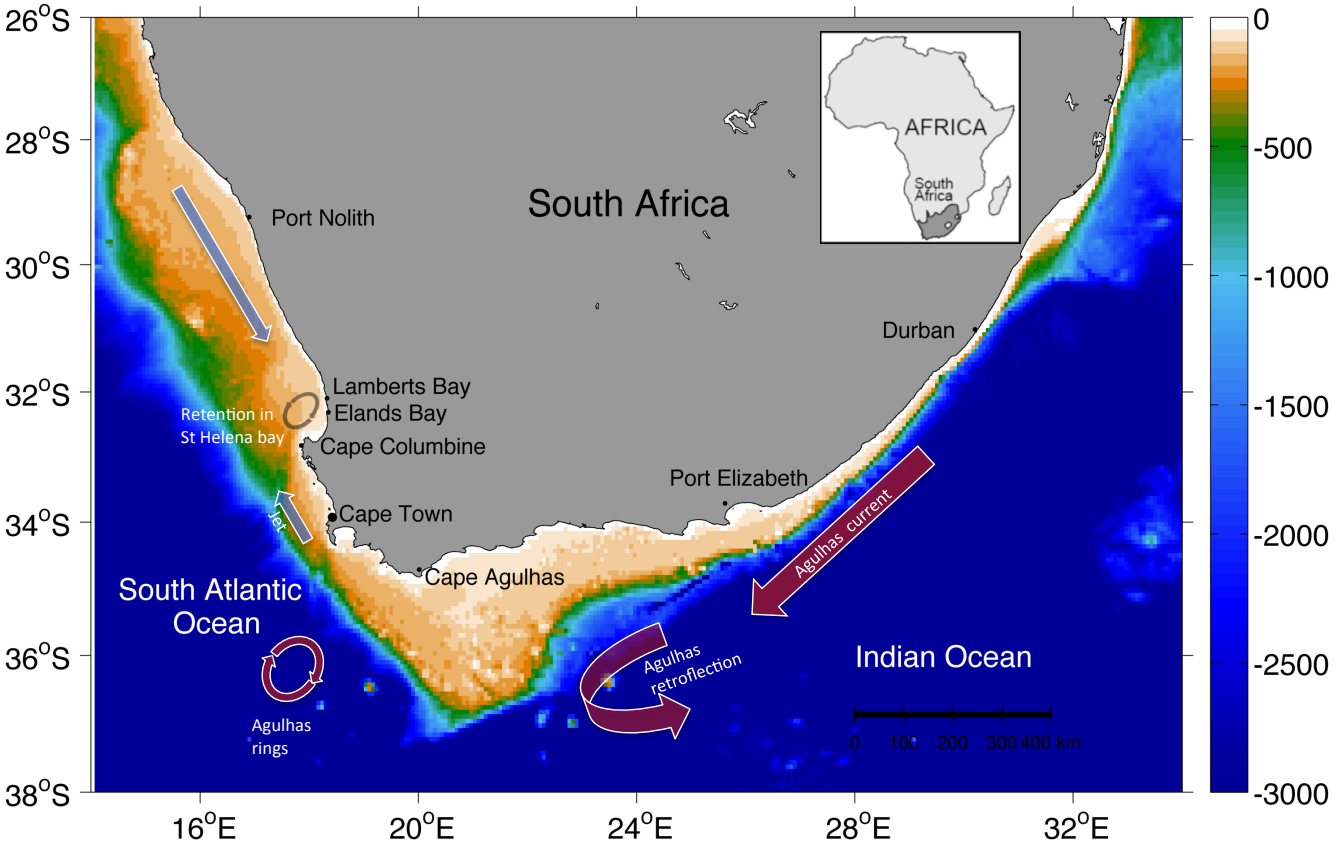

Figure 1.7: Map of South Africa with coastal bathymetry (m) and general oceanographic features. Adapted from Shannon (2006)

Physical drivers

In the southern Benguela, the area is dominated by the atmospheric South Atlantic subtropical anticyclone, causing high pressure cells that induce southerly wind stress. In this region, most hydrodynamic processes are governed by the prevailing winds (Pitcher et al., 1995) and thus strong coupling between wind patterns and bloom dynamics is observed (Fawcett et al., 2007). In the summer months, the prevailing winds are southerly, determined by the location of high pressure systems in the south Atlantic and the pressure field over the African continent, the gradient between the two and eastward moving cyclones (Nelson and Hutchings, 1983). Wind stress is intensified during summer months (September to March) when continental surface

heat flux creates low pressure systems and enhances zonal pressure gradients between both pressure systems. During winter (April to September), westerly winds predominate as the atmospheric circulation features move northward, leaving low pressure systems to dominate. In addition to this seasonality in southerly winds, synoptic scale wind patterns during the upwelling season drive the upwelling/downwelling cycles, ranging from 3 -10 days (Nelson and Hutchings, 1983). These south-easterly winds drive Ekman transport of the surface layer away from the shore, causing the replacement of surface water masses by cold, nutrient-rich upwelled waters from depth, composed mostly of South Atlantic Central Water (SACW). Downwelling occurs during periods of quiescent winds or light westerly winds, when surface waters are retained within bays. These strong pulses of upwelling cycles, driven by synoptic weather and wind patterns (Pitcher et al., 1998b), are the main drivers of short term variability of plankton dynamics, as seen in Margalef's Mandala (Margalef et al., 1979).

Harmful Algal Blooms

Harmful algal blooms (HABs) are common to many coastal regions of the world (Hallegraeff, 1993) and frequent on the west coast of South Africa (Horstman, 1981; Pitcher and Cockcroft, 1998; Cockcroft et al., 1998; Pitcher and Probyn, 2011). The mechanisms driving the proliferation of harmful species are the result of a complex mix of physical, chemical and biological interactions (Anderson et al., 2012). HABs have been reported to cause major impacts on public health, fisheries and aquaculture, spurring a global consortium of research in the last decade (GEOHAB), with the aim to understand driving mechanisms and ultimately establish monitoring and predictive programs. HABs are characterised by the accumulation and often dominance of particular toxic and non-toxic algal species, and can be separated by their impact (GEOHAB, 2001):

- the occurrence of rapid proliferation and/or high biomass of toxic algae that kill fish or shellfish,
- highly toxic cells in low cell concentrations, but can render shellfish or other seafood poisonous to humans and other marine mammals,

- the accumulation of non-toxic species at high biomass, causing ecosystem damage via hypoxia, anoxia or altering food-web dynamics (Glibert et al., 2005). This includes blooms that cause discolouration of water, more commonly known as red tides.

Globally, the frequency and magnitude of HABs, and consequently their ecosystem impacts, have increased (Anderson et al., 2012). The mechanisms causing this are suggested to include increases in coastal nutrient loading (Anderson et al., 2012 and references therein), changes in species dispersal and physical transport (bottom-up), as well as altered food-webs as a result of over-fishing, by impacting the community of grazers of harmful algal species (top-down). However, the diversity in HAB species and the mechanisms causing their proliferation is vast and studies are usually focused within a local context, thus no identified 'unifiying principles' can explain such phenomena at a global scale (Anderson et al., 2012).

Diversity in blooms:

Although harmful algal species are most commonly dinoflagellates, HABs cover a broad range in phylogenetic grouping: diatoms, haptophytes and cyanobacteria, employing a wide range from *r* to *K* strategies of growth (Haellegraff, 2010), toxicity patterns as well as filling several niches (Smayda, 2000). Furthermore, mixotrophic tendencies have become an accepted mode of nutrition for many harmful algal species observed (Glibert and Legrand, 2006). The diversity in species has traditionally been defined using nomenclatural classifications of species, but other methods have been suggested to be more appropriate from an ecological perspective. Smayda and Reynolds (2001) argued that quantifying HAB dynamics required focusing on the life-form properties rather than individual species. It is also acknowledged that DNA sequencing and molecular probing have brought novel insight into the molecular diversity of harmful algal species (Sellner et al., 2003 and references therein).

In the southern Benguela, HAB events are strongly coupled to meteorological forcing such as wind stress (direction and intensity) and insolation, where strong seasonality is observed with HABs reported most often during late summer/autumn months between March-May (Pitcher and Calder, 2000). HABs are particularly prevalent in St Helena Bay, equator-ward of Cape Columbine, where the broadening of the coastal shelf is subject to intense stratification, fol-

lowing sustained periods of wind relaxation and onshore transport of dinoflagellate populations (Pitcher and Boyd, 1996). The interplay between upwelling and downwelling favourable conditions provide 'ecological windows' when HAB events are most likely (Kudela et al., 2005; Bernard et al., 2006; Tilstone et al., 1994; Trainer et al., 2002; Ryan et al., 2009). The proliferation of HAB species is often associated with the relatively high utilisation of reduced forms of nitrogen (Collos et al., 2004; 2007, Kudela et al, 2010) and, in cases of eutrophication, urea (Glibert et al., 2006; Solomon et al., 2010). Such functional traits (e.g. nutrient utilisation) are well observed in dinoflagellates and small flagellates (Paerl, 1991; Berg et al., 1997; 2003) and are characteristic of nutrient-deplete downwelling waters. High growth rates of *Pseudo-nitzschia* spp., a diatom, on reduced forms of N have also been recorded (Howard et al., 2007; Cochlan et al., 2008; Seeyave et al., 2009) which is in contrast to an often observed diatom preference/affinity for nitrate (Collos, 1992; Lomas and Glibert, 2000). A review of published kinetic experiments carried out for harmful species reveals, on average, highest affinities (α) for reduced forms of nitrogen (Kudela et al., 2010 and references therein).

Monitoring blooms:

It is clear from the literature that HAB events are complex and remain unpredictable owing to the diversity of nutrient utilisation strategies, cell physiologies (Kudela et al., 2010), competition/predator-prey interactions (Chakraborty and Feudel, 2014) and the range of habitats in which they can occur (Smayda and Reynolds, 2001). Differentiating the phytoplankton assemblages through satellite remote sensing techniques is of benefit to HAB monitoring (Kudela et al., 2005; Bernard et al., 2009), where the scale of observation can be useful to monitor temporal and spatial variability and trends in bloom dynamics. As mentioned above, the initiation of HABs is a result of interactions between the biological, physical and chemical conditions for the bloom, which vary for each HAB species. Consequently, a single solution to monitoring and management may not exist and thus requires more locally designed methods of observation. For example, in the Gulf of Mexico, *Karenia brevis* commonly forms red tides which have caused significant economic losses to the region (Hoagland et al., 2009). Several studies have successfully applied algorithms to Sea-viewing Wide Field-of-view (SeaWiFS) data to

detect *K. brevis* blooms (Stumpf et al., 2003; Carvalho et al., 2010), providing information on bloom size and magnitude.

In the southern Benguela, by far the most common HABs to occur are those of dinoflagellate blooms, characteristically associated with exceptionally high biomass (as indexed by Chl-*a*), where values often exceed 30 mg m^{-3} (Pitcher and Weeks, 2006; Fawcett et al., 2007; Pitcher and Probyn, 2011). The standard global ocean color algorithms, e.g. for the Medium Resolution Imaging Spectrometer (MERIS) data, are not well constrained at Chl-*a* concentrations greater than 20 mg m^{-3} (Morel et al., 2007). This prompted the establishment of more specialised algorithms for high biomass waters, such as the Equivalent Algal Population (EAP) algorithm (Bernard, 2005; Evers-King et al., 2014), to accurately determine the high concentrations often observed in the southern Benguela. An additional output from the algorithm is an effective diameter (D_{eff}), which is a size metric that represents the bulk optical signal of a measured assemblage using the mean volume to surface area ratio of the entire distribution (Bernard et al., 2007). The detection of assemblage size characteristics is valuable in understanding HAB dynamics, as bloom initiation is often associated with changes in the gross size of algal assemblages (Bernard et al., 2014) and it is most often large dinoflagellate cells (>15 μm in diameter) that most commonly form harmful blooms in the southern Benguela (Pitcher and Calder, 2000).

The EAP algorithm was applied to an 11 year time series of MERIS data to assess temporal and spatial trends in Chl-*a* and D_{eff} (Evers-King, 2014). The use of D_{eff} enabled confirmation of two suggested patterns in the local variability in particle size distributions (Pitcher et al., 1992a): 1) large cells are typically dominant inshore and small cells offshore, 2) a size progression from small to large cells over event scale upwelling/downwelling cycles. Furthermore, the Chl-*a* and D_{eff} products derived from the EAP algorithm provide evidence that support the conceptual model as described by Pitcher and Nelson (2006) and illustrated in Fig 1.8.

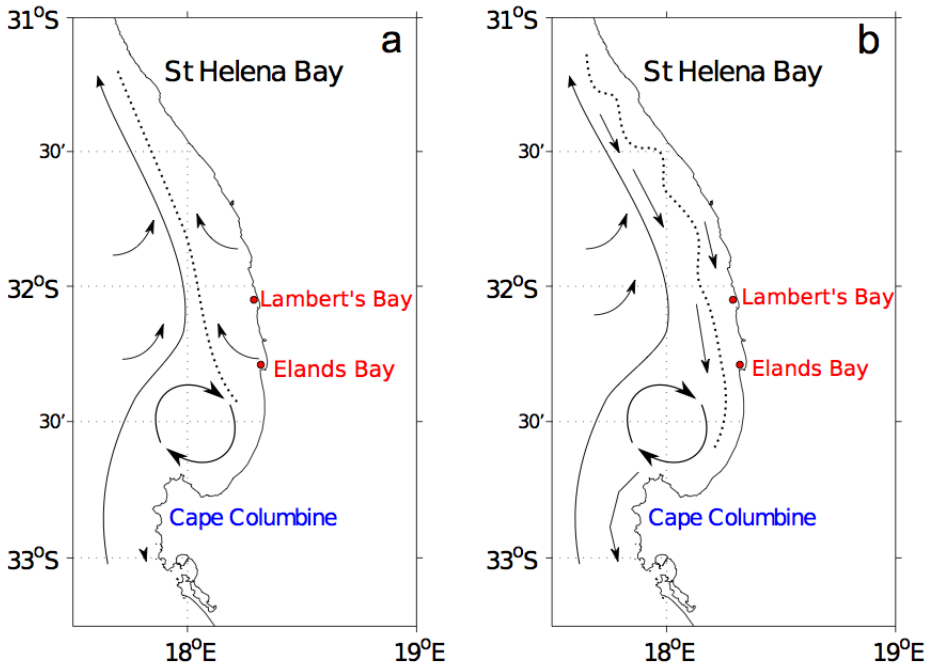

Figure 1.8: Schematic illustrating the major physical circulation features in St Helena Bay during a) upwelling and b) downwelling/relaxation scenarios that drive the spatial distribution of dinoflagellate populations. Dashed line indicates the spatial extent from the shore of dinoflagellates. Taken from Evers-King (2014) with permission from the author.

The approach used to determine D_{eff} from the EAP algorithm differs fundamentally from other algorithms that derive either dominant size class (Brewin et al., 2010; Uitz et al., 2010) or particle size distributions (Kostadinov et al., 2009), and it has yet to be quantitively compared to each of the other approaches (Evers-King et al., 2014). The advantage of the EAP algorithm over others in such a local context is its capacity to appropriately deal with exceptionally high biomass (Bernard et al., 2014). The algorithm product, D_{eff}, has proven to be useful in the tracking of high biomass blooms containing cells within the micro-plankton size range (10 - 50 μm) and has provided new insight into the spatial and temporal variability of HABs within the St Helena Bay area (Fig. 1.9).

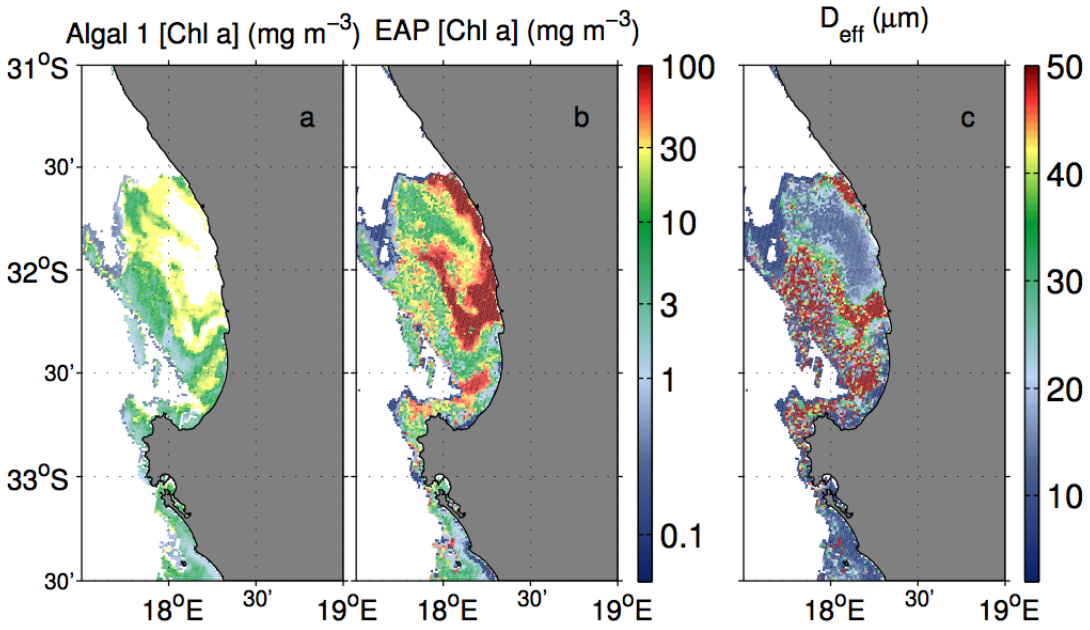

Figure 1.9: Products derived from MERIS level 2 imagery in St Helena Bay on the 5 April 2005. Comparisons between Chl-*a* products using a) Algal 1 (standard algorithm for case 1 waters) and b) Chl-*a* product from EAP algorithm (Bernard et al., 2009). c) shows the associated D_{eff} product from the EAP algorithm. Images kindly provided by Evers-King.

The use of aggregate properties to describe an assemblage as a single entity is not new. The effective diameter described above was adapted from atmospheric sciences, where single size proxies are used as equivalent descriptors of the aggregated bulk optical properties of the particle size distributions (Bernard et al., 2007). Similarly, in the plankton modeling community several models treat phytoplankton assemblages as a single entity through aggregate properties such as total biomass, mean trait and trait variance (Wirtz and Eckhardt, 1996; Bruggeman and Kooijman, 2007; Merico et al., 2009; Wirtz, 2013; Acevedo-Trejos et al., 2016). Such approaches are adopted with the aim to reduce the complexity in characterising natural communities and thus, the computational costs of modeling them.

Aims and Objectives

Phytoplankton are a key component in the functioning of marine systems and play a central role in the cycling of important elements. Representing diversity in biogeochemical models has become an increasingly popular area of research. Phytoplankton cell size is considered

a 'master' trait that can represent the functional diversity in phytoplankton, owing to empirical relationships observed between metabolism, cell size and the trade offs associated with growth. In this thesis, emphasis is placed on gaining further insight into the ecological significance of a bulk metric, effective diameter (D_{eff}), to represent the size-based diversity in phytoplankton assemblages. As a product derived from ocean-color data for high biomass blooms that are typical in the southern Benguela, D_{eff} has been used to assess synoptic-scale variability in phytoplankton assemblages, but has yet to be tested in an ecological/biogeochemical context.

Nitrogen, in its many forms, is identified as a key driver in phytoplankton community structure (and often HABs) in the southern Benguela, and will thus be used as a testing currency. The relationships, and variability therein, between phytoplankton cell size and the associated nitrogen dynamics are expected to provide a good platform for such an analysis.

The southern Benguela upwelling system is an ideal 'laboratory' to explore the usefulness of D_{eff}, as the system offers highly fluctuating dynamics of nitrogen and periodic shifts in the relative contributions of oxidised and regenerated forms to the total nitrogen inventory. Furthermore, owing to such high nutrient supply, the large fractions of the size spectrum of phytoplankton are periodically present, often in bi-modality, and thus supply a broad spectrum of cell size distributions. As opposed to employing cultured phytoplankton communities, using natural assemblages, measured *in situ*, provides the necessary means to test how well D_{eff} can describe nitrogen metabolism in relation to other, concomitant influences. The specific research questions that refer to each data chapter are as follows:

1) The southern Benguela upwelling system is periodically subject to HABs and monitoring their dynamics has become an evermore pressing priority for local research. Any discussion on phytoplankton dynamics in the southern Benguela would be incomplete without some focus on HABs. The development of the effective diameter (D_{eff}) approach was driven by the need to provide size information for these high biomass blooms. Can D_{eff} capture the principal biogeochemical properties of observed phytoplankton assemblages in high biomass?

2) Diatoms are the most abundant and diverse group of phytoplankton in the marine environment and display a wide range in strategies of nitrogen uptake. Sampling from a coastal

bay system provides a data set of diatom-predominant assemblages to explore the strategies of nitrogen utilisation under varying environmental conditions. What are the strongest factors that influence nitrogen uptake within diatoms? Given the wide range in cell sizes of diatoms, can D_{eff} represent nitrogen utilisation within diatoms as a group?

3) Establishing adequate means of representing phytoplankton diversity and its role in biogeochemistry is an important research area in phytoplankton models. Phytoplankton cell size distributions are hypothesised to be an accurate means to quantify nitrogen uptake by diverse, natural assemblages of phytoplankton. Can a size-based approach to phytoplankton diversity and nitrogen dynamics account for the variability observed in measured *in situ* nitrogen uptake by natural populations?

This thesis covers the nitrogen dynamics observed in diverse, natural phytoplankton assemblages and uses these case studies to inform understanding of the relationships between nitrogen uptake and a size metric, D_{eff}. The nitrogen utilisation by diverse groups of phytoplankton is detailed in relation to environmental variables for three *in situ* case studies. These descriptions in themselves provide valuable information on the utilisation of nitrogen during high biomass, harmful algal blooms and in diatom dominated assemblages.

Chapter two explores two case studies of particular interest at the Lamberts Bay study site, where exceptionally high biomass is observed with the proliferation of two common harmful algal species: *Myrionecta rubra* and *Prorocentrum triestinum*. The dynamics of community structure and environmental variability are linked to the utilisation of the different nitrogen sources (NO_3^-, NH_4^+ and urea). Some inferences are made on the physiology of the two species of interest and are compared along the upwelling/downwelling axes. The relationships between the single-value size proxy, D_{eff}, and the uptake of nitrogen are quantified.

Chapter three takes advantage of a diatom-dominated data set to explore the nitrogen dynamics during bimonthly sampling over the period of a year in a coastal bay system, Saldanha Bay. Limitations on nitrogen uptake rates are linked to environmental variables as well as qualitatively to community structure. The results of uptake kinetic experiments throughout the sampling period are compared, to assess the variations in Michaelis-Menten uptake parameters

within diatoms under varying environmental conditions. Finally, the relationships between D_{eff} and nitrogen uptake rates are assessed.

Chapter four explores several means to predicting size-integrated nitrogen uptake rates via Michaelis-Menten uptake kinetic parameters. Size distributions from the three case studies are converted to an integrated biomass value and compared to *in situ* particulate nitrogen to validate the use of Coulter Counter size distributions. Comparisons are made between measured and estimated uptake rates. Estimated uptake rates are calculated using kinetic parameters that are scaled to size, but the use of constant parameters is also included in the analysis to compare allometric and non-allometric estimations.

Chapter five summarises the major conclusions of this thesis and offers suggestions for further work which would enhance our understanding of the role that diversity plays in a broader ecological context. Suggestions are made for further research into the use of phytoplankton size distributions as a tool to improve our mechanistic understanding of functional diversity in nitrogen dynamics.

Chapter 2

Can effective diameter (D_{eff}) capture the nitrogen utilisation by high biomass blooms at upwelling/downwelling timescales?

Abstract

High biomass, and often harmful, algal blooms are a prevalent feature in the southern Benguela. Large scale monitoring of such blooms is facilitated by the development of the ocean color Equivalent Algal Population (EAP) algorithm, which provides an algal size proxy, effective diameter (D_{eff}). This product has previously been used to assess synoptic scale variability in high biomass, large-celled blooms but has yet to be assessed in terms of biogeochemical relevance. This study describes the nitrogen dynamics of two separate high biomass blooms that occurred late austral summer of 2004 and 2005 in Lamberts Bay, South Africa. The nitrogen dynamics of the blooms are related to D_{eff} with the aim of establishing the degree to which D_{eff} represents the nitrogen physiology of the communities, within the constraint of allometry. In 2004, *Myrionecta rubra,* a mixotrophic ciliate, was present in both upwelling and downwelling conditions

and observed in close association with a diatom genus, *Skeletonema* spp. *Myrionecta rubra* proliferated to high biomass (104 μmolN L^{-1}), with high rates of primary productivity (303 mgC m^{-3} h^{-1}) and high NO_3^- uptake rates (0.30 μmol N L^{-1} h^{-1}). In 2005, *Prorocentrum triestinum,* a common HAB species, was also observed in high biomass (147 μmol N L^{-1}) and primary productivity peaked at 340 mgC $m^{-3}h^{-1}$. Diatoms were the most efficient utilisers of NO_3^- and total nitrogen in both case studies, irrespective of cell size. Urea appeared to be an important source of nitrogen during both harmful algal blooms. The uptake rates of regenerated forms of nitrogen were correlated with D_{eff} (NH_4^+: r=-0.54, p<0.05; urea: r=-0.59, p<0.05), indicating that the bulk dynamics of regenerated forms of nitrogen can be adequately represented by D_{eff}. By comparison, the observed positive relationship between D_{eff} and the uptake of NO_3^- was not significant (r=0.27, p>0.05). The uptake of regenerated nitrogen is thus well captured by D_{eff} but not the uptake of NO_3^-.

Introduction

Nitrogen is a major limiting nutrient in the marine environment (Dugdale, 1967), with a complex cycle and strong interactions with the uptake of carbon and other elements (Gruber, 2008). Coastal upwelling systems cover merely ∼2% of the global ocean, but their contribution to global primary production is disproportionately significant (Ryther, 1969), and they are thus important regions to consider in global nitrogen dynamics.

Different forms of nitrogen, in its oxidised (NO_3^-) or reduced forms (NH_4^+, urea), are utilised by different components of phytoplankton communities (Probyn, 1985; Stolte and Riegman, 1995; Litchman et al., 2007). Small phytoplankton cells (<2 μm) are considered principal utilisers of reduced forms of nitrogen and large cells (>2 μm) are frequently observed to utilise nitrate when available in high concentrations (Probyn, 1985; Chisholm, 1992; Thingstad, 1998; Agawin et al., 2000; Barnes et al., 2011; Acevedo-Trejos et al., 2013). However, several studies (Dauchez et al., 1996; Bury et al., 2001) suggested the size/nutrient source relationship is not clear cut and is strongly influenced by taxonomic variability (Chisholm, 1992). The relationship is even more

confounded in extreme conditions, i.e. during harmful algal blooms (HABs), when adaptive strategies can be adopted under nutrient-limited or highly competitive conditions. The southern Benguela is characterised by frequent high biomass blooms that can have adverse effects on the ecosystem, thus any discussion of the phytoplankton and nitrogen dynamics in the region would be incomplete without their inclusion.

Harmful algal blooms and the role of nitrogen

The term HAB covers a broad spectrum of events (Zingone and Enevoldsen, 2000), and is defined by GEOHAB (2001) as high biomass blooms, toxic or not, which have direct or indirect negative consequences for marine ecosystems and/or human health. HABs can be distinguished by two main forms of causing harm: either by producing toxins that enter the marine food chain, or via their accumulation in high biomass, causing hypoxia, anoxia or altering food-web dynamics. The second situation, the accumulation of high biomass, is more commonly known as a red tide (Glibert et al., 2005) and is a prevalent feature in the southern Benguela.

Margalef's Mandala (Margalef, 1978) was a seminal conceptual model of the balance between turbulence and nutrient availability in determining the dominance of diatoms or dinoflagellates in phytoplankton assemblages. The Mandala was extended to explain red tides, which occur during low turbulence and high nutrient availability (Margalef et al., 1979). However, in upwelling systems, which are often affected by HABs (e.g. Kudela et al., 2005, 2010), this model is not always applicable (Smayda, 2000). In the southern Benguela for example, red tides are often observed towards the end of the upwelling season in stratified, nutrient-deplete conditions (Seeyave et al., 2009). Several studies have further developed Margalef's Mandala as understanding improved of phytoplankton physiology and ecology (Smayda and Reynolds, 2001; Cullen et al., 2007; Wyatt, 2014). Most recently, Glibert (2016) added several axes to the Mandala, placing particular emphasis on nutritional physiology, differentiating between nutrient preferences for NO_3^-/NH_4^+ by large/small cells and the outcome of new and regenerated production respectively. Distinction was also made between two groups of HAB dinoflagellates: high biomass bloom-forming *Prorocentrum* spp, and low biomass, toxic species such as *Alexandrium*

spp. (Glibert, 2016). The review by Glibert (2016) exemplifies advances in our understanding of phytoplankton physiology and ecology, and the benefit of using trait-based approaches to conceptualise the complexity of plankton dynamics.

Numerous studies of red tides in the southern Benguela focus on the physical dynamics associated with HAB development. Well established patterns are evident in the interplay between upwelling and downwelling-favourable winds (Pitcher et al., 1998b; Fawcett et al., 2007), water column stability and increased thermal stratification (Pitcher et al., 1998b), and alongshore advection and in-shore accumulation of blooms (Pitcher and Boyd, 1996). The interplay between upwelling and downwelling favourable conditions provides an ecological window when HAB events are most likely (Pitcher et al., 1998b; Bernard et al., 2006; Kudela et al., 2010), when prolonged relaxation and onshore advection occur and rates of phytoplankton growth exceed those of dispersion and mortality (Tilstone et al., 1994; Smayda, 2000; Trainer et al., 2002). This has also been observed in other upwelling areas (Tilstone et al., 1994; Trainer et al., 2002; Ryan et al., 2009).

In terms of nutrient dynamics, the proliferation of HAB species is often associated with reduced forms of nitrogen (Kudela et al., 2010), often showing preferences for ammonium (Collos et al., 2004; 2007) and, in cases of eutrophication, urea (Glibert et al., 2006; Solomon et al., 2010). Such utilisation traits are well observed in dinoflagellates and small flagellates (Paerl, 1991; Berg et al., 1997; Berg et al., 2003) and are characteristic of nutrient conditions during relaxation of upwelling. However, nutrient affinities of species that cause harmful blooms (either in high biomass or in toxic latency) are varied and reflect the physiological diversity of harmful algal species. Seeyave et al. (2009) found high affinities for both NO_3^- and NH_4^+ during a *Pseudo-nitzschia* sp. bloom, and highest affinities for NH_4^+ in separate blooms of harmful dinoflagellates *Alexandrium catenella* and *Dinophysis acuminata*. The nutrient utilisation strategies of the harmful algal species observed implies that they do not always follow the hypothesised diatom preference for NO_3^- (Malone, 1980a) and dinoflagellate preference for regenerated forms of nitrogen (Glibert and McCarthy, 1984). Similarly, blooms of mixotrophic species can be responsible for ecologically catastrophic events (Horstman, 1981; Burkholder

et al., 2008), but data and our understanding of their nutrient utilisation traits remain poor (Mitra and Flynn, 2010). In a review by Kudela et al. (2010), it is evident that HABs in upwelling areas occupy numerous ecological niches provided by 'ecological windows' and the shifts between upwelling/downwelling dynamics. As such, HABs are evidenced to employ a wide range of nutrient utilisation strategies, exhibiting moderate to high affinities for NO_3^- as well as regenerated nitrogen (NH_4^+, urea).

The monitoring of HABs via remote sensing

Owing to diversity in the type and impact of harmful blooms, the causes of blooms and their impacts are ecosystem specific (Zingone and Enevoldsen, 2000), and thus methods of monitoring are usually contextualised to a specific ecosystem. Remote-sensing can provide data on harmful algal blooms by revealing several characteristic features surrounding bloom development and maintenance, such as large scale environmental changes, elevation of biomass to exceptionally high concentrations and, in some instances, information on assemblage structure such as organism size (Bernard et al., 2009; Kostadinov et al., 2010; Evers-King et al., 2014) or functional group probability (Stumpf et al., 2003). Information on changes in sea surface temperatures (SST) and retention or advection of water masses could indicate ecological windows that are known to be optimal conditions for the potential proliferation of certain blooms (Pitcher et al., 1998b; Sordo et al., 2001). Miller et al. (2006) were able to derive HAB likelihood indices based on spectral responses of different species; *Karenia mikimotoi*, *Chattonella verruculosa* and cyanobacteria. Their multivariate classification uses input data to 'train' the algorithm in combining distinct spectral responses and optimal environmental conditions.

In blooms that are dominated by a single species, proxies such as increases in Chl-*a* have been shown, in some cases, to be sufficient to detect harmful algal blooms. In the Gulf of Mexico, Sea-viewing Wide Field of View Sensor (SeaWiFS) data were used to detect *Karenia brevis* blooms (e.g. Stumpf et al., 2003) by detecting localised increases in Chl-*a* above running mean or median background levels. In instances where species do not dominate the biomass, detecting such HABs is only possible by monitoring conditions associated with their

proliferation, i.e. 'ecological associations' (Miller et al., 2006). Such is the case for instances of *Pseudo-nitzschia* spp., which occurs regularly in upwelling regions but comprises merely 10% of total chlorophyll (Stumpf and Tomlinson, 2005), Alternatively, the detection of certain pigments particular to harmful algal species can also be adopted. Cyanobacteria blooms were detected in the Baltic Sea using MERIS bands 6 and 8, by detecting the absorption features of phycocyanin, a pigment present primarily in cyanobacteria (Kutser et al., 2006).

In the southern Benguela, harmful algal blooms are often characterised by exceptionally high biomass, with Chl-*a* concentrations exceeding 30 mg m^{-3} (Pitcher and Weeks, 2006; Fawcett et al., 2007; Pitcher and Probyn, 2011). These high biomass waters, with ocean color signals dominated by the contribution of phytoplankton, provide good opportunity for the application of algorithms offering some assemblage descriptors. For example, the Equivalent Algal Population (EAP) algorithm (Bernard et al., 2009) was developed for the region, where a single metric (effective diameter) can be derived that represents the bulk optical signal of an entire assemblage, considering the assemblage as a single entity.

Effective diameter as a size proxy

Several simple descriptors of algal size or formulations for size distributions are employed to represent phytoplankton or particle size distributions. The most commonly used function is a power law function, the Junge distribution (Junge, 1963). Such a function is adequate for oligotrophic environments, which are characteristically dominated by small cell sizes (Chisholm, 1992) and follow the smooth, negative exponential of Junge-type representations. In eutrophic systems however, an alternative function is required that can account for complex shapes as the dominance of one or more size classes leads to bimodal or polydispersed distributions that deviate markedly from Junge distributions. Single parameters that adequately describe the combined or average optical properties of complex particle size distributions have been established and are used in the field of atmospheric physics (Hu and Stamnes, 1993; Alexandrov and Lacis, 2000). Similarly, several numerical models quantify phytoplankton assemblages by a single parameter, e.g. total biomass, mean trait or trait variance, and consider the assemblage as

a single entity (Wirtz and Eckhardt, 1996; Bruggeman and Kooijman, 2007; Merico et al., 2009; Acevedo-Trejos et al., 2015, 2016; Wirtz, 2013).

The EAP algorithm was locally contextualised to account for the high biomass that is prevalent in the southern Benguela, and offers two products to describe the assemblages from remote sensing. A singular descriptive variable output of the EAP algorithm, known as the effective diameter (D_{eff}), was tested in the southern Benguela, and has been shown to accurately represent the optical properties of typical particle size distributions (Bernard et al., 2007, 2009; Robertson Lain et al., 2014; Evers-King et al., 2014). Bernard et al. (2009) and Evers-King et al. (2014) assessed the impact that algal and non-algal particle size distributions had on absorption and scattering signals in the southern Benguela, where bimodal or polydispersed distributions are common. Owing to complexity in phytoplankton size distributions, defining the parameter to represent such diverse distributions is not without difficulties. When conducting size estimates of D_{eff}, greatest errors occurred when Chl-*a* was estimated incorrectly and/or at concentrations < 10 mg m^{-3}. However, overall, the results revealed that D_{eff} was able to give an indication of the broad size structure of the community, and would be useful in discriminating between large or small cell size dominance in certain bloom scenarios. Estimates of D_{eff} represent a good analogue to existing allometric trait-based approaches in that they offer either optical or physiological properties based on a simple size continuum. Great potential exists to use D_{eff} to study the synoptic variability and spatial scales offered by satellite remote sensing of phytoplankton blooms, harmful or not. To date no assessments have been made as to its biogeochemical relevance.

Application of D_{eff} to Harmful Algal Blooms

HABs are often associated with changes in the dominant size of algal assemblages (Bernard et al., 2006) and it is most often large dinoflagellate cells (>15 μm in diameter) that commonly form harmful blooms in the southern Benguela (Pitcher and Calder, 2000). D_{eff} was applied to an 11 year time series to assess synoptic variability and temporal trends in phytoplankton assemblages (Evers-King, 2014). Several key patterns in cell size distributions were confirmed

when using the D_{eff} output. General patterns in the dominance of large cells inshore and at frontal features, and dominance of small cells offshore have been observed (Crichton et al., 2013) and satellite constructions of effective diameter have confirmed this (Evers-King, 2014). Further, the MERIS time series and D_{eff} provided evidence for the coastal circulation patterns predicted by Pitcher and Nelson (2006), where an inshore poleward current and the accumulation of large cells inshore can be seen during downwelling conditions.

In this chapter, two case studies will be used to explore the usefulness of D_{eff} from a biogeochemical point of view. The first case study involves a bloom of *Myrionecta rubra* (previously known as *Mesodinium rubrum*), which is a large planktonic ciliate with a cell diameter up to 100 μm (including cilia), showing both heterotrophic and autotrophic behaviour (Hansen and Fenchel, 2006; Herfort et al., 2011). *Myrionecta rubra* causes non-toxic red tides globally (Lindholm, 1985; Crawford, 1989; Herfort et al., 2011 and references therein) and is often seen in very high biomass with exceptionally high productivity. The second case study involves a bloom of *Prorocentrum triestinum*, which is a common HAB dinoflagellate found in many parts of the globe (Labib, 1996; Ault, 2000; Douding and Goebel, 2001; Fawcett et al., 2007), with average cell length 15-22 μm and diameter 7-12 μm (Douding and Goebel, 2001). *Prorocentrum triestinum* has the highest measured division rates of its genus (Kim, 1986). The little that is known of the physiology of *P. triestinum* is derived from culture experiments and, to date, no description of its *in situ* nutrient utilisation has been published.

This chapter aims to describe the nitrogen utilisation in the two separate case studies in Lamberts Bay, South Africa, providing information on the biogeochemical conditions and nitrogen physiology during these harmful algal blooms. The environmental conditions will be described in relation to species composition and community size structure. The second aim is to estimate the effective diameter of the bloom organisms and assess how well the nitrogen dynamics are related to this size descriptive metric in the two HABs. If D_{eff} can be used to represent the bulk biogeochemical properties of an assemblage, it could potentially be used to quantify key biogeochemical features of the region at scales provided by the wealth that is the ocean color archive.

Methods

Sampling

Samples and measurements were taken in austral summer from a fixed station position (32° 05.020´S, 18° 16.010´E), 3.5 km offshore from Lamberts Bay, on the west coast of South Africa (Fig. 2.1). When bloom waters containing assemblages of interest had been advected away from the station, measurements and samples were taken at selected patches, within close proximity to the fixed station. Two study periods were selected, one of 15 days (25 February - 11 March 2004) and the other of 16 days (15 March - 6 April 2005). Only days with a complete set of variables (microscopy, Coulter Counter, temperature, uptake rates and nutrient concentrations) were used in the analysis. Daily vertical temperature and fluorescence profiles were obtained with a Sea-Bird Electronics Seacat CTD profiler. Samples for phytoplankton counts were collected in 200 mL bottles from the surface and 5 m depth and fixed in a final concentration of 2.5% buffered formalin for enumeration. For incubations and other measurements, water from the surface was collected in a 20 L black bucket, and a 5 L Niskin bottle was used to collect water at 5 m, which was decanted into a second black bucket. Incubations to measure nitrogen uptake for both surface and subsurface waters were simulated as *in situ* on land, where temperatures were controlled by a separate chiller unit for surface and subsurface samples, and light was simulated at 50%. Subsurface samples were predominantly taken from 5 m, but on two occasions samples were drawn respectively from 3.5 m and 10 m. Water was transported back ashore within 1 hour of collection for incubations, Coulter Counter analyses, nutrient analyses and Chl-*a* analyses.

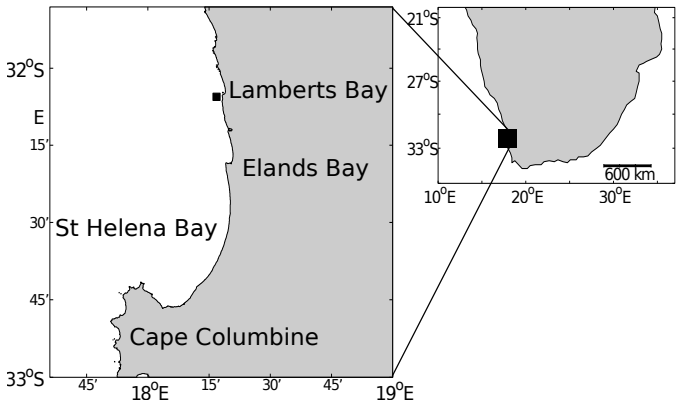

Figure 2.1: Sampling location (■) 3.5 km offshore from Lambert's Bay on the southern Namaqua Shelf.

Coulter Counter Analysis

The size spectra of samples were measured using a Beckman Multisizer 2 Coulter Counter. An aperture size of 140 μm was used, with a capacity to measure particles from 2-86 μm. Filtered seawater (using 0.2 μm Nucleopore) was used as a diluent in cases of high biomass where the aperture became blocked. Calibration of the aperture was carried out at the start of every sampling period using calibration beads with a modal size of 20 μm, as recommended by Beckman Coulter Counter. A discrete sample volume of 40 mL was used to count particles per size class and was blank corrected with 0.2 μm filtered seawater. Discrete particle size distributions (PSDs) represent the number of particles (N) per unit volume (cells L^{-1}) within each of the size classes, which were log-spaced equivalent spherical diameter (ESD) size bins. Total assemblage volume, V (μm^3), per size bin was calculated as:

$$V = N\frac{4}{3}\Pi r^3 \tag{2.1}$$

where cell radius (μm) is half the ESD and all cells are assumed spherical. Effective diameters (D_{eff}), the ratio of the third to second moment (ESD^3/ESD^2) or essentially the volume/surface area ratio of the distribution, were calculated to characterise the entire size distri-

bution of the assemblage by a single value (Bernard et al., 2007, 2009):

$$D_{eff} = \frac{\int_1^{bins} \frac{\pi}{6} ESD^3}{\int_1^{bins} \frac{\pi}{4} ESD^2} \tag{2.2}$$

Wind data

Hourly averages of wind speed and direction were obtained from Lamberts Bay Nortier station of the South African Weather Service, located 8.4 km north-east of the sampling station. Wind data were decomposed into north (u) and east (v) components and rotated 21.5° eastward. A lanczos high pass filter was applied and alongshore wind speeds were calculated, with positive values indicating equator-ward winds. Neutral wind stress (τ) was calculated according to Smith (1988), applying a running mean to a period of 12 hours and thus smoothing the data to reduce small scale variability:

$$\tau = \rho_{air} C_D U^2 \tag{2.3}$$

where ρ_{air} is the density of air, C_D is a dimensionless drag coefficient and U is the wind speed (m s^{-1}) at 10 m. Calculations were computed from scripts in the Woods Hole Air-Sea toolbox available at `http://woodshole.er.usgs.gov/operations/sea-mat/air_sea-html/`.

Community structure

Species were counted using inverted microscopy following the Utermöhl method (Utermöhl, 1958). Dominance within assemblages was considered by cell numbers (cells L^{-1}), where the dominant taxon (as used in the GLM analysis) is considered >40%. In the case of *Myrionecta rubra,* dominance was considered from 30% given its large cell size.

Primary production

Primary production was measured using the ^{14}C method (Parsons et al., 1984). At each depth sampled, three light samples and one dark sample were inoculated with 0.2 μmol 2uCi

$NaH^{14}CO_3$ and incubated *in situ* at their respective depths for 4 hours over midday. At the end of the incubation period, water samples were filtered onto Whatman GF/F filters, air-dried for 1.5 h and placed in scintillation vials to which 0.5 mL HCl was added to remove any remaining inorganic ^{14}C. Vials were shaken vigorously after the addition of scintillation fluor (Instagel) and stored in the dark. The activity of filters was assayed by liquid scintillation counting using a Beckman LS1800.

Nutrients

Manual determinations of all nutrients were carried out within 2 hours of collection and after filtration through a 47 mm Whatman GF/F filter. Nitrate was analysed according to the cadmium reduction method of Nydahl (1976), where flow rate is controlled by a peristaltic pump. Nitrite (NO_2^-), silicate (Si), phosphate (PO_4^{3-}), ammonium (NH_4^+) and urea were analysed in triplicate following Grasshoff (1983), scaled down to 5 mL samples. Urea was analysed using sulfuric acid reagent and a manganous chloride mixed reagent and placed in the oven for 3h at 75° C, following Koroleff (1983).

Chlorophyll-*a* (Chl-*a*)

For the determination of Chl-*a*, 100 mL samples were filtered onto 25 mm Whatman GF/F filters. Filters were placed in 10 mL centrifuge tubes with 9 mL of 90% acetone and stored in a freezer for pigment extraction. After 24 hours, samples were centrifuged at 200 rpm for 10 minutes prior to measuring flourescence of the supernatant using a Turner flourometer. The flourometer was regularly calibrated with available commercial Chl-*a* (Sigma Anacystis).

Uptake Incubations

Water from each depth was decanted into two 1 L Nalgene polycarbonate bottles and one 2 L Nalgene bottle. The 2 L bottle was inoculated with $^{15}NH_4Cl$, well mixed and split into two 1 L portions. Of this, 1 L was decanted into a polycarbonate bottle for ammonium uptake measurements (Fig. 2.2). The other 1 L bottles were inoculated with a stock solution of either

$^{15}NO_3^-$ or Urea ($CO(^{15}NH_2)_2$), with adjustments of the ^{15}N spike volume to equate to ~10% of the ambient nutrient concentrations. The volume of added stock solutions varied according to concentrations measured the previous days or, in the case of NO_3^-, on temperature. The three 1 L polycarbonate bottles (NO_3^-, NH_4^+ and Urea) were incubated for a period of 2-4 hours under natural light. The 1 L bottle spiked with $^{15}NH_4^+$ was filtered on a 47 mm ashed Whatman GF/F filter. A 900 mL sub-sample of the filtrate was frozen for later determination of the ^{15}N:^{14}N ratio for initial aqueous enrichment (R_0) of NH_4^+ by mass spectrometry. The remaining 1 L was used to determine the initial nutrient concentrations.

Incubations were terminated by filtration on 47 mm ashed GF/F filters, washed with artificial sea water and Milli-Q and then dried at 75 ℃ overnight. Sub-samples were punched out of each filter and wrapped in tin capsules for later determination of particulate ^{15}N:^{14}N by a Finnigan MAT mass spectrometer (Department of Archeometry, University of Cape Town). The filtrate was used for analysis (S_T) of ambient concentrations at the end of the incubation (T_t) for final aqueous enrichment (R_t).

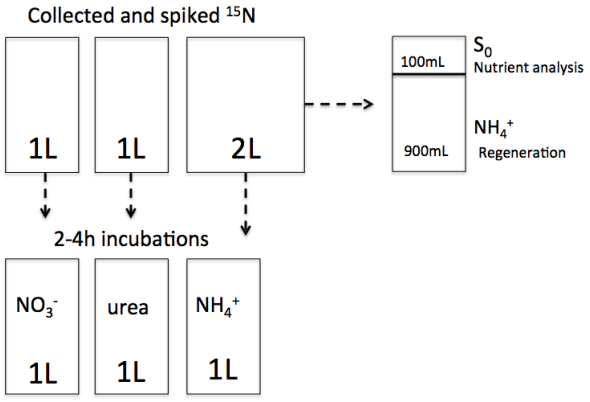

Figure 2.2: Simple schematic of the different bottles collected and deployed for *in situ* incubations. The 2 L bottle was spiked with $^{15}NH_4^+Cl$ and decanted into two 1 L bottles. One was frozen for later determination of final aqueous enrichment (R_t), and the 1 L other included in the *in situ* incubations.

Isotope dilution

A measured amount (0.9 μmol) of NH_4Cl carrier solution (10 μmol mL^{-1}) was added to the 900 mL of remaining NH_4^+ filtrate (Fig. 2.2), to ensure sufficient NH_4^+ concentrations for diffusion recovery and detection, prior to freezing. Within 1 month after the sampling period, the bottles were defrosted and a heaped spoon of magnesium oxide (MgO) was added to the thawed bottle to raise the pH to ∽9 so that NH_4^+ would be released in its gaseous form, NH_3. Based on Probyn (1987), halved precombusted 25 mm Whatmann GF/F filters were wetted with 0.1 mL of potassium hydrogen sulphate ($KHSO_4$) solution and suspended from the bottle lid to recover the diffused NH_3. The bottles were left for ± 2 weeks, after which time the filters were removed, dried overnight at 60℃ and packed into tin capsules for mass spectrophotometer ^{15}N:^{14}N determination. These values are given as r_0 and r_t, stipulated in equation 2.8 as r_x.

Calculations

All abbreviations and units for variables and parameters in the calculations are given in Table 2.1.

Uptake Rates The net transport rates (ρ) of nitrogen (μmolN L^{-1} h^{-1}) from the substrate into the cell were calculated as:

$$\rho = \nu * PN \tag{2.4}$$

where ν is the specific uptake rate (h^{-1}) and PN is the particulate nitrogen (μmolN L^{-1}). Biomass specific uptake rates (ν) of N were calculated as in Dugdale and Wilkerson (1986):

$$\nu =^{15} N_p/T * R \tag{2.5}$$

where $^{15}N_p$ is the particulate A% excess at T_t corrected for natural abundance (= $A\%E_{sample}$-$A\%E_{natural}$), T is the incubation time (h) and R is the aqueous Atom % (^{15}N/total $^{15+14}N$) ratio. The calculation of *R* for NH_4^+ is markedly different from that of NO_3^- and urea, owing to significant

regeneration of NH_4^+ during the incubation period. *R* for NO_3^- and urea corrects for the natural abundance of $^{15}N_{natural}$ (0.3663%) as well as the purity of the supplier's assay of ^{15}N stock standard (*spike)*:

$$R = \frac{(spike * 99.6 + S_0 *^{15} N_{\%natural})}{(spike * S_0)} \tag{2.6}$$

For νNH_4, *R* was calculated using Glibert et al. (1982), with the notation R_G, assuming an exponential decrease in *R* over the time course:

$$R_G = (R_0/ln(R_0/R_T)) * (1 - (R_T/R_0)) \tag{2.7}$$

R_0 and R_T were the calculated atom % and give the ratio of ^{15}N to $^{15+14}N$ in aqueous phase after spiking at the start and end of the incubation respectively. R_0 and R_T, hereafter each denoted in equations for the sake of simplicity as R_x, were calculated using aqueous measurements of ^{15}N, as follows:

$$R_x = \frac{(0.9 * S_x + 9) * r_x - 9 *^{14} N_{\%nat.abundance}}{(0.9 * S_x)} \tag{2.8}$$

where r_x is the atom% of $^{15}NH_4^+$, measured by diffusion from the aqueous phase. In the calculation of uptake rates, aqueous enrichments (A%) were corrected for natural abundance of 0.3663 (A%E). It can be expected that the relative standard deviation for these measurements of nitrogen uptake rates is ca. 10%, given what has been found in previous experiments (Gandhi et al., 2010; Cavagna et al., 2011) of similar atom % enrichments. For urea uptake the standard deviation is expected to be slightly higher, as seen in Bronk and Glibert (1993).

Table 2.1: List of variables and parameters used in the text and for uptake calculations

T	Incubation duration	
S_0	measured nitrogen concentration at start of incubation	$\mu molL^{-1}$
S_T	measured nitrogen concentration at end of incubation	$\mu molL^{-1}$
R	^{15}N:$^{15+14}$N in aqueous phase	atom % excess
R_G	^{15}N:$^{15+14}$N in aqueous phase from Glibert (1982) calculation	atom % excess
R_0	^{15}N:$^{15+14}$N in aqueous phase at start of incubation	atom % excess
R_t	^{15}N:$^{15+14}$N in aqueous phase at end of incubation	atom % excess
R_x	Used in equation to denote either R_0 or R_t	atom % excess
^{15}Np	Particulate ^{15}N	atom %
ν	Biomass specific uptake rate	h^{-1}
ρ	Net transport rate	$\mu molL^{-1}h^{-1}$
r_0	measured regenerated aqueous^{15}N:$^{15+14}$N at start of experiment	atom % excess
r_T	measured regenerated aqueous^{15}N:$^{15+14}$N at end of experiment	atom % excess
r_x	Used in equation to denote either r_0 or r_t	atom % excess
spike	purity of the suppliers assay of ^{15}N stock standard	$\mu molL^{-1}$

Data Analysis

In order to quantify the influence of the different variables on the uptake rates, several general linear models (GLM) were explored, assuming a Gaussian error distribution.

$$vN\,(h^{-1}) = \beta_0 + \beta_1\, total\, N\,(\mu mol\, L^{-1}) + \beta_2\, D_{eff}\,(\mu m) + \alpha_{taxon} + \varepsilon \tag{2.9}$$

where β_0 is the intercept, β_1 is the coefficient for total nitrogen, β_2 is the coefficient for the effective diameter (μm), α_{taxon} is a vector of parameters describing the influence of each phytoplankton group (diatoms, dinoflagellates, *Myrionecta rubra*, *Prorocentrum triestinum*, mixed) and ϵ represents the residual error. Groups in this instance are categorised by percentage in cells per litre, where >40% dominance of a specific group in an assemblage. *Myrionecta rubra* is an exception, where dominance (cells L^{-1}) lies between 32-63%. Where no clear dominance was found the assemblage was considered mixed. The same GLM model was used for the uptake of total N, NO_3^-, NH_4^+ and urea. Mass specific uptake rates were used in the analysis to reduce the potential bias associated with the high biomass accounted for in absolute uptake rates. Further analyses were carried out for each nitrogen source to assess which groups were

taking up which nitrogen source at what rate, by comparing the least squares mean uptake rate per group after statistically removing the effect of cell size and ambient nutrient concentration. Vector parameters for the community structure are divided into five taxonomic groups, where the relative sizes of the values indicate which taxa have low or high uptake rates.

Results

Wind patterns in both case studies in 2004 and 2005 were dominated by upwelling-favourable, southerly winds, with sustained periods of wind relaxation and reversal. Cumulative net wind transport was much higher in 2004, i.e. winds were stronger (Fig. 2.3) than 2005 (Fig. *2.7*). On average, particulate nitrogen, Chl-*a* and primary productivity were higher in 2005 than 2004. Average effective diameters were greater and *f*-ratios higher for the entire assemblage during 2004 than 2005 (Table 2.2). *Myrionecta rubra* dominated in 2004 in association with *Skeletonema* spp. and *Prorocentrum triestinum* dominated in 2005.

Table 2.2: Summary data from the fixed station in 2004 and 2005 at Lamberts Bay: Nutrient concentrations (NH_4^+, NO_3^-, urea, NO_2^-); Chlorophyll-*a* (Chl-*a*), particulate nitrogen (PN); *f*-ratio and primary productivity (PP), effective diameter of the entire assemblage (D_{eff}) and dominant species (%). * indicates a patch away from the station. ** indicates a sample where *Syracosphaera pulchra* (49%) is in high coexistence with *Prorocentrum triestinum* (46%). % dominance by numbers of cells.

date	NH_4^+	NO_3^-	Urea	Chl-*a*	PN	*f*-ratio	PP	D_{eff}	Dominant Species	
	(μmol N L^{-1})	(μmol N L^{-1})	(μmol N L^{-1})	(mg m^{-3})	(μmol L^{-1})		(mgC m^{-3}h^{-1})	(μm)		(%)
29/02/2004	0.10	1.27	0.15	17.96	42.75	0.61	63.30	31.54	*M. rubra*	63
01/03/2004	0.80	20.41	0.66	3.55	6.52	0.50	17.29	15.55	mixed	-
02/03/2004	1.04	22.95	0.47	3.09	4.06	0.64	17.59	12.79	mixed	-
03/03/2004	0.66	22.05	4.39	6.85	7.82	0.40	31.95	17.09	*Skeletonema* spp.	55
07/03/2004	0.19	20.46	0.57	10.29	9.19	0.81	86.17	15.02	*Skeletonema* spp.	58
27/02/2004*	0.42	0.10	0.31	13.49	16.67	0.09	66.05	15.33	Mixed	32
08/03/2004*	0.17	0.72	0.25	58.17	34.44	0.59	291.58	22.22	Mixed	-
09/03/2004*	0.10	5.59	0.35	54.51	26.04	0.82	152.59	23.54	Mixed	-
10/03/2004*	0.08	0.61	0.93	149.07	104.09	0.56	303.26	29.61	*M. rubra*	34
11/03/2004*	0.55	23.60	0.90	39.79	18.54	0.75	67.45	27.63	*M. rubra*	46
Mean	**0.41**	**13.29**	**1.57**	**32.10**	**25.34**	**0.58**	**122.87**	**21.03**		
SD	**0.34**	**10.36**	**1.44**	**41.22**	**27.24**	**0.17**	**142.28**	**6.81**		
16/03/2005	0.50	0.11	2.64	46.47	53.49	0.04	169.89	13.05	*P. triestinum*	64
17/03/2005	0.50	0.05	0.91	13.99	24.35	0.04	137.79	14.83	mixed	-
18/03/2005	0.19	0.13	2.63	11.04	21.65	0.07	79.28	13.34	*P. triestinum*	56
21/03/2005	0.31	0.18	1.47	14.70	27.93	0.10	118.57	15.94	*S. pulchra***	49
24/03/2005	0.00	0.02	0.52	42.97	42.34	0.07	125.46	13.14	*P. triestinum*	82
29/03/2005	0.03	0.06	0.25	163.69	129.37	0.15	339.87	14.27	*P. triestinum*	98
30/03/2005	0.13	0.23	1.19	172.45	122.49	0.16	234.84	14.90	*P. triestinum*	98
31/03/2005	0.08	0.06	0.54	184.15	109.57	0.10	154.74	14.67	*P. triestinum*	90
01/04/2005	0.33	1.15	0.99	201.68	146.69	0.36	175.76	16.33	*P. triestinum*	88
02/04/2005	3.35	20.34	1.60	9.64	17.41	0.48	4.97	29.42	*Protoperidinium* spp.	46
03/04/2005	0.35	22.86	1.33	21.92	45.91	0.62	13.55	29.78	*Protoperidinium* spp.	50
05/04/2005	0.54	0.57	0.99	39.61	49.85	0.30	23.16	31.86	*C. furca*	33
Mean	**0.53**	**3.81**	**1.26**	**76.86**	**65.92**	**0.21**	**131.49**	**18.46**		
SD	**0.91**	**8.33**	**0.76**	**77.99**	**47.20**	**0.19**	**96.63**	**7.26**		

Case Study 1: *Myrionecta rubra*

Environmental conditions A period of relaxed northerly winds was observed from 10 February until 24 February (Fig. 2.3). At the start of the study (25 February), the winds reverted to predominately upwelling-favourable, and remained so for the rest of the study, with the exception of a two day relaxation period, which occurred on 6 March (Fig. 2.3). Diurnal variability was evident in a shift between light northerly winds in the morning and southerly winds in the afternoon. Cumulative winds show a net equator-ward direction, indicating upwelling-favourable conditions. Temperatures at the start of the study were up to 17℃ and strong stratification was observed in the upper 5 m (Fig. 2.4a), reflecting the prior relaxation in upwelling-favourable winds. With the increase in wind stress from 27 February (shown by the greater distance between black points indicated in Figure 2.3), temperatures gradually cooled until the entire water column was well mixed from 1 March onwards, and surface temperatures were around 11℃ for the remainder of the study (Fig. 2.4a) .

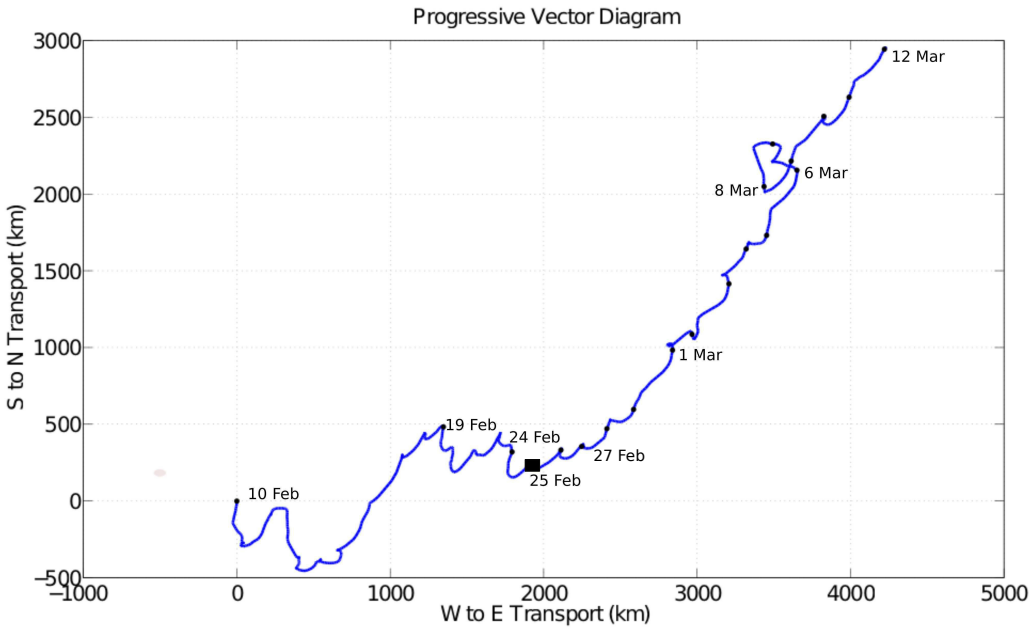

Figure 2.3: Progressive wind plot from Nortier Weather Station at Lamberts Bay. Data starts from 10 February and sampling period starts 25 February. Black dots for the start of each day are placed at 24:00 hrs from the previous day. ▮ indicates the start of the sampling period. Data provided by Weather SA.

Myrionecta rubra peaked in abundance at 1 x 10^6 cells L^{-1} on 29 February (Fig. 2.4). At the

onset of upwelling conditions, temperatures cooled and a diatom *Skeletonema* spp. gradually increased in numbers, with concentrations as high as 3 x 10^6 cells L^{-1}. Highest Chl-*a* was observed below the thermocline (Fig. 2.4b) at 5 m, where there were low counts of all species at the surface between 25 February-7 March (Fig. 2.4b and c). *Myrionecta rubra* numbers were low at the sampling station, but patches sampled away from the station showed a strong *M. rubra* presence (Table 2.2). Maximum biomass was observed during *M. rubra* dominance ($\sim$46%), measured by PN (104 μmolN L^{-1}) and Chl-*a* concentration (149 mg m^{-3}), and was associated with primary productivity values of 303 mgC m^{-3} h^{-1}. There was high variability in NO_3^- concentrations and a large range in biomass (PN) as well as Chl-*a* concentrations during *M. rubra* dominance.

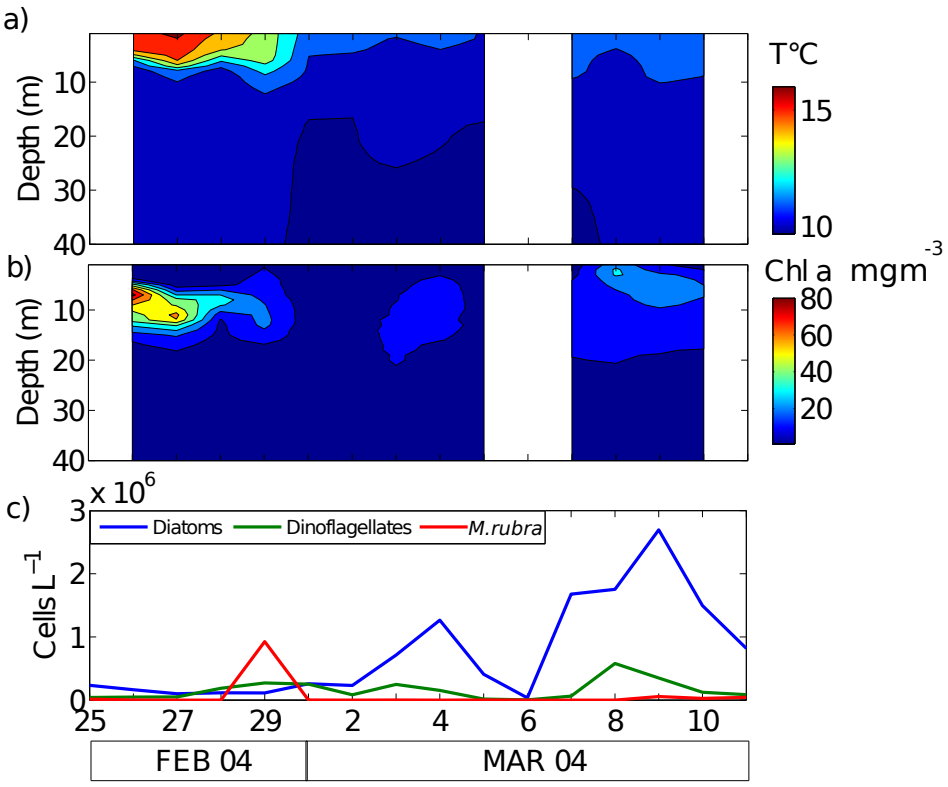

Figure 2.4: Time series from 25 February to 11 March 2004 at Lamberts Bay showing CTD-derived a) temperature, b) Chl-*a* and c) microscopy counts of phytoplankton cells at 0m. White bands indicate missing data. Data from Pitcher and Probyn.

Nitrogen uptake NO_3^- concentrations were initially low (<5 μmolN L^{-1}) (Fig 2.5a,d) but, with the onset of upwelling-favourable winds from 27 February (Fig. 2.3), concentrations of

NO_3^- increased (±20 μmolN L^{-1}) (Fig. 2.5a,d), reflecting a period of active upwelling. ρNH_4^+ was relatively consistent throughout the sample period (0.067 ±0.03 μmolN L^{-1} h^{-1}). As NO_3^- concentrations increased, the persistence of 11°C waters at the surface was maintained (Fig. 2.4) and NO_3^- uptake rates steadily increased and reached a maximum of 0.35 μmolN L^{-1} h^{-1} in association with the diatom *Skeletonema* spp. Average % dominance (by cell numbers) for *M. rubra* was 46% (Table 2.2). When *M. rubra* contributed most to total biomass (as illustrated by largest effective diameters and high cell counts), ρNO_3^- was relatively high (maximum of 0.30 μmolN L^{-1} h^{-1} and maximum *f*-ratio=0.74) but never exceeded the rates observed when *Skeletonema* spp. dominated total cell counts. At selected patches away from station 3, ρNO_3^- reached a maximum (0.55 μmolN L^{-1} h^{-1}) (Fig. 2.6b). Although *M. rubra* were not as numerous (cells L^{-1}) as the diatom/dinoflagellate species (Fig. 2.6c), their large cell diameters (±30 μm) indicates their disproportionate dominance of the assemblage biomass and nitrogen uptake signal.

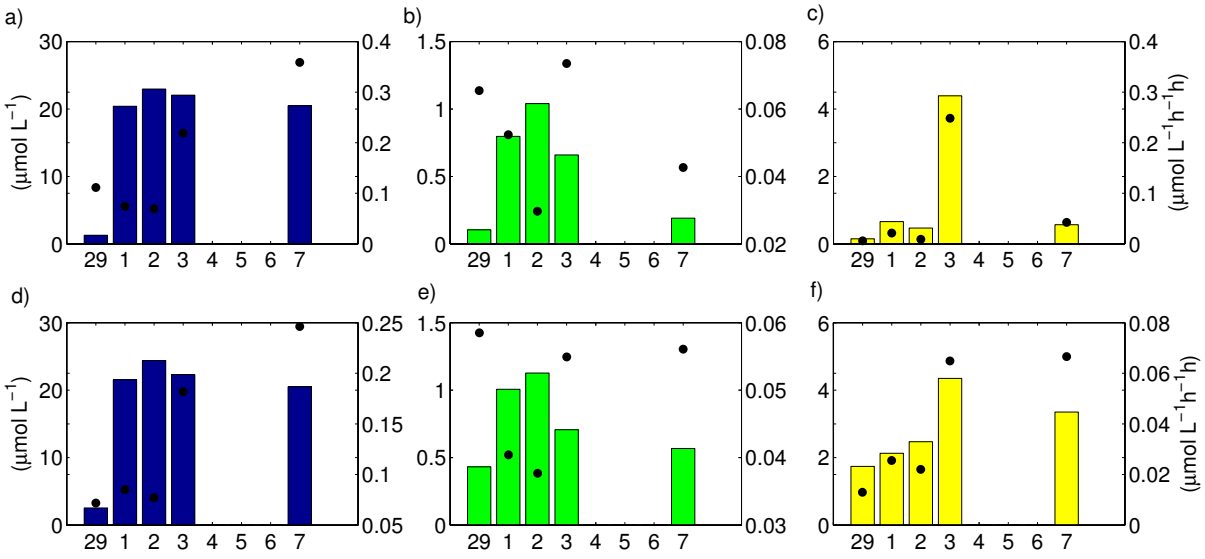

Figure 2.5: Time series of the nitrogen dynamics at Lamberts Bay station for the sample period between 29 February to 7 March 2004. Left axis, nutrient concentrations (μmol N L^{-1}) of NO_3^- (blue bars), NH_4^+ (green bars) and urea (yellow bars) and right axis, uptake rates (μmol N L^{-1} h^{-1}) (black dots) at a-c) 0 m and d-f) 5 m. Data from Probyn.

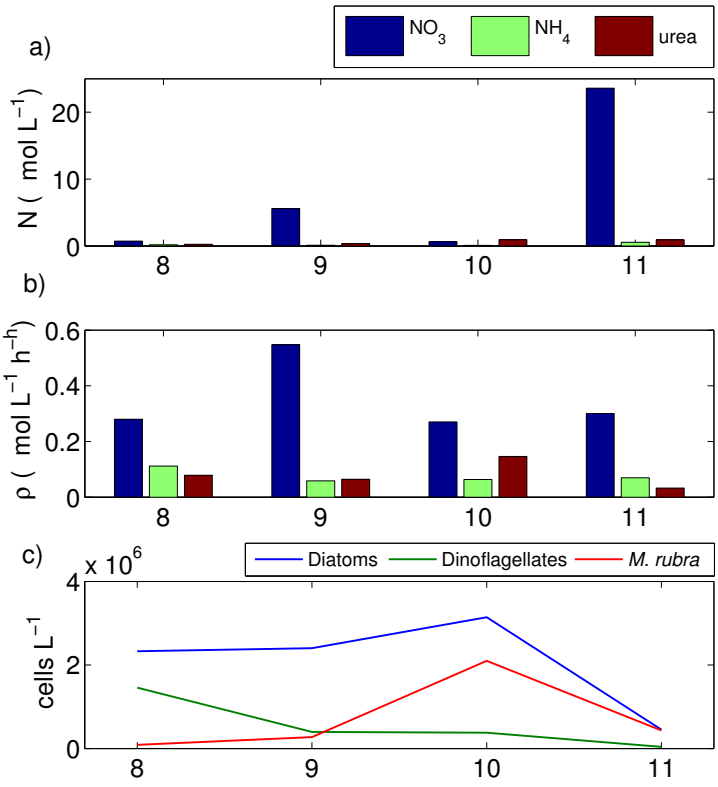

Figure 2.6: Nitrogen dynamics in Lamberts Bay, 8-11 March 2004, at high biomass patches away from station 3. a) N concentrations, b) absolute uptake rates of nitrogen and c) dominant community structure. Data from Pitcher and Probyn.

Case Study 2: *Prorocentrum triestinum*

Environmental conditions The 2005 study, starting 15 March, was preceded by predominately southerly, upwelling-favourable winds (Fig. 2.7). From 15-20 March, the wind reversed to north-westerly before southerly winds recommenced. Two further relaxation events occurred from 26-27 March and 4-6 April. Surface temperatures remained at 16°C from 15-24 March, with warm waters extending as deep as 20 m on 19 March (Fig. 2.8b). The thermocline shallowed after 24 March, with surface expression of cold waters of 11°C from 1 April onwards. The relaxation event of 4 April was reflected in the 1°C temperature increase in surface waters.

The community showed an initial dominance of diatoms (*Chaetoceros* spp.) followed by high dinoflagellate numbers (*Prorocentrum triestinum*) from 29 March until 2 April (Fig. 2.8c). Cell counts were comparatively low (ranging between 2.2 - 9 x 10^6 cells L^{-1}) between 16-23 March,

after which counts gradually increased and the assemblage was dominated by *Prorocentrum triestinum*, reaching a maximum of 34 x 10^6 cells L^{-1} on 30 March. *Prorocentrum triestinum* dominated the assemblage from 29 March - 1 April (Table 2.2), comprising as much as 88-98% (% contribution by cells L^{-1}). Maximum rate of primary productivity during this time was 339 mgC m^{-3} h^{-1} and was seen in association with highest particulate nitrogen (146.69 μmol L^{-1}). As the water column became more mixed from 2 April, cell numbers were dominated by a dinoflagellate *Ceratium furca*, peaking in dominance on 5-6 April.

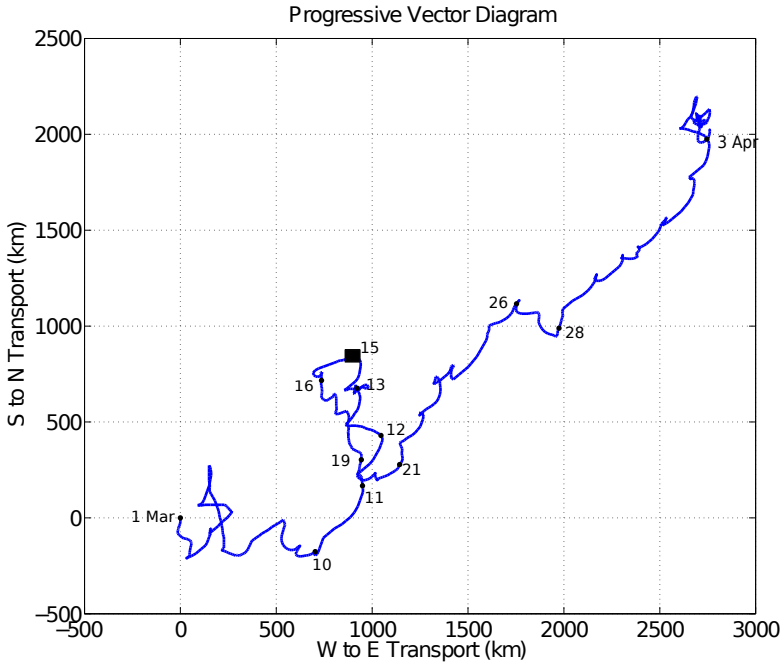

Figure 2.7: Progressive wind plot from Nortier Weather Station at Lamberts Bay in 2005. Data starts from 1 March and sampling period starts 15 March 2005. Black markers thereafter indicate the start of each day. Note the difference in axes values compared to the progressive wind plot for 2004, with net transport much reduced during the 2005 sample period. ▉ indicates start of sampling period. Data provided by Weather SA.

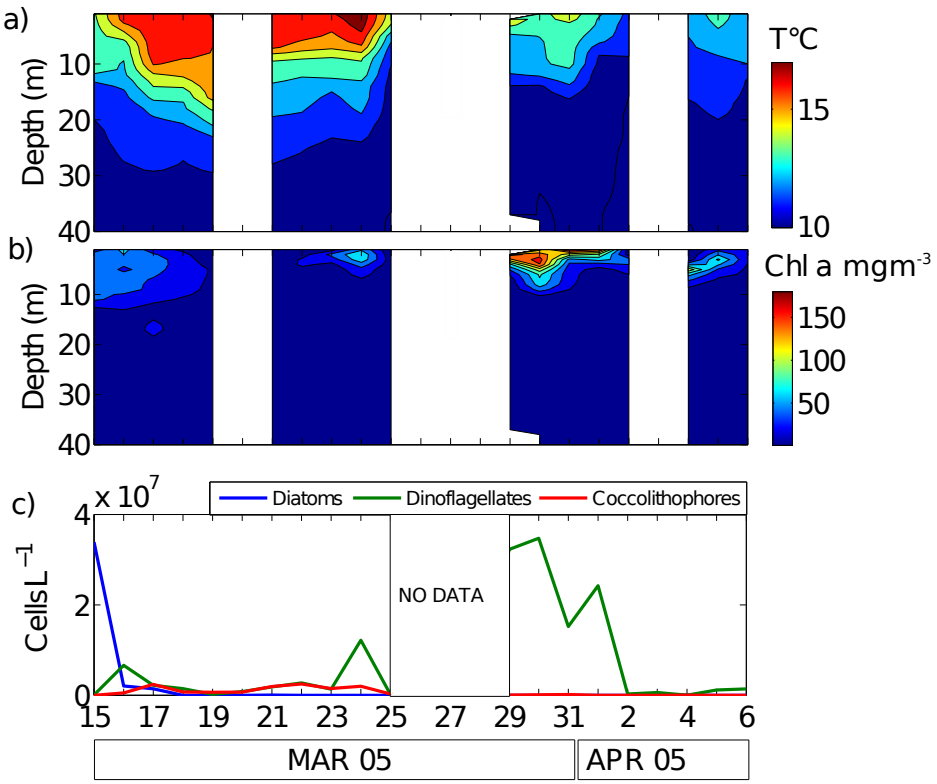

Figure 2.8: Time series from 15 March to 6 April 2005 at Lamberts Bay showing CTD-derived a) temperature, b) Chl-a and c) microscopy counts of phytoplankton cells at 0 m. White bands indicate days when data were not collected or are missing. Data from Pitcher and Probyn.

Nitrogen uptake Initially, urea concentrations were highest of all nitrogen species, with a maximum of 2.6 μmol N L^{-1} on 16 March (Fig. 2.9c,f). The stratified water column and nutrient-depleted conditions were reflected in the uptake rates, with surface uptake rates of urea and NH_4^+ ranging between 0.1 and 0.4 μmol N L^{-1} h^{-1} and NO_3^- being relatively low. Highest uptake rates during *P. triestinum* dominance were those of urea, suggesting it was an important source of nitrogen during stratified conditions.

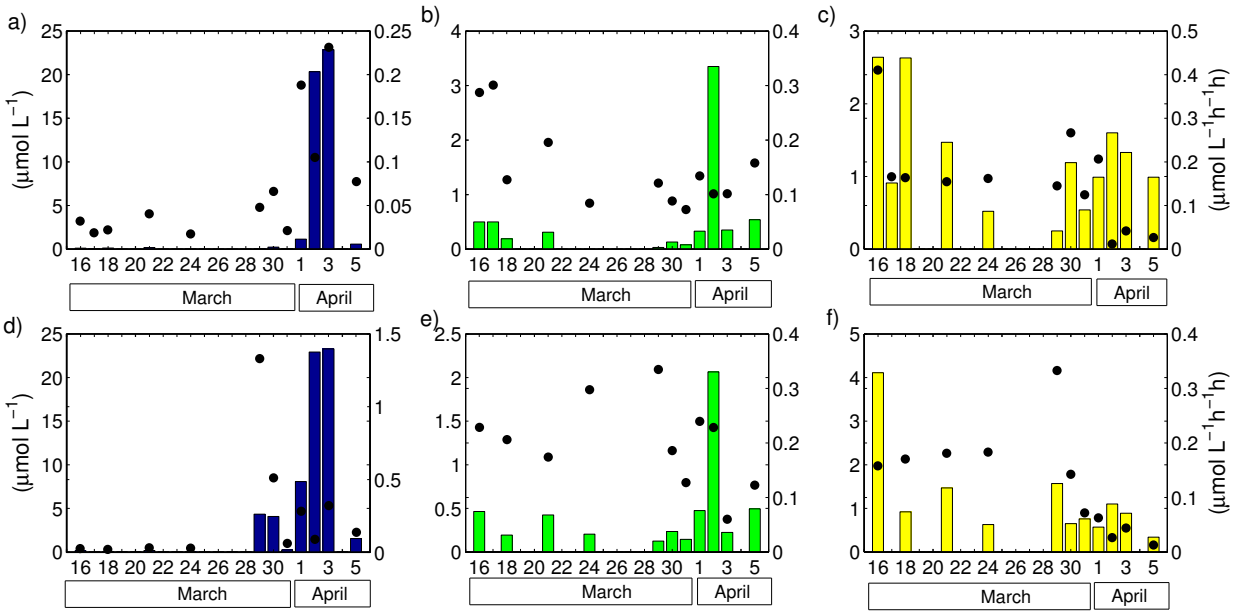

Figure 2.9: Summary of nutrient dynamics at Lamberts Bay station for 2005 between 16 March and 5 April. Left axis, nutrient concentrations (µmol N L^{-1}) of NO_3^- (blue bars), NH_4^+ (green bars) and urea (yellow bars) and right axis, uptake rates (µmol N L^{-1} h^{-1}) (black dots) at a-c) 0 m and d-f) 5 m. Data from Probyn.

Nitrogen resource partitioning A GLM was used to assess how much of the variability in mass specific uptake rates could be explained by different predictive variables, in order to assess whether *M. rubra* and *P. triestinum* displayed any particular strategy for nitrogen utilisation. The GLM model for nitrogen uptake that best matched the data incorporated the effects of ambient nitrogen concentration (total nitrogen, NO_3^-, NH_4^+ or urea), cell size and taxa (diatoms, dinoflagellates, *M. rubra*, *P. triestinum* and mixed) (Fig. 2.10). Ambient nutrient concentration and taxa had significant influences on the uptake of total N and NO_3^-, and the influence of cell size was significant only for NH_4^+ (Table 2.3). When removing the effects of total N concentration and size from the predicted values (Fig. 2.11), the least squares mean uptake rates of each group indicated that uptake rates by diatoms on a whole were faster for all nitrogen species. Statistically, *P. triestinum* was not dissimilar to dinoflagellates as a whole group, and *M.rubra* took up total nitrogen relatively fast but not as fast as diatoms.

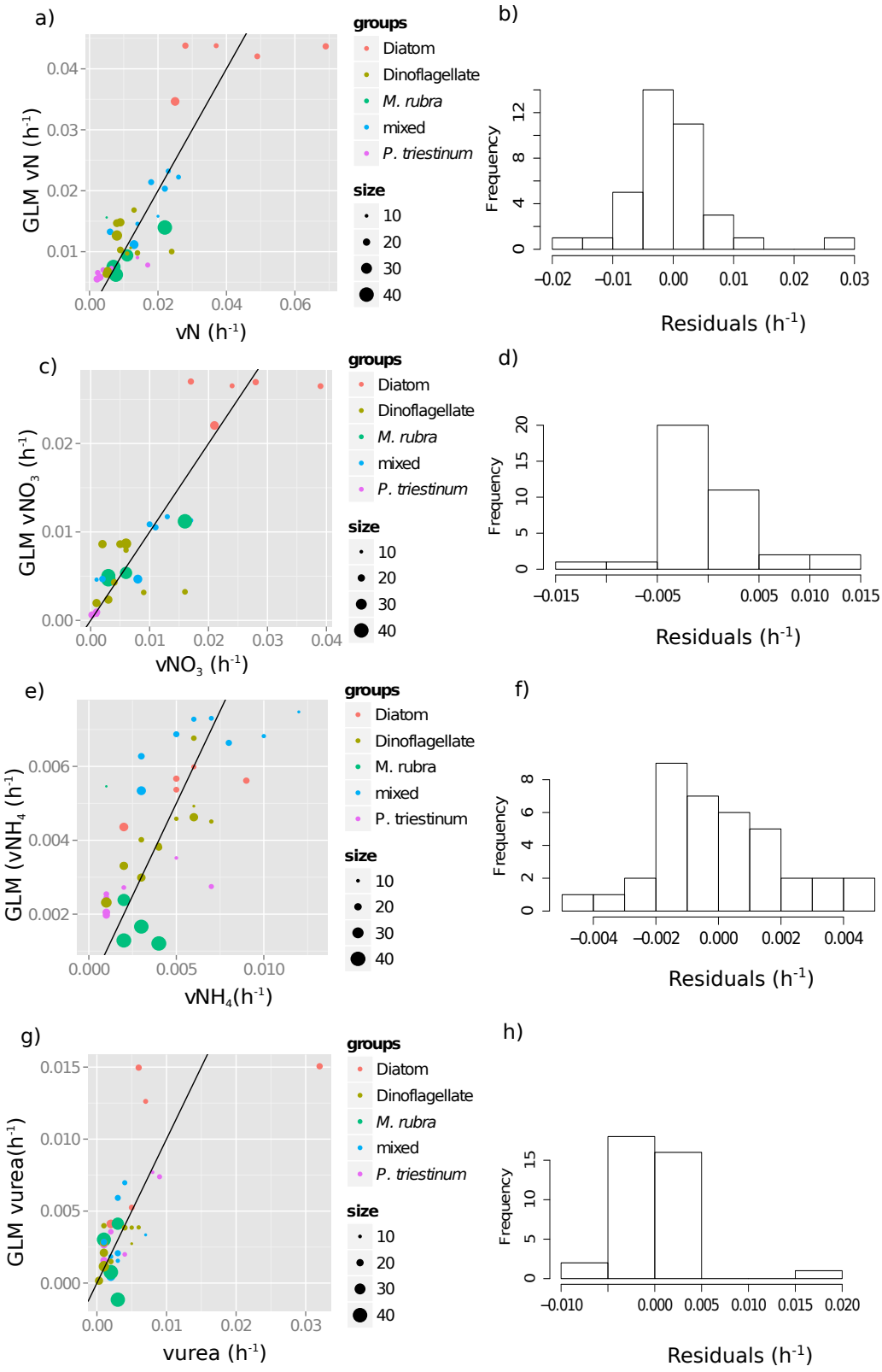

Figure 2.10: Results of the GLM. Comparison between observed *in situ* and predicted values of the different nitrogen components (a,c,e,g) and the distribution of model residuals indicating normality (b, d, f, h). Size represents the effective diameter (D_{eff}) in μm and are estimates of the dominant size class following equation 2.2. Dominant groups are defined by >40% dominance of a specific group in an assemblage. *Myrionecta rubra* is an exception where dominance (cells L^{-1}) lies between 32-63%. Where no clear dominance was found the assemblage was considered mixed.

Table 2.3: Summary statistics of the GLM for the uptake of each nitrogen source (following equation 2.9), with N corresponding to either total nitrogen, NO_3^-, NH_4^+, urea. DF= 36 * indicates significance (critical value=0.05)

Parameter	Coefficient	SE	t	p
Total N	**r^2 = 0.67**	**AIC=-239.74**		
β_0	0.0393	0.0055	7.115	6.5 x10^{-8} *
β_1 total N	0.0003	0.0001	2.353	0.02 *
β_2 size	-0.0003	0.0002	-1.365	0.18
αDino	-0.0269	0.0045	-6.014	1.3 x10^{-6} *
α*M. rubra*	-0.0224	0.0063	-3.552	0.001 *
αmixed	-0.0217	0.0047	-4.656	1.0 x10^{-5} *
α*P. triestinum*	-0.0286	0.0054	-5.295	2.1 x 10^{-6} *
NO_3^-	**r^2 = 0.70**	**AIC=-275.98**		
β_0	0.0206	0.0032	6.52	3.33 x10^{-8} *
β_1 NO_3^-	0.0003	-0.0001	3.18	0.003 *
β_2 size	0.0000	0.0001	-0.08	0.94
αDino	-0.0185	0.0026	-7.07	7.3 x10^{-8} *
α*M. rubra*	-0.0159	0.0037	-4.30	3.1 x10^{-8} *
αmixed	-0.0170	0.0027	-5.85	2.11x10^{-6} *
α*P. triestinum*	-0.0198	0.0032	-6.27	6.5 x10^{-7} *
NH_4^+	**r^2 = 0.75**	**AIC=-338.09**		
β_0	0.007	0.001	5.07	1.9 x10^{-5} *
β_1 NH_4^+	0.001	0.001	1.38	0.18
β_2 size	0.000	0.000	-2.24	0.03 *
αDino	-0.002	0.001	-1.27	0.22
α*M. rubra*	-0.001	0.002	-0.64	0.53
αmixed	0.001	0.001	0.67	0.51
α*P. triestinum*	-0.003	0.003	-2.21	0.03 *
Urea	**r^2 = 0.75**	**AIC=-292.22**		
β_0	0.0049	0.0035	1.41	0.17
β_1 urea	0.0026	0.0008	3.45	0.001 *
β_2 size	-0.0001	0.0001	-0.67	0.51
αDino	-0.0040	0.0025	-1.62	0.12
α*M. rubra*	-0.0036	0.0031	-1.16	0.25
αmixed	-0.0033	0.0027	-1.26	0.22
α*P. triestinum*	-0.0034	0.0026	-1.27	0.21

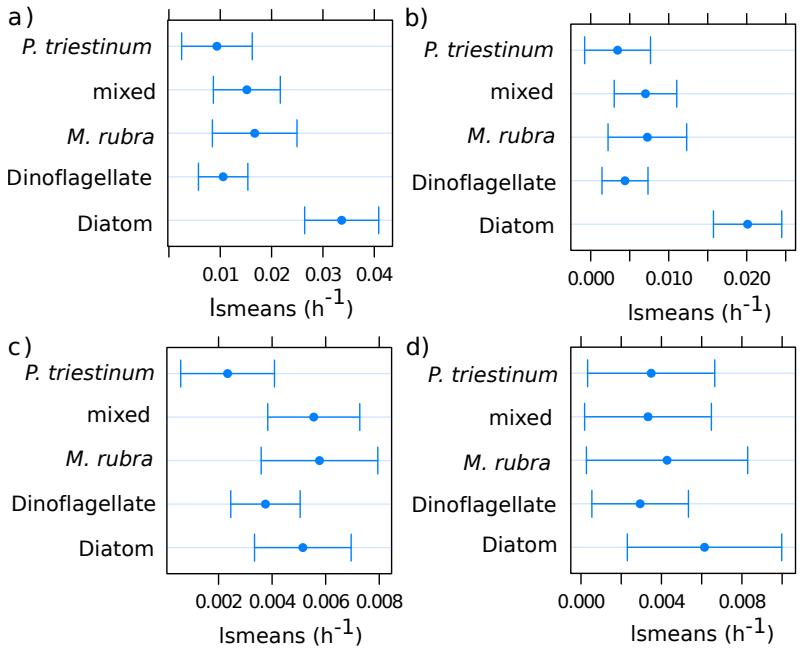

Figure 2.11: Comparison of least square means (lsmean) of the uptake rates of the different nitrogen sources by different phytoplankton groups, a) total N b) NO_3^-, c) NH_4^+, and d) urea. These values represent uptake rates after removing the effects of size and ambient nutrient concentration.

Effective diameter as a size proxy Measured mass-specific uptake rates (h^{-1}) and calculated effective diameters were combined for 2004 and 2005. A significant negative relationship existed between D_{eff} and the uptake of regenerated forms of N (Fig. 2.12b,c) but not for NO_3^- (Fig. 2.12a). Highest NO_3^- mass-specific uptake rates were by diatoms. Largest cell sizes were when *M. rubra* dominated total biomass. A large range in vNH_4^+ was observed when the assemblage was dominated by *P. triestinum,* which was also associated with high uptake rates of urea.

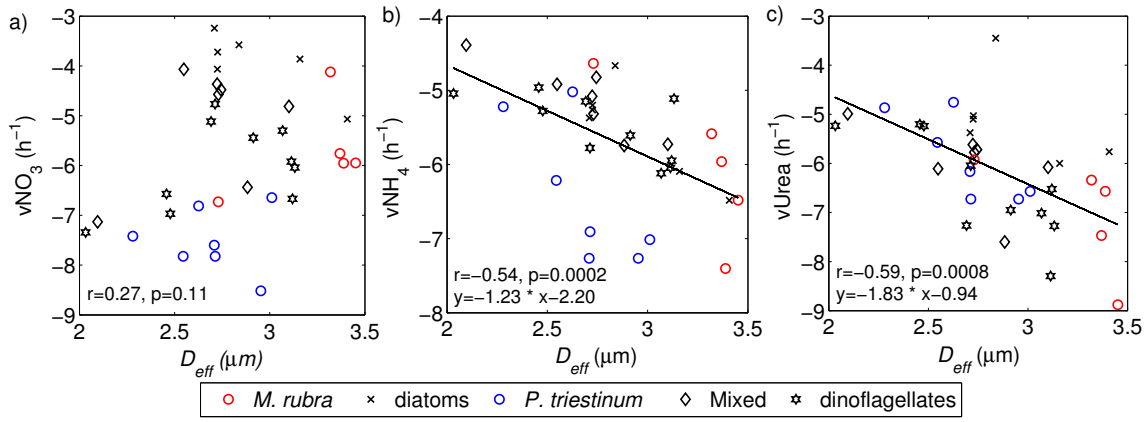

Figure 2.12: Log-log relationships between mass-specific transport rate (v) and D_{eff}, of a) NO_3^- b) NH_4^+ and c) Urea (h^{-1}) with colours representing >40% dominance of a specific group in an assemblage. *Myrionecta rubra* is an exception where dominance (cells L^{-1}) lies between 32-63%. Where no clear dominance was found the assemblage was considered mixed.

Samples dominated by small-celled phytoplankton (<20 µm) corresponded to warmest observed temperatures and low *f*-ratios (Fig. 2.13). Assemblages characterised by a large D_{eff} (>20 µm) were not observed in water warmer than 14°C. D_{eff} and *f*-ratios were variable between 10 and 14°C. Assemblages with *P. triestinum* dominance were characterised by D_{eff} between 6-28 µm, within a temperature range of 13-18°C, with maximum *f*-ratios of 0.36. Assemblages with *M. rubra* dominance had large D_{eff} (28-40 µm) with *f*-ratios as high as 0.74. *M. rubra* were mainly found in cool waters, associated with high *f*-ratios (0.74-0.1), and *P. triestinum* were found in warm waters and with low *f*-ratios. Independently, temperature and *f*-ratio have a strong negative correlation (r= -0.66, p=0.008), and D_{eff} and *f*-ratio are positively correlated (r= 0.46, p=0.008).

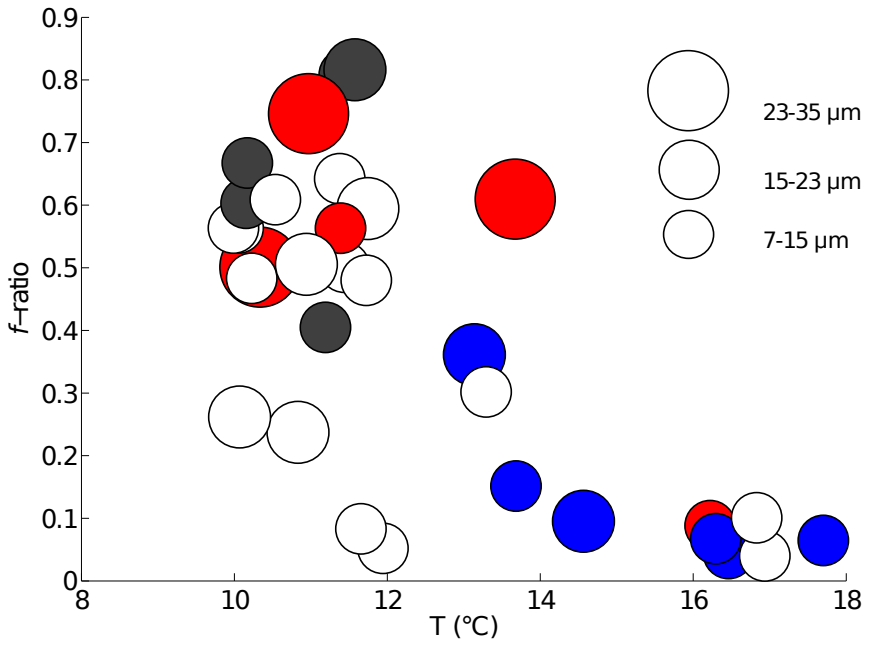

Figure 2.13: The relationship between effective diameter (D_{eff}), *f*-ratio and temperature for all data collected in 2004 and 2005 from 0 m and 5 m. The size of the data point is proportional to the D_{eff} of the assemblage (normalised to the mean D_{eff} for proportionate plotting) , categorised into three size bins: 7-15 µm, 15-23 µm and 23-35 µm. The shading corresponds as follows: Red - *M. rubra*; blue- *P. triestinum*; Black - Diatoms; White - mixed.

Discussion

The nitrogen dynamics of two case studies were explored in relation to environmental variables and community structure. The two separate case studies are of particular interest due to the proliferation of two harmful algal species to exceptionally high biomass. In 2004, a ciliate, *Myrionecta rubra,* a large cell (±30 µm diameter), displayed high *f*-ratios when NO_3^- was available and was present along the entire temperature range of the upwelling/downwelling cycle, between 10-17°C. *Prorocentrum triestinum*, a dinoflagellate with an observed average D_{eff} of 14 µm, displayed higher uptake rates of regenerated forms of nitrogen. Aside from the varying conditions and influences on the nitrogen utilisation by the different assemblages, these assessments reveal the diversity of strategies employed by harmful algal species. These data also provide a suitable platform for testing how well the single size proxy, D_{eff}, could represent

the principal nitrogen signals observed during these two separate blooms. Such a metric is the output of an algorithm (applied to MODIS sensor data) that was developed to provide a relevant indication of the potential of harmful algal blooms in the region, which are characteristically large celled, high biomass blooms.

Characteristic features of the case studies

Ecological windows Wind patterns for both 2004 and 2005 were typical of southern Benguela summer months, with upwelling-favourable winds dominating. Both 2004 and 2005 study periods were preceded by relaxed winds, and warm, nutrient-deplete surface waters. These periods of sustained wind relaxation (between 2-5 days), characteristic of late summer (March-April), are considered to be an optimal window for HAB development in the southern Benguela (Pitcher and Nelson, 2006; Fawcett et al., 2007). Wind and wind-driven processes influencing phytoplankton species composition (Margalef et al., 1979), bloom retention and advection Pitcher and Weeks (2006) are key determinants in the presence and proliferation of HABs. Shifts between pulses of upwelling-favourable winds and relaxation are well established patterns in the succession between diatoms (upwelling-favoured) and dinoflagellates (downwelling/relaxation-favoured) (Pitcher et al., 1991). Variability in diurnal wind patterns (i.e. coastal breezes) as well as local inertial surface currents are suggested to be of first order significance to phytoplankton phenology (Lucas et al., 2014). Processes that function at such timescales could explain how very different water column dynamics and community structure can occur at similar stages in the upwelling/downwelling favourable wind cycle, as seen in this study.

Myrionecta rubra were present over the entire upwelling/downwelling cycle (Fig. 2.14), even in recently upwelled waters as cold as 10°C. The ability to withstand fluctuating conditions is suggested to be linked to its mixotrophic capabilities (Stoecker et al., 1989) and mobility (Jonsson and Tiselius, 1990). *Myrionecta rubr*a displayed high levels of patchiness, as was evidenced by the additional sampling away from the fixed station. A high degree of patchiness appears to be characteristic of *M. rubra* blooms, as other studies have also observed similar patterns in spatial heterogeneity (Montagnes and Lynn, 1989; Bulit et al., 2004). Crawford

(1989) hypothesised that *M. rubra* bloom proliferation is from the combined effects of high light intensity, low turbulence and increased organic compounds produced by a preceding diatom bloom. A decrease in water column turbulence has also been suggested to play an important role in the initial surface aggregation of large numbers of bloom-forming *M. rubra* cells (Crawford, 1989; Herfort et al., 2011). The proliferation *of M. rubra* in association with diatoms has often been observed (Cloern et al., 1994; Crawford, 1989) and is reaffirmed in this study.

Dinoflagellate blooms are well known to be associated with very specific habitat conditions (Smayda and Reynolds, 2003). In this study, *P. triestinum* blooms were observed in waters above 15°C (Fig 2.14) and their observed proliferation fits with Smayda and Reynolds' (2003) characterisation of Prorocentroids (Type II) being found nearshore with a relatively accessible nutrient supply. They further suggest that the selection of species *within* a given life form (in this case - Type II) is stochastic. Their conceptual model focused on dinoflagellates, as they are the most common HAB species group, owing to their ability to occupy a wide range of niches (Smayda and Reynolds, 2003). However the model does not address the full diversity of HAB species.

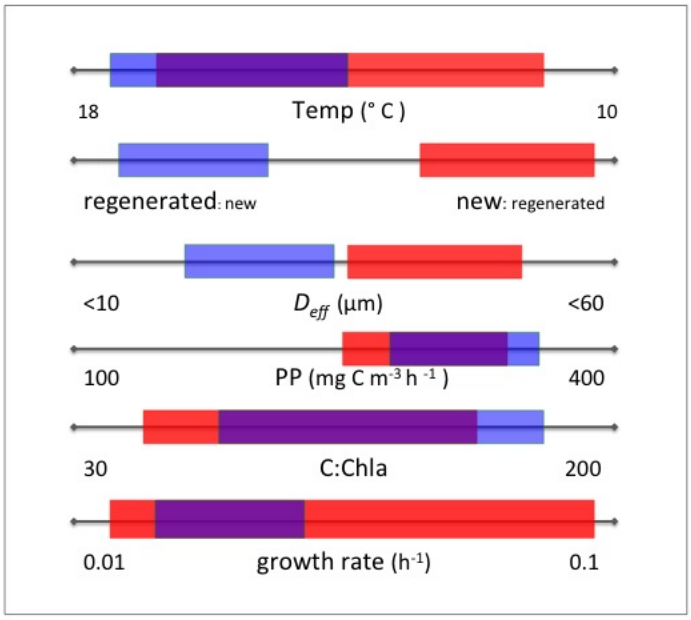

Figure 2.14: Approximate placing of *Myrionecta rubra* (red), *Prorocentrum triestinum* (blue) or both (overlapping) along environmental and biological axes. See Table 2.2.

Approximated physiology: *M. rubra* On average, particulate nitrogen and primary productivity were greater in the samples dominated by *M. rubra* than in those dominated by *Skeletonema* spp. (Table 2.4). Some of the highest previously recorded primary productivity rates from planktonic organisms were during *M. rubra* blooms. Packard et al. (1978) reported values of 1200 mgC m^{-3} h^{-1}, and similarly Smith and Barber (1979) observed a maximum rate of particulate C synthesis of 2187 (mg C m^{-3} h^{-1}) at 50% of incident light. Several studies indicate photosynthetic efficiency of *M. rubra* during blooms (in the form of P/I curves) is comparable to that of diatoms (Stoecker et al., 1989; Platt et al., 1980). Although, at times, *Skeletonema* spp. cells were as numerous as *M. rubra*, based on their cell size (8-12 μm) and volume:carbon ratios (Verity et al., 1992; Menden-Deuer and Lessard, 2000), they did not contribute as much, in terms of biomass, to the total assemblage as *M. rubra*. The data in this study suggest that *M. rubra* rates of primary productivity were higher than those observed during high *Skeletonema* spp. cell densities (Table 2.4). Reported values may even represent an underestimation of productivity rates as *M. rubra* are known to be sensitive to confinement and rapid nutrient exhaustion, and their cells frequently rupture during sampling, potentially biasing measured values.

The approximated carbon-based growth rates are comparable to values measured by Herfort et al. (2011) in the Colombia River estuary, which ranged between 0.7 -1.4 (d^{-1}). The values are seemingly high when compared to those recorded *in situ* by Crawford et al. (1997) or in culture by Yih et al. (2004), but maximum values have been recorded up to 3.5 d^{-1} in culture studies of ciliates (Strom and Morello, 1998). The steady increase in *Skeletonema* spp. numbers and high growth rates indicate active growth of the diatom in the presence of *M. rubra.*

The C_p:Chl-*a* ratios given in Table 2.4 represent an upper limit estimate of phytoplankton carbon for a given Chl-*a* concentration. These values are well within the inverse of the values published by Behrenfeld et al. (2009) in their approximations of Chl-*a*:C from satellite Chl-*a* and backscattering determinations. Changes in the cellular C_p:Chl-*a* are associated with community composition and acclimation to light and nutrient regimes (Sathyendranath et al., 2009) and the approximations presented here are based on carbon values that were converted assuming a Redfield N:C ratio of 1:6.625 molar. Although C:N:P ratios are observed consistently at a global

scale (Redfield, 1958), deviations from this ratio have been observed at several temporal scales and between different phytoplankton communities. Assuming a constant Redfield ratio, will no doubt introduce some error into the C_p:Chl values presented in this study.

Approximated physiology: *P. triestinum* *Prorocentrum triestinum* displayed exceptionally high biomass (max. 146 μmol N L^{-1}) and high rates of primary productivity (339 mg m^{-3} h^{-1}), and it appears that urea was the main source of nitrogen during their proliferation. Active growth is suggested during *P. triestinum* proliferation as growth rates were on average higher when they dominated than when not.

Table 2.4: Temperature (T), particulate nitrogen (PN) and primary productivity (PP) values and standard error in samples dominated by the species of interest. For approximated phytoplankton C_p:Chl-*a* ratios, PN was converted to PC, using the Redfield ratio (10C:1N). 30% of the total C:Chl-*a* was considered as C_p:Chl-*a* (Behrenfeld et al., 2005). Carbon-based growth rates were approximated assuming μ (h^{-1}) = PP (mg m^{-3} h^{-1})/PC (mg m^{-3}). Growth rates are scaled from per hour to per day (Brown et al., 1991) for comparisons with other studies.

Dominance	T (℃)	PN (μmol N L^{-1})	PP (mg C m^{-3} h^{-1})	Approx. C_p:Chl-*a*	Approx. growth rate (d^{-1})
M. rubra (~45%, ~7 X10^6 cells L^{-1}) n= 5	10.3 - 16.2	40.9 $\pm$14.7	138.7$\pm$42.9	49.4 $\pm$18.71	0.33 $\pm$0.09
Skeletonema spp. (~49%, ~12 X10^5 cells L^{-1}) n= 5	10.2 - 11.6	12.7±3	75.2±19	32.5±3.8	0.49±0.07
P. triestinum (~75%, ~13 X10^7 cells L^{-1}) n= 7	13.1-17.7	88.4±17	182.8±29.4	35.4±6.0	0.20±0.03
mixed (n= 14)	10.1-16.9	42.6±4.3	81.2±15.3	55.0±3.8	0.16±0.03

Nitrogen resource partitioning

With regard to the harmful species, *M. rubra* and *P. triestinum,* both displayed higher rates of urea uptake than NH_4^+. This supports results found by Anderson et al. (2002), Li et al. (2010) and Solomon et al. (2010) that urea is an important source of nitrogen for species associated with HAB events. During high cell densities of *P. triestinum*, ρurea was higher than ρNH_4^+, with substrate urea concentrations exceeding those of NH_4^+ uptake (Fig. 2.9). Culture experiments

show that, on a per cell basis, dinoflagellates have significantly higher urease activity (and thus urea uptake rates) than diatoms, cyanobacteria, or pelagophytes (see Solomon et al., 2010). Also, in the field, rates of urease activity typically peak in summer months, and are considered to be a reflection of not just direct and indirect effects of temperature, but also community composition and urea concentrations. Li et al. (2010) found that urea was the preferred organic N source during a *Karenia mikimotoi* (harmful dinoflagellate) bloom in the East China Sea. Their measured half saturation constants for NH_4^+ uptake were substantially higher (2.15 μmolN) than those for urea (1.35 μmolN), indicating that lower concentrations of urea than ammonium can be used for growth, i.e. high affinity shows a greater ability to take up nutrients at low ambient concentrations. Moreover, culture experiments on *Pseudo-nitzschia,* a HAB-forming diatom, showed that it produces more domoic acid when grown on urea than on NO_3^- or NH_4^+ (Howard et al., 2007).

Diatoms were observed to take up total N and NO_3^- at faster rates than any other phytoplankton group, as has been observed in other studies (Dortch et al., 1984; Lomas and Glibert, 2000). Interestingly, the GLM did not predict the uptake rates of NO_3^- by diatoms particularly well, as evidenced by their uniformly predicted values in Fig. 2.10. The GLM best predicts the uptake rates as a function of ambient nutrient concentration, cell size and taxon. With regard to ambient concentrations, typically high NO_3^- concentrations are associated with high *f*-ratios (Eppley and Peterson, 1979) and large-celled communities (e.g. Malone, 1980b; Probyn, 1985; Harrison, 1990), and usually dominated by diatoms (Margalef, 1979; Dortch et al., 1984). However, several studies have found weak correlations between uptake rates and availability of NO_3^- (Furnas, 1983; Glibert and Garside, 1992; Dauchez et al., 1996) due to variable preconditioning conditions and physiological state (i.e. nutrient starved/replete). Diatoms are known to have large internal stores of NO_3^- (e.g. Dortch et al., 1984; Lomas and Glibert, 1999) and can thus regulate their uptake according to how much is needed. Reasons for this are hypothesised to be for mechanistic energy balances in the cell during transient conditions of temperature and light. NO_3^- uptake in excess of nutritional requirements and the subsequent internal storage are further hypothesised to be a strategy of dissipating the electron flow during photosynthesis

(Lomas and Glibert, 1999; Glibert et al., 2016). Another circumstance observed in upwelling systems is that measured substrate concentrations at the time of uptake measurement may not reflect the available substrate nutrient concentrations. This is the "shift up phase" mentioned Dugdale et al. (1990) and previously noted in Schaecter (1968). Phytoplankton take time to respond to new inputs of nutrients and so a lag exists and maximum attainable uptake rates increase as the body of water moves away from the upwelling centre (Wilkerson and Dugdale, 1987). The measured rates in this study could reflect such a circumstance and, in the case of diatoms, uptake rates are not constrained solely by ambient concentration and community structure. Accounting for silica limitation in the GLM might have improved the estimates of uptake rates as silica is an essential component of diatom physiology and is thus a key factor in the regulation of diatom growth (Paasche, 1980). In this study, silica was not measured in 2004, but in 2005 N:Si ratios were all below 2:1 (unpublished data). Gilpin et al. (2004) considered >4:1 Si limited, and <2:1 N limited. An earlier study in the Cape Peninsula by Brown and Hutchings (1987) reported ratios within the same range (1 - 2.2). The authors concluded that silicate may *sometimes* limit the growth of diatoms in the system studied, but NO_3^- was the limiting nutrient in their observations.

Further suggestion for the poor GLM estimates of NO_3^- uptake, is the potential bias that could have been incurred by defining community structure, both in terms of D_{eff} and the dominant taxon. The different algal species were considered dominant with >40% contribution to total cells L^{-1}, except in the case of *M. rubra,* which was >30%. The rates expressed in this study are representative of the entire assemblage. Although particular emphasis has been placed upon teasing out the signals from each of the dominant groups in the blooms, these can only be considered as approximates.

Effective diameter as a size proxy

The generally observed trends in the literature are that NO_3^- is taken up by large cells, and regenerated nitrogen is taken up by small cells (Probyn, 1985; Acevedo-Trejos et al., 2013). Qualitatively, this is observed in the data set within the micro-plankton size range measured

(2-60 μm), and the relationships between D_{eff} and the mass specific uptake of NH_4^+ (r=-0.54, p=0.0008) and urea (r=-0.59, p=0.0002) are significant. This is considered a reflection of the physiological efficiencies of small cells compared to large cells, where small cells have greater affinity and faster uptake rates per unit biomass than large cells (Aksnes and Egge, 1991; Edwards et al., 2012), owing to their smaller surface area:volume ratios (Raven, 1997). The significant size/uptake relationships for regenerated forms of nitrogen in this study suggest that effective diameter can represent the assemblage scale properties of regenerated nitrogen dynamics. The situation for NO_3^-, however, seems more complicated. As seen in the results from the GLM, NO_3^- uptake was not predicted with the additive effects of ambient concentration, cell size and taxon. A strong linear relationship exists between mass specific uptake rate and ambient NO_3^- concentration (r=0.67 , p=0.0001), suggesting that, overall, ambient concentrations may play a first order influence on NO_3^- uptake. This is unsurprising, given the large range in ambient concentrations (0.02-24 μmolN L^{-1}). Although clear patterns are observed between cell size and NO_3^- availability in several studies (Kostadinov et al., 2010; Acevedo-Trejos et al., 2013), the size/NO_3^- uptake relationship can be highly variable (Probyn, 1985; Dauchez et al., 1996). The relationships can be attributed to physiological acclimation to rapidly shifting conditions (Bonachela et al., 2011; Smith et al., 2009) and taxonomic influences (Platt, 1985). This seems to be the case in this study. Despite the significant positive correlation between *f*-ratio and D_{eff} (r= 0.46, p=0.008), the highest NO_3^- uptake rates were not measured in samples with the largest D_{eff} (Fig. 2.12a). Diatoms appeared to take up NO_3^- at a faster rate than any other group observed (Fig. 2.11b) and, when removed from the regression analysis, the r value improved but was still not significant. High NO_3^- uptake values were also found in samples containing a mixotrophic dinoflagellate *Ceratium furca.* This is the one circumstance where D_{eff} failed to represent the size fraction with the greatest contribution to total biomass. The effective diameter was underestimated due to bimodal distributions that occurred in samples where *P. triestinum* and *C. furca* were both high in numbers, peaking at different parts of the size spectrum. As *P. triestinum* numbers declined, *C. furca* numbers increased. This was evident in four samples during 2005. After removing such samples, the correlation between vNO_3^- and

D_{eff} became significant (r=0.39, p=0.04). It is likely that D_{eff} represented the bulk dynamics of NO_3^- 90% of the time (n= 30) and that inherent taxonomic adaptations in NO_3^- assimilation, by most notably diatoms, was an important influencing factor. Complications of quantifying community structure by bulk metrics were also highlighted by Acevedo-Trejos et al. (2015). Their trait based model assessed the mechanisms and trade-offs shaping the size structure of phytoplankton communities, and described their assemblages using total biomass, mean size and size variance (as a measure of functional diversity). They explicitly assume unimodality in the size structure of the emergent phytoplankton communities, as accounting for multi-modality would require more parameters and add to model complexity.

Conclusions

The nutrient utilisation strategies of two separate, high biomass blooms, respectively dominated by *Myrionecta rubra* and *Prorocentrum triestinum*, were explored. In both case studies, the shift in local wind patterns from relaxed, light northerly to southerly winds with increasing wind stress had a strong influence on the thermal and physical dynamics of the water column.

Myrionecta rubra were present throughout the downwelling/upwelling cycle, were spatially heterogeneous across a range of temperatures from 11-17℃, and occurred in high biomass (104 μmolN L^{-1}) and high Chl-*a* concentrations (150 mg m^3). NO_3^- and urea were important nitrogen sources during their proliferation and calculated *f* ratios were high. *Myrionecta rubra* dominance was observed in association with a diatom *Skeletenoma* spp.

Prorocentrum triestinum dominated after a prolonged period of strongly stratified water, with temperatures between 11-16℃. They displayed an ability to utilise NO_3^- (*f* ratios from 0.1-0.6) but it is suggested that urea, which was in elevated concentrations, was an important N source. Urea uptake rates were high during their proliferation, and their apparent capacity to utilise this N resource could have contributed to their proliferation and dominance over other phytoplankton species. Growth rates were, on average, higher when they dominated. Exceptionally high primary productivity (339.8 mg C m^{-3} h^{-1}) was observed during *P. triestinum* proliferation.

The data were used to assess whether the single size descriptor, effective diameter, could

adequately represent the aggregate physiological properties of the assemblages. This is important for two main reasons. Firstly for the meaningful interpretation of data products that can be derived from the ocean color EAP algorithm designed for the southern Benguela, and secondly to inform allometric dependencies of different phytoplankton communities. A significant, negative correlation between NH_4^+ and D_{eff} (slope=-1.2, p<0.05) and urea uptake rates and D_{eff} (slope=-1.8, p<0.05) was evident, reflecting the physiological efficiencies of small versus large cells. All cells require NH_4^+, and per unit biomass small cells take up nutrients at a faster rate. This was captured in the data when using the bulk metric to describe the aggregated size properties of the assemblage; D_{eff} is an adequate representation of the assemblage size distribution. The non-significant relationship between NO_3^- uptake and D_{eff} represents several important factors that are known to cause marked deviations from the generally observed allometric relationships for NO_3^- uptake. Most notably, taxonomic variations and adaptations to fluctuating NO_3^- availability, characteristic of upwelling systems, influence NO_3^- uptake rates. The presence of diatoms as well as occasional bi-modality in size distributions restricted the usefulness of D_{eff} in estimating NO_3^- dynamics in this data set. However, the significant positive relationship between *f*-ratios D_{eff} implies that, in general terms, D_{eff} can capture the bulk nitrogen signals of natural assemblages.

Chapter 3

An investigation into the use of effective diameter to represent the nitrogen dynamics in diatom-dominated assemblages: The case of Saldanha Bay, South Africa

Abstract

The effective diameter (D_{eff}) is a single value proxy representation of phytoplankton size distributions that has been shown to represent the bio-optical properties of natural assemblages in the southern Benguela. The previous chapter shows that D_{eff} can also represent the dynamics of regenerated nitrogen in natural assemblages of phytoplankton, but not NO_3^-. This chapter explores further the use of D_{eff} to represent the nitrogen dynamics observed in Saldanha Bay, South Africa between January 2012 and January 2013. Assessments were also made of the nitrogen uptake rates in relation to environmental forcing and community structure, and comprise the first measurements of nitrogen uptake in the bay. Summer waters in the bay were nutrient-

limited at the surface and light-limited at depth, with low depth-integrated *f*-ratios (min: 0.04). Winter months were characterised by high nutrient availability throughout the water column, low biomass and highest depth-integrated *f*-ratios (max: 0.56). Diatoms were dominant throughout the seasonal cycle, with highest biomass and large cell sizes (up to 60 μm) observed in summer, and lowest biomass and small cell sizes observed in winter (<20 μm). Ambient nitrogen concentrations were the driver in the observed variability in the absolute uptake of all nitrogen sources. In the diatom-dominated community, V_{max} values for NO_3^- and NH_4^+ range between 0.007-0.17 μmol N $L^{-1}h^{-1}$ and 0.025-2.76 μmol N $L^{-1}h^{-1}$ respectively. Variation is observed in estimates of K_s for NO_3^- (0.23-42.57 μmol N L^{-1}) and NH_4^+ (0.18-14.02 μmol N L^{-1}). Michaelis-Menten models did not describe the kinetics of urea uptake. The effective diameter could not represent the dynamics of nitrogen uptake in low biomass, diatom-dominated assemblages in Saldanha Bay.

Introduction

Diatoms (Bacillariophyta) are key players in the ocean carbon, nitrogen and silicon cycles, constituting the most abundant, diversified, and ecologically important group in the marine environment (Sarthou et al., 2005). They occupy the entire nine orders of magnitude of the range in phytoplankton cell volume (Litchman and Klausmeier, 2008). Diatoms contribute a large component to marine biomass, particularly in nutrient-rich coastal systems, and account for 25-40% of total primary productivity in the global ocean (Smetacek, 1999), exceeding the contribution of all terrestrial rain forests combined (Field et al., 1998). Diatom dominance tends to occur whenever conditions are optimal for growth (Kudela, 2009), contributing disproportionately to biomass in spring blooms and coastal upwelling events, as diatoms are particularly well adapted to conditions that favour large cells (Chisholm, 1992). Their proliferation requires that silicic acid and other major nutrients are non-limiting (Egge and Aksnes, 1992) but diatoms have also been observed to be well adapted to areas of low nutrient input (Leynaert et al., 2001) by reducing cell volumes and increasing their surface area to volume ratios (Kiørboe, 2008). As a

group, diatoms are considered NO_3^- specialists (Glibert et al., 2016), suggested to be a result of their higher nitrate reductase activity (Lomas and Glibert, 2000), which is necessary for the assimilation of NO_3^- into the cell.

Diverse nitrogen utilisation strategies

Many models explicitly represent diatoms as a single group (e.g. Bopp et al., 2005; Le Quéré et al., 2005) and use average parameters (e.g. for growth, nutrient uptake, mortality etc) to represent the taxonomic and functional diversity of the entire group. Several reviews have found a wide range of half saturation constants for N (Sarthou et al., 2005; Collos et al., 2005), with strong genus-specific responses to high NO_3^- levels (Collos et al., 1997), indicating diversity in nutrient utilisation strategies under varying environmental conditions. Sartouh et al. (2005) reported values between 0.02 μM to 10.2 μM, with an average value of 1.6 $\pm$ 1.9 μM (n = 35). Collos et al. (2005) reported K_s values between 0.4 and 53 μmol N L^{-1} and argue that K_s appears to covary with ambient nitrate concentrations rather than within a given taxonomic group. Positive relationships between NO_3^- concentrations and K_s have been reported (Harrison et al., 1996; Smith et al., 2009) with much of the variability in K_s in those studies explained by nutrient prehistory. Interspecific competition for nutrients and cell surface area (Collos et al., 1997), temperature (Lomas and Glibert, 1999) or cellular acclimation in response to internal and ambient nutrient concentrations (Smith et al., 2009), are all factors that could affect uptake kinetic parameters. With regard to the effect of size, Maguer et al. (2011) found the influence of cell size was greater for NO_3^- than NH_4^+, where V_{max} was consistently higher in cells larger than 10 μm, potentially reflecting larger specific storage of NO_3^- relative to their biomass. A review by Litchman et al. (2007) found that diatoms as a group displayed higher NO_3^- uptake rates for a given cell size than other functional groups such coccolithophores, dinoflagellates or chlorophytes. Within diatoms, they found a strong relationship between K_s and cell size.

The effects of cell size

The general patterns in size distribution, and the inherent limits size imposes on metabolism, is consistent within diatoms as a group. Large diatoms tend to dominate plankton communities under high-nutrient conditions owing to their low surface area-volume ratios (Raven, 1980) and subsequent requirement for high nutrient concentrations. On the other hand, small diatoms are adapted to low nutrient concentrations, as seen in smaller half saturation constants than those of larger cells (Eppley et al., 1969; Edwards et al., 2012). Terseleer et al. (2014) used a size based approach to model the functional diversity within diatoms and characterised diatom size succession as a trade off associated with cell size along a bottom-up (resource acquisition) and top-down (grazing pressure) gradient (Steiner, 2003). Small cells are better competitors at nutrient acquisition but are more susceptible to grazing, whereas large cells can proliferate due to slower rates of predator growth in response to blooms (Irigoien et al., 2005). Terseleer et al. (2014) argued that the diverse strategies of nutrient uptake and growth within diatoms as a group could be resolved using size succession. Barton et al. (2013) assessed intra-group ecology of diatom and dinoflagellate taxa and found greater variation in the mean cell volumes over the seasonal cycle for diatoms than for dinoflagellates. This was attributed to the mixotrophic strategies employed by dinoflagellates for the same cell size, which were less constrained by ambient nutrient concentrations.

This chapter takes advantage of a predominantly diatom-dominated data set collected in Saldanha Bay, in the southern Benguela, over the period of a year. In the previous chapter it was found that D_{eff} could represent the regenerated nitrogen dynamics of high biomass blooms. The case for NO_3^- was confounded by several data points that were diatom dominated, as well as a few samples displaying bi-modality in size distribution. It was suggested that the physiological NO_3^- utilisation strategies of diatoms were more important than allometric considerations in determining the uptake rates of NO_3^-. This current chapter explores this tenet further, as such an assessment could help interpretation of allometric deviations within diatoms as a group.

This chapter aims to describe the utilisation of the different nitrogen sources in relation to

community structure and seasonally varying environmental gradients and is the first description of its kind in Saldanha Bay. Uptake kinetic experiments are used in addition to *in situ* incubations to infer the nitrogen capabilities of the particular diatom communities present. The size distribution and nitrogen utilisation are then used to assess how well the effective diameter can represent the physiological properties of natural, diatom-dominated assemblages.

Methods

Sampling

Sampling was carried out in Saldanha Bay during seven periods between January 2012 and January 2013. Each sampling period consisted of three days of experimentation, with the exception of January 2013 when six days were sampled. Data presented in this study were collected from a fixed station in Big Bay (33°01.748' S, 18°00.888' E), in close proximity to an oyster farm (Fig. 3.1). Vertical temperature and flourescence profiles were obtained with a Sea-Bird Electronics Seacat CTD profiler for each sampling day. Depths of 0, 3, 6 and 9 m were sampled as a representation of the water column, which in entirety is 12 m deep. Water from each depth was collected using two casts of a 5 L Niskin water sampler and used to fill 10 L black buckets. Water from the buckets was used to measure nitrogen uptake in *in situ* incubations, which were prepared on board and deployed from the vessel. Two out of the three days per sampling period were dedicated to *in situ* incubations with the remaining day being used to conduct uptake kinetic experiments on shore. Protocols for *in situ* incubations and uptake kinetic experiments are detailed below. Each bucket was brought back to the laboratory for nutrient analysis, Coulter Counter measurements, and Chl-*a* analysis.

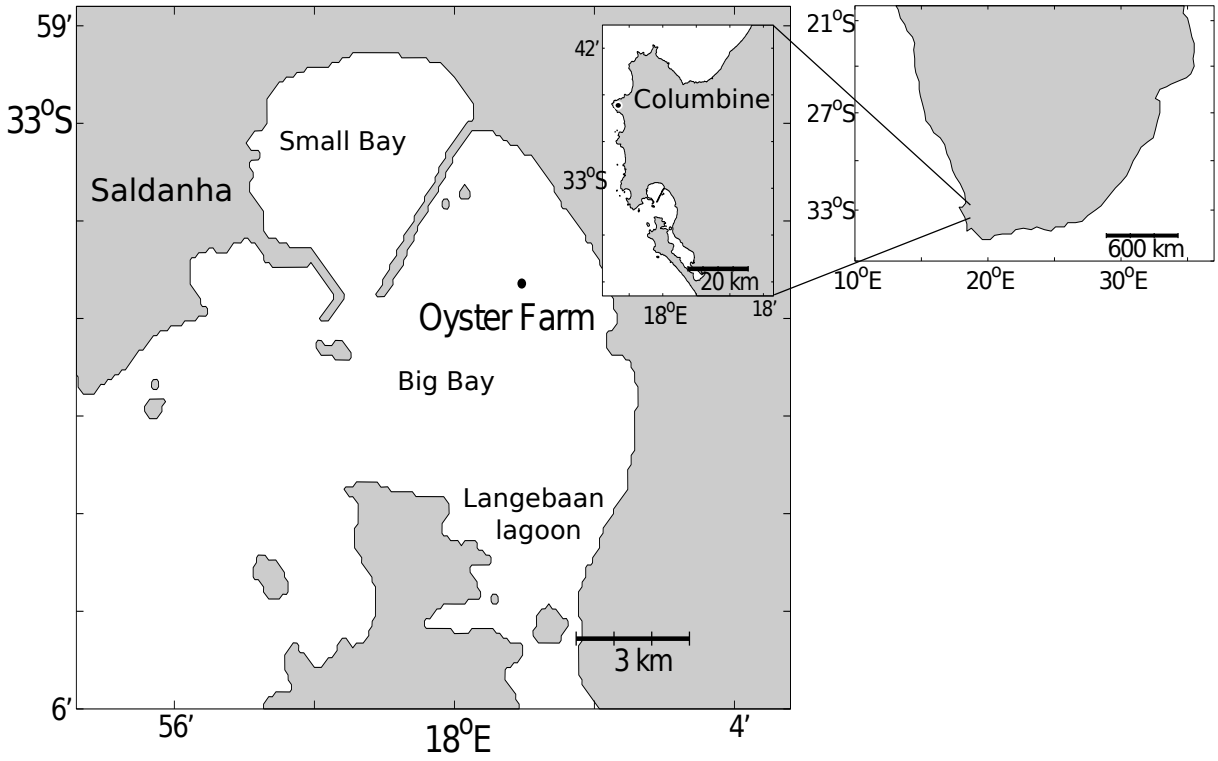

Figure 3.1: Map of sample site in Saldanha Bay on the west coast of South Africa. (●) indicates sample site in close proximity to the oyster farm in Big Bay.

Wind data

Hourly averages of wind speed and direction were obtained from Cape Columbine weather station of the South African Weather Service, located approximately 30 km north-west of the Big Bay sampling station. Refer to Chapter 2 for details of processing.

Particle size distributions

A Beckman Coulter Multisizer IV was used to measure particle size distributions between 7-70 μm and were presented here using means and standard deviations from all sample depths (0, 3, 6 and 9 m) . Effective diameters (D_{eff}) were calculated as in Chapter 2 (eq. 2.2).

In situ incubations

Uptake of NO_3^-, NH_4^+ and urea were measured over a 24 hour period in *in situ* incubations. The protocol for uptake incubations follows that already detailed in Chapter 2, with the exception that the 1 L polycarbonate bottles (NO_3^-, NH_4^+ and urea) were incubated *in situ* at their respective depths (0, 3, 6, and 9 m) for a period of 24 hrs on a custom-made rig. Isotope dilution has not been taken into account. The 24 hrs incubation time could results in an underestimate of NH_4^+ uptake rates under conditions of active regeneration within the incubation bottle.

Community structure

Phytoplankton samples from each depth were collected in two 100 mL bottles and fixed in 2.5% buffered formalin. Species were counted using inverted microscopy (Utermöhl, 1958). Pie diagrams were compiled showing relative abundance (cells L^{-1}) and relative particle volume (μm^3). Cell volumes of only the most dominant species were included. In cases where biovolumes were not found in the literature, estimates were calculated from available width and length data (e.g. $\mathrm{https://www.eoas.ubc.ca),}$ using appropriate formulae for geometric shapes according to Sun and Liu (2003). Certain assumptions were made regarding the geometric shape of the species present, and thus values in Table 3.1 represent rough estimates of biovolume and are not considered to be exact, and in some cases may be an overestimate. Species diversity was calculated via Shannon's diversity index (H').

Table 3.1: Biovolumes of the dominant phytoplankton species, sources and the equations used to calculate biovolume from width (a) and length (b) and height (c) as found in several phytoplankton databases online.

species	biovolume (μm^3)	equation	chain-forming	reference
Diatoms				
Chaetoceros spp.	342		Yes	Olivieri et al. (1984)
Pseudo-nitzschia spp.	1237.5		Yes	Olivieri et al. (1984)
Thalassionema nitzschioides spp.	2250	$Vol = a \cdot b \cdot c$		https://www.eoas.ubc.ca
Thalassiosira spp.	19454.5		Yes	Olivieri et al. (1984)
Skeletonema costatum	13800	$Vol = a \cdot b \cdot c$		https://www.eoas.ubc.ca
Dityllum brightwelli	54125		Yes	https://www.eoas.ubc.ca
Detonula pumila	40644	$Vol = \Pi \cdot b^2 \cdot ((\frac{b}{4})\text{-}(\frac{a}{12}))$	Yes	Naz et al. (2013)
Dinoflagellates				
Gyrodinium spp.	11000	$Vol = \left(\frac{\prod}{12}\right) a \cdot b^2$		
Ceratium lineatum	31800	$Vol = \left(\frac{\prod}{12}\right) a \cdot b^2$		
Ceratium furca	52539	$Vol = \left(\frac{\prod}{12}\right) a \cdot b^2$		https://www.eoas.ubc.ca
Prorocentrum micans	17638	$Vol = \left(\frac{\prod}{12}\right) a \cdot b^2$		https://www.eoas.ubc.ca
Prorocentrum triestinum	378	$Vol = \left(\frac{\prod}{12}\right) a \cdot b^2$		http://species-identification.org/
Peredinium spp.	3512	$Vol = \left(\frac{\prod}{12}\right) a \cdot b^2$		

Kinetics protocol

Samples for kinetic experiments were collected from 3 m depth and brought back to the laboratory on shore. Eight 250 mL bottles were filled with the collected water for each nutrient: NH_4^+, NO_3^-, Urea. Each 250 mL bottle for the different nitrogen source was spiked with the same volume of 100% ^{15}N solution (0.05 mL) to account for ambient concentrations (putatively 10% final enrichment). To obtain a concentration gradient, separate bottles were spiked with an increasing volume of a 10% ^{15}N stock solution (Table 3.2). All bottles were gently inverted 20 times once all inoculations were done, and a 25 mL scintillation vial was filled and filtered immediately for determination of initial concentrations of the respective nutrients (S_0). The samples were incubated for an average of 3.5 hours over midday, screened with 50% neutral density film, with periodic rotation of the bottles to allow for mixing. The temperature was maintained at ambient seawater by water flow through a chiller unit. The incubation was terminated by filtering each

bottle and the filtrate was collected to carry out nutrient analyses for ambient nutrient concentrations at the end of the experiment. The filter, a 25 mm precombusted GF/F filter, was rinsed with artificial seawater and Milli-Q, dried at 60℃ and used for mass spectrometry analysis as described in Chapter 2.

Table 3.2: Example protocol for either NH_4^+, NO_3^- or urea, and the volumes for each inoculation of i) 100% and ii) 10% ^{15}N stock solution. Increasing concentration of 10% stock solution were used to obtain a concentration gradient for uptake rates. Time In refers to time bottles were placed in the incubator, Time Out refers to its termination via filtration (S_t).

N	**100% Solution.**	**10% solution**	**Nominal concentration**	**Time In**	**Time Out**
	(mL)	(mL)	(μmol N L^{-1})	(h)	(h)
1	0.05	0.0	0.2	11:00	14:15
2	0.05	0.1	0.6	11:00	14:15
3	0.05	0.2	1	11:00	14:15
4	0.05	0.25	1.2	11:00	14:15
5	0.05	0.5	2.2	11:00	14:15
6	0.05	1.25	5.2	11:00	14:15
7	0.05	2.5	10.2	11:00	14:15
8	0.05	5	20.2	11:00	14:15

The 10% ^{15}N spiking solution was made up as follows:

2 mL of 100% ^{15}N (~0.1 μmol/0.1 mL) = 2 μmol ^{15}N

2 mL of std stock (10 μmol/1 mL) = 20 μmol ^{14}N

18 mL milli Q = 22 μmol/22 mL

$\approxeq$ 1 μmol/mL (depending on ^{15}N concentration)

Actual concentrations of the 100% ^{15}N spike solution were measured spectrophotometrically and incorporated into calculations. Presented nutrient concentrations are an exponential average (S), which assumes that the decrease in concentration from start of incubation (S_0) to end of incubation (S_t) is not linear over time (3.1).

$$S = \frac{S_0}{ln(S_0/S_t)} * (1 - (S_t/S_0) \tag{3.1}$$

Uptake kinetic parameters

The uptake kinetic parameters V_{max} (μmol N L^{-1} h^{-1}) and K_s (μmol N L^{-1}) were estimated via the Michaelis-Menten hyperbola function, using a least squares curve fit to the measured nutrient concentration (μmol N L^{-1}):

$$V = \frac{V_{max} * S}{K_s + S} \tag{3.2}$$

The affinity for each nutrient was calculated using Healey (1980):

$$\alpha = \frac{V_{max}}{K_s} \tag{3.3}$$

Data analysis

Patterns in community composition per sample were analysed using Multi Dimensional Scaling plots and a cluster analysis at 70% similarity between samples, per sample month and depth. Cell counts (cells L^{-1}) were standardised to total values and square root transformed.

The influence of different explanatory variables (ambient concentrations of NO_3^-, NH_4^+ or urea) on the uptake rates was explored using several general linear models (GLM), assuming a Gaussian error distribution.

$$vnitrogen\,(h^{-1}) = \beta_0 + \beta_1 + \beta_n + \varepsilon \tag{3.4}$$

where β_0 is the intercept, β_1 is the coefficient for the different nitrogen sources (total N, NO_3^-, NH_4^+ or urea), β_n is the coefficient for whichever variable(s) predicted the uptake of each nitrogen species best and ϵ represents the residual error. Changes in the Akaike information criterion (AIC) values were considered significant with a difference of 2, which was used to assess the significance of adding variables to the model.

Results

A summary of depth-integrated N concentrations and uptake rates is provided in Table 3.3.

Table 3.3: Depth-integrated (0-9 m) nitrogen concentrations (NH_4^+, NO_3^-, urea), total nitrogen uptake rates, *f*-ratios (NO_3^-/[NO_3^-+NH_4^++urea]) and particulate organic nitrogen (PON). Presented values are an approximation of the integral of each variable, estimated via a trapezoidal function.

	Date	NH_4^+	NO_3^-	urea	*f*-ratio	PON	Chl-*a*	Uptake
		(mmol N m^{-2})	(mmol N m^{-2})	(mmol N m^{-2})		(mmol N m^{-2})	mg m^3	(mmol N m^{-2} d^{-1})
SB1	17/01/2012	4.5	3.4	21.1	0.12	76.3	8.78	13.4
SB1	19/01/2012	1.5	0.4	15.4	0.09	80.3	12.54	9.5
SB2	13/03/2012	2.8	29.6	17.3	0.21	97.1	81.32	7.5
SB2	15/03/2012	0.7	10.5	3.6	0.27	74.4	82.26	5.5
SB3	15/05/2012	2.9	0.6	15.2	0.21	137.4	100.55	11.9
SB3	17/05/2012	5.4	10.3	5.1	0.22	143.3	68.76	9.1
SB4	02/07/2012	4.8	104.8	13.2	0.44	80.3	22.60	10.2
SB4	04/07/2012	11.1	120.5	9.7	0.33	90.6	50.26	13.6
SB5	11/09/2012	1.2	3.9	3.6	0.42	118.1	94.89	4.9
SB5	13/09/2012	3.5	4.5	7.4	0.27	79.7	21.28	7.5
SB6	20/11/2012	1.4	12.9	4.2	0.29	91.2	65.60	7.0
SB6	22/11/2012	2.3	17.5	3.5	0.37	83.2	47.71	6.0
SB7	19/01/2013	4.5	10.4	5.4	0.18	90.7	43.09	7.7
SB7	21/02/2013	2.7	4.0	1.9	0.24	85.4	63.05	7.9
SB7	23/01/2013	7.0	2.8	3.0	0.16	82.4	54.30	8.1

Water column and community dynamics

Temperature profiles of the bay showed a clear seasonal pattern (Fig. 3.2b). Strong stratification occurred during summer months (November-May), with surface temperatures reaching almost 20℃. During winter months (May-September), temperatures are homogeneous throughout the water column, where minimum temperatures reached 11.9℃. A subsurface Chl-*a* maximum was observed during summer months (January, March and September) at the thermocline, which varied between 4-10 m (Fig. 3.2d). Depth-integrated Chl-*a* reached a maximum of 100.55 mg m^{-3} in March (late summer), with an average value of 54.47 mg m^{-3} over the entire sampling period (Table 3.3). Lowest biomass, as expressed by particulate organic nitrogen (PON), was observed from late summer to spring (March to September) in association

with a mixed water column and highest nutrient availability (Fig. 3.3). During summer months when thermal stratification was strong (Fig. 3.2), there were generally higher concentrations of all nutrients at depth than at the surface (Fig. 3.3b). Urea concentrations (Fig. 3.3c) were low during winter and highest during summer at depth, but remained low in surface waters.

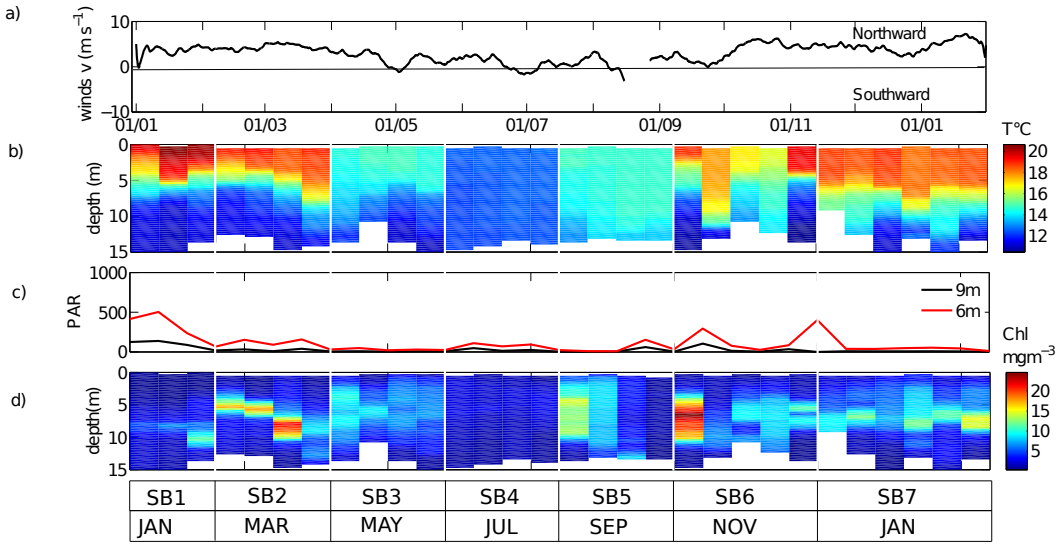

Figure 3.2: Results from Saldanha Bay site showing a) v component of winds as a 1 week running mean from 01 January 2012 to 31 January 2013, b) daily CTD measurements of temperature, c) daily estimates of extracted PAR from 6 m and 9 m and d) Chl-*a* throughout the water column per sample period. Thin, vertical white lines separate each sample period as this is not a continuous time series.

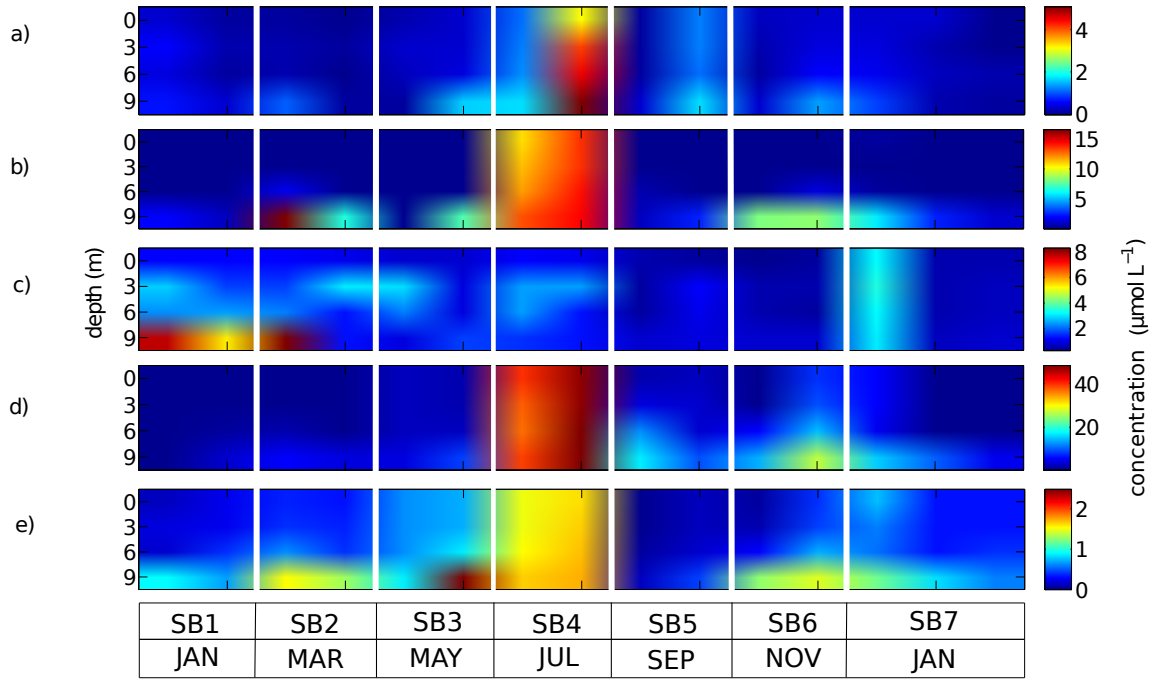

Figure 3.3: Nutrient concentrations at each depth (0, 3, 6 and 9 m) for a) NH_4^+, b) NO_3^-, c) Urea, d) Si, and e) PO_4^{3-}. Thin, vertical white bands separate each sampling period as this is not a continuous time series. Colourbars represent nutrient concentrations in µmol L^{-1}.

Community structure was distinctive for each sample month, where clustering at 70% similarity indicated very little overlap in species composition between sample periods (Fig. 3.4a). No significant difference in community composition was seen with depth (Fig. 3.4b), indicating that species composition was consistent throughout the water column for each sampling period. Particulate nitrogen was highest at depth (6 m and deeper) during summer months and more homogeneous throughout the water column during winter, with marginally higher particulate nitrogen at the surface (Fig. 3.5a). Assemblage biomass was maintained by small-celled communities (D_{eff} 10.84 µm) during winter (July) (Fig. 3.5c) and large cell sizes (up to 60 µm in diameter) at all other times of the year. Species composition was dominated numerically by diatoms throughout the year (Fig. 3.6a), with highest species diversity observed in winter, as quantified by Shannon's diversity index H'. The estimated biovolumes (Fig. 3.6b) indicate the groups that contributed most to the assemblage volume. Although, numerically, *Chaetoceros* spp. dominated assemblages, due to their relatively small sizes their contribution to total assemblage volume was surpassed by other diatom species. Assemblages were relatively diverse,

comprising several chain-forming diatom species throughout the year, with *Psuedo-nitzschia* spp. contributing most frequently to assemblages during the upwelling season (summer). A large-celled dinoflagellate, *Ceratium furca,* contributed most to assemblage volume during May but dinoflagellates were not observed to dominate the assemblage during other any sample period, although they were present in background numbers in most samples (Fig. 3.6a)

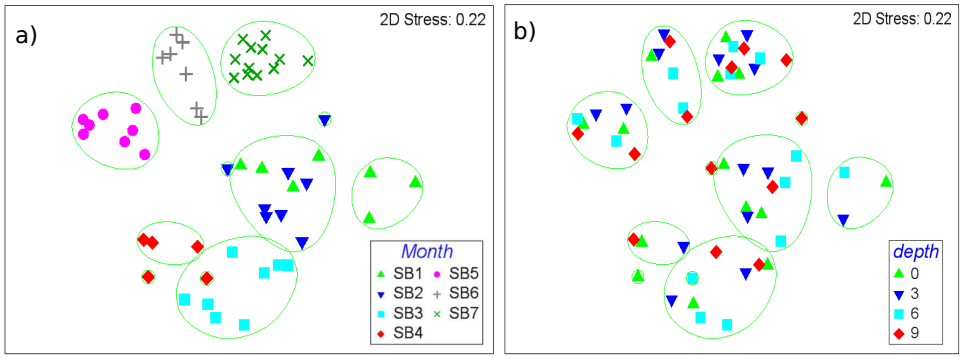

Figure 3.4: Results of Multi Dimensional Scaling plot showing clusters of samples based on species composition by numbers with a) month and b) depth. Green rings indicate 70% similarity between samples.

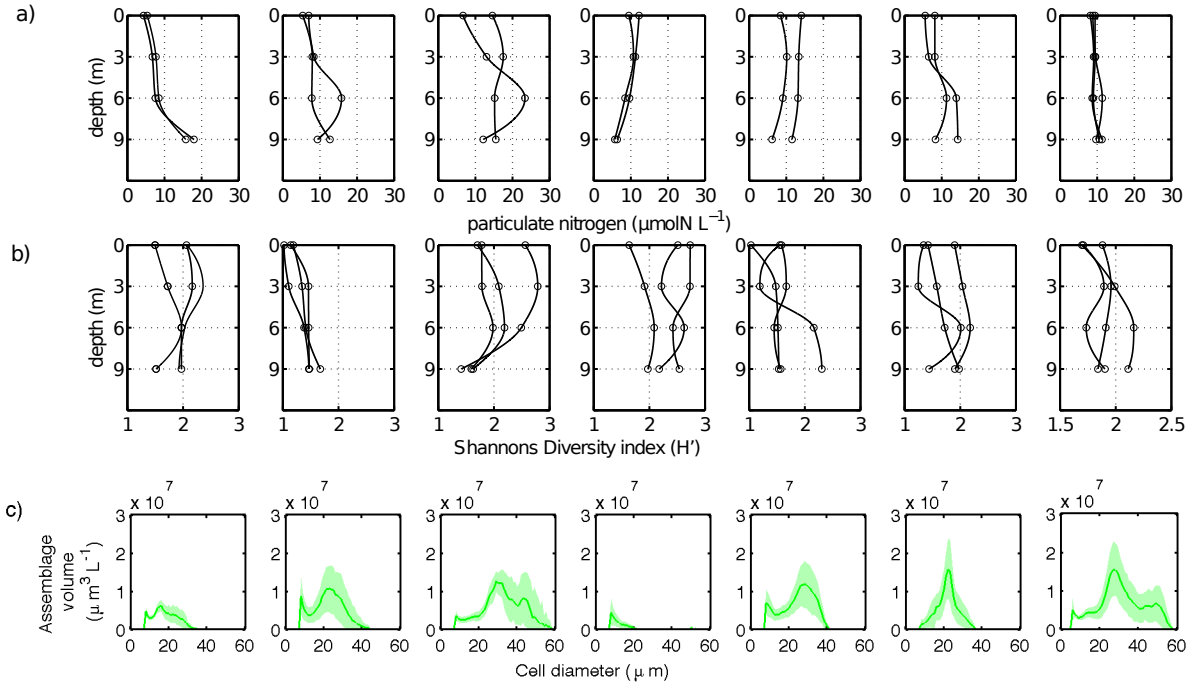

Figure 3.5: Summary of a) depth profiles of particulate nitrogen for each sample, b) Shannon's Diversity index (H') for all sample days and c) particle size distributions of all depths with the green line indicating mean total volume of the assemblage over all depths/samples and shaded area corresponding to standard deviations.

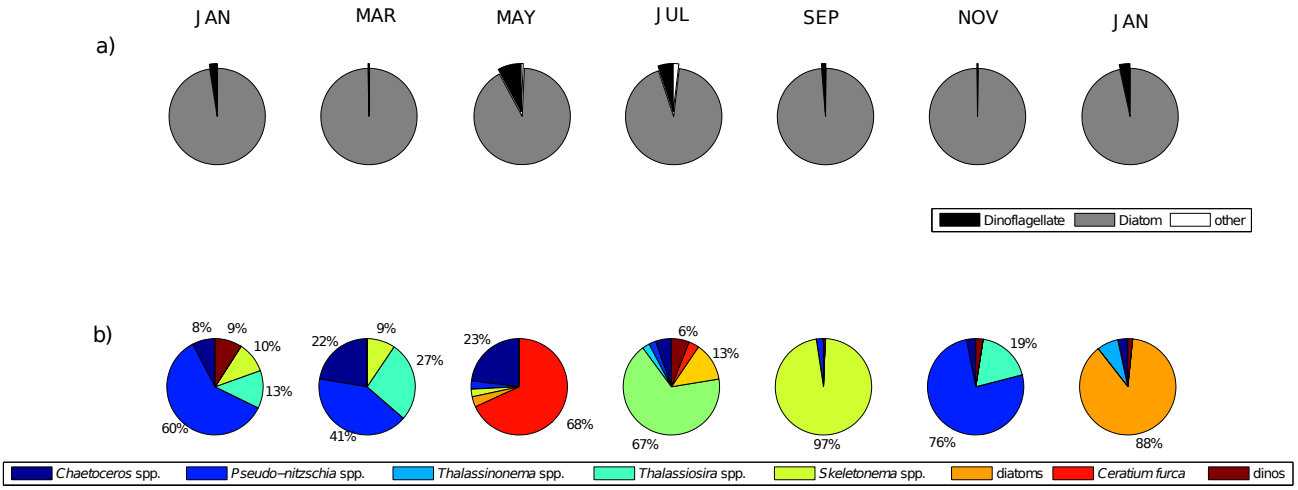

Figure 3.6: Pie diagrams showing community structure per sample period, represented as average values of all sample days per trip. a) relative abundance by numbers (cell L^{-1}) and b) relative biovolume of most contributing genera, excluding species in 'other' category.

Uptake kinetics

Michaelis-Menten (MM) curves were fitted to each kinetic experiment for NH_4^+ and NO_3^- but not for urea (Fig. 3.7) as the data did not indicate an increase in uptake rates with saturation at increasing urea concentrations. The range of experimental nutrient concentrations was consistent for each treatment but V_{max} parameters were variable throughout all samples for NO_3^- (0.007 - 0.175 μmol $L^{-1}h^{-1}$) and NH_4^+ (0.025 - 2.767 μmol $L^{-1}h^{-1}$) (Table 3.4). K_s values were highly variable for both NO_3^- (0.237-42.59 μmol L^{-1}) and NH_4^+ (0.185-14.023 μmol L^{-1}). The high K_s observed for NO_3^- during SB5 and SB6 indicates that uptake rates had not yet reached the asymptote of the Michaelis-Menten curve. Highest affinity for NO_3^- was observed in January (SB7) and highest affinity for NH_4^+ in September (SB5) (Table 3.4).

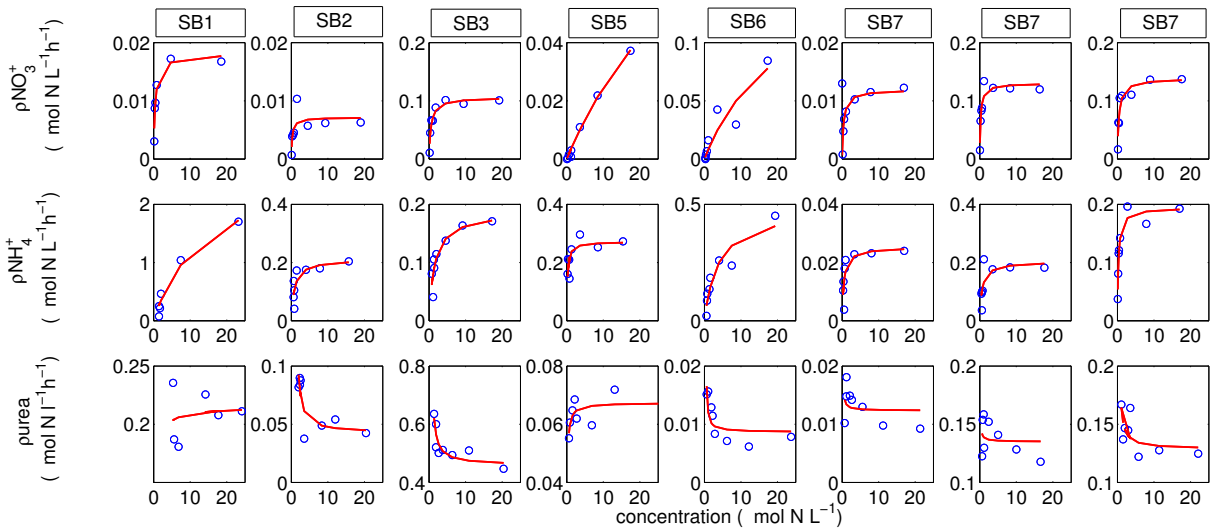

Figure 3.7: Model fits of the Michaelis-Menten equation $V = V_{max} * S/(Ks + S)$ using a non-linear least squares curve fit in Matlab for all kinetic experiments for NH_4^+ , NO_3^- and Urea, from SB1 to SB7. No kinetic experiments were undertaken during SB4 and three were done during SB7. Nutrient concentrations are reported as μmol N L^{-1} and absolute uptake rates as μmol N L^{-1} h^{-1}.

Table 3.4: Summary of particulate nitrogen (PN) (μmol N L^{-1}), calculated V_{max} (μmol N $L^{-1}h^{-1}$), K_s (μmol N L^{-1}), and nutrient affinity α (*sensu* Healey, 1980).

		PN	V_{max}**NO**$_3^-$	K_s**NO**$_3^-$	V_{max}**NH**$_4^+$	K_s **NH**$_4^+$	α**NO**$_3^-$	α**NH**$_4^+$
SB1	18/01/2012	8.1	0.018	0.424	2.767	14.023	0.043	0.197
SB2	14/03/2012	3.5	0.007	0.251	0.211	0.818	0.028	0.258
SB3	16/05/2012	13.5	0.106	0.510	0.187	1.500	0.208	0.125
SB5	12/09/2012	4.1	0.129	42.579	0.272	0.185	0.003	1.471
SB6	21/11/2012	2.9	0.175	21.593	0.486	3.793	0.008	0.128
SB7	18/01/2013	0.7	0.012	0.409	0.025	0.471	0.029	0.054
SB7	20/01/2013	8.1	0.130	0.237	0.203	0.616	0.548	0.330
SB7	22/01/2013	8.2	0.139	0.408	0.194	0.273	0.340	0.712

Limitations on nitrogen uptake

Mass-specific nitrogen uptake appeared to be limited by ambient nitrogen concentration and, in some cases in the deeper samples, by light (Fig. 3.8). Positive linear relationships were observed between the respective mass-specific uptake rates and ambient nitrogen concentrations (NO_3^-: r=0.69, p<0.05; NH_4^+: r = 0.69, p<0.005; urea: 0.44, p<0.005). These relationships were

observed only when samples with PAR values <1% of incident light levels were disregarded in the regression analyses (Fig. 3.8 a,c). The uptake of both NH_4^+ and urea were also linearly related to their ambient concentrations and the effects of light limitation were more pronounced in vNH_4^+ than vurea. The availability of NH_4^+ above concentrations of 1 μmol L^{-1} appeared to have an effect on the uptake of NO_3^- (Fig. 3.8b), an observation also supported by the results of the GLM (Table 3.5). Ambient concentrations of NO_3^- and NH_4^+ were significant predictors of vNO_3^- and were included in the most appropriate model, as assessed by the lowest AIC number (-517.65), but they predict only 27% of the variability (r^2= 0.27). Additional factors such as effective diameter, taxon and PAR improved the model's ability to predict vNO_3^- (r^2= 0.38) but with little change to the AIC value (-516.23) and the only significant variables were ambient NO_3^- (p=0.001) and NH_4^+ (p=0.05) concentrations. The effects of Si appeared to have little effect on the predictions of vNO_3^-. In the case of vNH4, 62% (r^2= 0.62) of the variability could be explained by ambient NH_4^+ concentrations (p=0.001) and taxon (p=0.05), most notably for *Pseudo-nitzschia* spp. dominated (p=0.01) and mixed assemblages (p=0.05). Mixed assemblages comprised predominantly *Dityllum brightwellii* and *Detonula pumila*. Predictions of vurea using the GLM were much weaker than the other nitrogen species. Ambient urea concentrations could explain 14% of the variability (p=0.05); the effects of taxon, PAR and temperature were not significant.

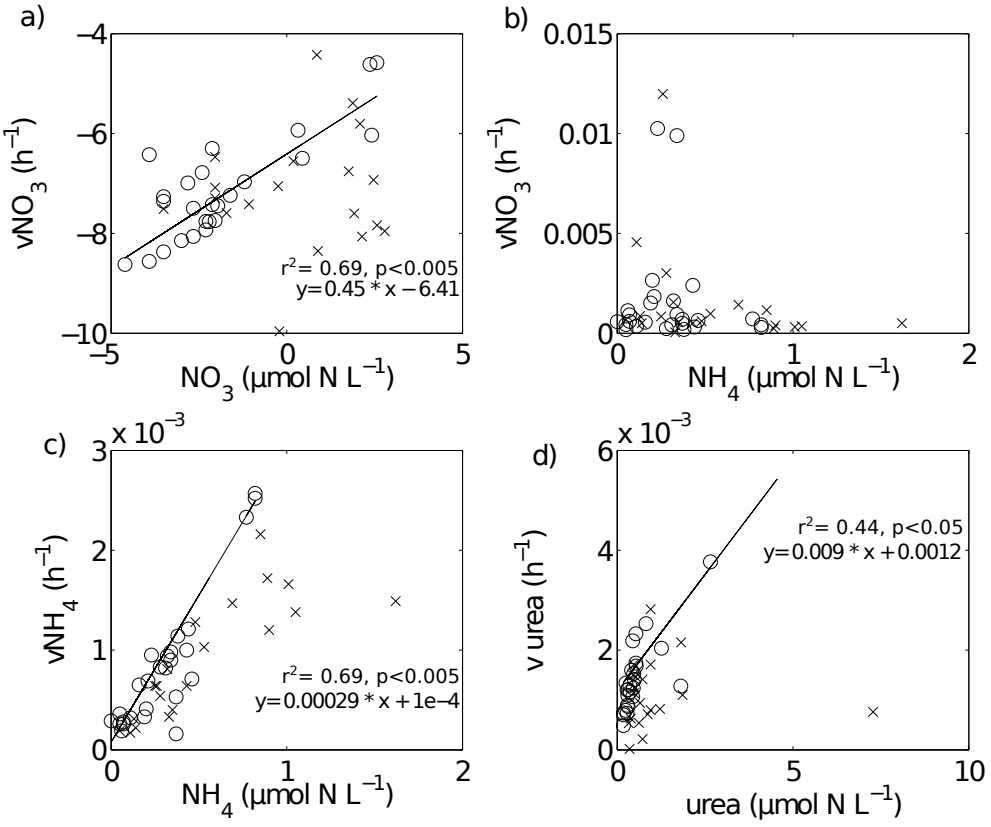

Figure 3.8: Relationships between ambient nutrient concentration and mass-specific uptake rates of a) NO_3^- (expressed as log-log), b) NO_3^- as a function of NH_4^+ c) NH_4^+ and d) urea. Crosses indicate samples that are <1% (~40 kWh) of incident light levels and were not included in the calculations of the regressions and correlation coefficients.

Table 3.5: Summary statistics from GLM to predict mass-specific uptake rates of NO_3^-, NH_4^+, urea and the significant predictor variables. DF=54

Parameter	Coefficients	SE	t	p
NO_3^- **r^2= 0.27**	**AIC= -517.65**			
$vNO_3^-\ (h^{-1}) = \beta_0 + \beta_1 NO_3^- + \beta_2\, NH_4^+ + \varepsilon$				
$\beta_1 NO_3^-$	3.22e-4	4.41e-4	3.887	<0.005
$\beta_1 NH_4^+$	-2.85e-3	9.97e-4	-2.86	0.01
NH_4^+ **r^2= 0.62**	**AIC= -678.7**			
$vNH_4^+\ (h^{-1}) = \beta_0 + \beta_1 NH_4^+ + \beta_2\, Group + \beta_3\, PAR + \varepsilon$				
$\beta_1 NH_4^+$	0.00155	0.00021	6.88	1e-8
β_2Group: mixed	0.008	0.00021	3.83	3e-4
β_2Group: *Pseudo-nitzschia* spp.	0.005	0.00020	2.80	0.007
Urea **r^2= 0.14**	**AIC= -587.89**			
$vUrea\,(h^{-1}) = \beta_0 + \beta_1\, urea + \beta_2\, Temp + \varepsilon$				
$\beta_1$urea	0.00038	0.00014	2.64	0.009

Effective diameter as a size proxy

No significant relationship existed between the mass-specific uptake of the different nitrogen species and D_{eff} (Fig. 3.9). However, further investigation revealed significant relationships between vNH_4^+ and log values of D_{eff} in the samples characterised by *Psuedo-nitzschia* spp. and *Skeletonema* spp. (slope=-2.74, r^2=0.38, p<0.005). Significant relationships were also observed between urea and log values of D_{eff} in the combined samples of *Psuedo-nitzschia* spp., *Skeletonema* spp. and mixed diatom assemblages (slope= -2.07, r^2= 0.27, p<0.005). Also evident in the data presented in Figure 3.9 is the representation of certain groups along the size spectra, as expressed by D_{eff}. In particular, samples of high *Thalassiosira* spp. volumes were characterised by a small D_{eff} (~10 μm) and had relatively high vNO_3^-. Two data points with small D_{eff} and large vNO_3^- (Fig. 3.9 a) correspond to surface samples with high NO_3^- (10-13 μmol N L^{-1}) and high light availability (400-700 kWh) during the winter sampling period. The samples with high *Ceratium furca* volumes were characterised by the largest effective diameters and appeared to take up urea relatively quickly (Fig. 3.9 c), but assemblages of *Pseudo-nitzschia* spp. displayed higher rates.

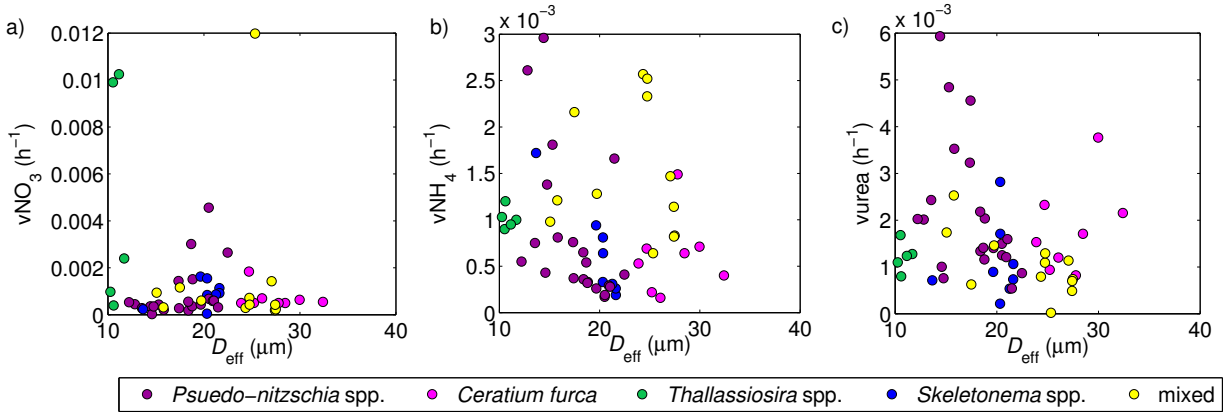

Figure 3.9: Relationships between mass-specific uptake rates and effective diameter (D_{eff}). a) vNO_3^- b) vNH_4^+ and c) vurea. The species groupings give an indication of the taxon with the greatest % contribution to assemblage volume but do not indicate complete dominance of assemblage. Approximate values of biovolumes per species (as indicated in Table 3.1) were used to define the groups.

Discussion

Over the study period (January 2012-January 2013), Saldanha Bay was dominated by diatoms but with different species composition in each sample month. A strong seasonal signal in water column dynamics was observed between winter and summer months. During summer months, strong thermal stratification was observed and NO_3^- concentrations were highest below the thermocline (between 6 and 9 m). Winter was characterised by homogeneous NO_3^- concentrations throughout the water column. The uptake of NO_3^-, and consequently *f*-ratios, were maximum during winter/spring months, in association with maximum NO_3^- availability. Uptake kinetic parameters (V_{max} and K_s) were variable over the study period, with highest deviance observed in half saturation constants for NO_3^-. Urea uptake did not conform to Michaelis-Menten enzyme kinetics. No significant relationship was observed between effective diameter and the mass-specific rates of nitrogen uptake.

Water column dynamics

The results of water column dynamics confirm what is generally known of the hydrodynamics of the bay (Monteiro and Largier, 1999). Temperature profiles observed over the entire sampling period showed strong stratification during mid/late summer months with high NO_3^- concentrations restricted to depth. During winter and early spring, the water column was well mixed and characterised by high nutrient availability across all depths. Saldanha Bay is modulated by the adjacent coastal waters via density-driven exchanges, in which nutrient-rich waters enter the bay at depth as upwelling-favourable winds relax (Monteiro et al., 1998; Monteiro and Largier, 1999; Probyn et al., 2000). In contrast to what often occurs in coastal waters, surface heating maintains strong stratification in the bay during coastal upwelling events (Monteiro and Largier, 1999) and nitrate-rich waters do not protrude to the surface during the upwelling-favourable season. In addition, associated with the strong thermocline, the subsurface Chl-*a* maximum was located from 4-7 m, acting as an effective 'nutrient trap' (Williams et al., 2013; Probyn et al., 2015) preventing input of NO_3^- to surface waters, which were thus nitrate-deplete.

During winter months, lowest Chl-*a* and cell abundances occurred in conjunction with highest nutrient concentrations, with overall highest nutrient uptake rates observed at 0 m and 3 m. Spring/early summer (September) marked the onset of highest biomass and cell abundances as light became less limiting. These results demonstrate nitrate-limited surface waters during summer, and light-limited bottom waters during winter, as exemplified in Figure 3.10.

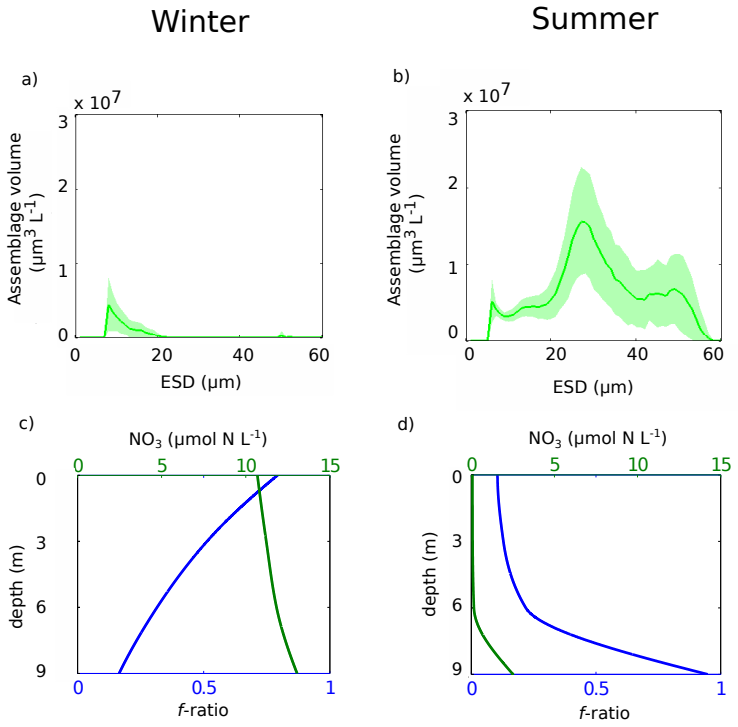

Figure 3.10: Example conditions during winter (a,c) and summer (b,d) of size spectra (a,b) and f-ratio and NO_3^- concentrations (c,d). Example size distribution examples represent the mean (green line) and standard deviations (green shading) of all measured depths. *f*-ratio (blue line) and NO_3^- concentrations (green lines) are depicted as averages. Winter data are from 2 July 2012, and summer data are from 21 January 2013. F

Limitations to nitrogen uptake

The linear relationship between mass specific uptake rates and the different nitrogen sources (with the exclusion of apparently light-limited samples from depth) is similar to that observed by Dugdale et al. (2006). Although seemingly contradictory to the Michaelis-Menten hyperbolae achieved in the kinetic experiments, the linear relationship between vNO_3^- and NO_3^- may be indicative of the “shift up” phase in the upwelling cycle (Wilkerson and Dugdale, 1987) following

nutrient depleted conditions. This linear relationship from *in situ* specific NO_3^- uptake rates has been similarly observed by Lomas and Glibert (1999; 2000) up to concentrations of ~60 μmol N L^{-1}, and for NH_4^+ in Dugdale et al. (2007), as seen in their Figure 4a.

It is also suggested that vNO_3^- was likely repressed/inhibited by high ambient NH_4^+ concentrations, as seen by Dortch (1990), who proposed that at concentrations >1 μmol N L^{-1}, NH_4^+ will suppress NO_3^- uptake. There is a wide range of observed NH_4^+ concentrations in the literature that cause a repression of NO_3^- uptake (Glibert et al., 2016 and references therein). NH_4^+ concentrations as low as 0.1 μM have been observed by Wheeler and Kokkinakis (1990) in oligotrophic environments, and as high as 4-10 μM in other field observations (Dugdale et al., 2007; Glibert et al., 2014). The threshold appears to be high in coastal systems. For example, in Bodega Bay (Dugdale et al., 2006) and San Francisco Bay (Dugdale et al., 2007), the repression of vNO_3^- occurred at NH_4^+ concentrations between 4-12 μmol N L^{-1}. The data from this study suggest that a large proportion of the NO_3^- inventory was inaccessible to the algal assemblage when NH_4^+ concentrations were >1 μmol N L^{-1} (Fig. 3.8b). Statistically, the variability in the uptake rates of all nitrogen species was best accounted for by relevant ambient concentrations (Table 3.5).

Uptake kinetic parameters

The results of the kinetic experiments confirm several key processes of connection between community structure and the nutrient utilisation strategies employed in response to the availability of the most limiting resources. On average, higher V_{max} and lower K_s values (*sensu* Dortch, 1990) observed for NH_4^+ (Table 4.5) indicate an overall preference for NH_4^+ over NO_3^-. This has been a common observation in cultured (Syrett, 1981) and field observations of phytoplankton communities (e.g. McCarthy et al., 1977). NH_4^+ is generally considered the preferred nitrogen source by phytoplankton (McCarthy, 1980; Syrett, 1956; Losada et al., 1981) especially as N becomes more limiting (Glibert et al., 2016). The reasons for NH_4^+ preferences are considered to be the higher energetic costs associated with assimilating NO_3^- (Syrett, 1981), whereby significantly more energy must be spent to first reduce NO_3^- to NO_2^-, and then to NH_4^+,

requiring additional transport systems and ATP (Mulholland and Lomas, 2008).

Collos et al. (2005) reported covariation between K_s (μmol L^{-1}) values and ambient NO_3^- concentrations (μmol L^{-1}), with a regression equation of: log K_s= 0.62 log NO_3^- - 0.09. No significant relationship between K_s and ambient concentrations of NO_3^-, or NH_4^+ were observed in this data set. However, after removing the exceptionally high K_s values from September (SB5) and November (SB6), the relationship between K_s and NO_3^- becomes significant. The equation follows closely to that observed by Collos et al. (2005): log K_s= 0.56 log NO_3^- - 0.02 : (r^2= 0.85, p=0.02). Doing this is considered to be justified for two main reasons: 1) The linear relationship proposed by Collos et al (2005), in the authors' own words, 'should be used with caution', as some groups, such as diatoms, are known to have genus-specific responses to high NO_3^- levels (Collos et al., 1997, 2005) and thus taxonomic adaptations may override the short term effects of fluctuating conditions; and 2) the exceptionally high K_s values (21; 42 μmol L^{-1}) correspond to high NO_3^- availability and assemblages with an abundance of *Skeletonema costatum* (September) and *Pseudo-nitzschia*/*Thalassiosira* spp. (November). The high K_s values reflect a linear dependency on NO_3^- in the uptake kinetic experiments for these two samples, where saturation did not occur in concentrations >20 μM NO_3^-.

A culture study of *Skeletonema costatum* (Serra et al., 1978) found that NO_3^- only reached saturation in concentrations >6 μM, and it was suggested that such a threshold may differentiate between transporter/uptake systems within the cell, i.e. 'multi-phasic systems' (Collos et al., 2005). Biphasic kinetic patterns have also been observed in Chesapeake and Delaware Bays by Lomas and Glibert (1999) at concentrations >30 μM. The activation of a second uptake system could be a good indication that NO_3^- is no longer limiting. Collos et al. (1997) also found a shift from the classic Michaelis-Menten kinetics to 'linear' kinetics as the population shifted from *Chaetoceros* spp. to a larger diatom *Thalassiosira* spp. The presence of a multi-phasic uptake system for NO_3^- represents the differences between active uptake, potentially after a period of N starvation and the active filling of storage vacuoles (Collos et al, 1997; Lomas and Glibert, 2000), and passive uptake, in which diffusion dominates uptake when NO_3^- becomes no longer limiting. It has since been noted that including multi-phasic uptake systems in model

estimates of NO_3^- limited plankton growth would improve model estimates of NO_3^- in upwelling areas of fluctuating and exceptionally high NO_3^- availability (Dugdale et al., 2007).

Urea uptake kinetics did not conform to Michaelis-Menten. What is apparent across the urea experiments is a peak in uptake rates at low concentrations (Fig. 3.7). Similar behaviour has been observed in studies of other systems (Eppley et al., 1971; Kristiansen and Lund, 1989; Tamminen and Irmisch, 1996; Bronk et al., 2004), and is also observed in kinetic studies of other organic substrates (glucose, amino acids) (Gocke et al., 1981). Potentially erroneously high determinations of ambient concentrations were originally suggested by Eppley et al. (1971) as an experimental artefact leading to the urea curves. Kinetic experiments carried out by Tamminen and Irmisch (1996) found a similar effect in their results but they suggested that chemical analyses to derive urea concentrations may have something to do with over estimations of urea uptake rates at such low concentrations. When they used the kinetic sum (Ks +Sn), as calculated via a linear transformation of the Michaelis-Menten curves (Wright and Hobbie, 1966), rather than ambient nutrient concentrations, they had a much more realistic curve. Tamminen and Irmisch (1996) call into question the concept of 'biologically available' urea, whereby chemical analyses may induce some degree of manipulation to the samples which 'can bring some absorbed, chelated or biologically loosely bound compartments into solution'. The curve observed in their Figure 1 (Tamminen and Irmisch, 1996) was explained by the over estimations made when analysing urea concentrations at such low concentrations (Grasshoff, 1976). Alternatively, Bronk et al. (2004) suggested that low atom % enrichment concentrations, relative to high substrate concentrations could cause errors in calculated uptake rates at substrate concentrations <0.05 μmol N L^{-1}. They saw similar curves in their urea kinetic experiments in *Karenia brevis* blooms in the Gulf of Mexico and reported urea atom % enrichment values between 4-85% . Nominal ^{15}N label concentrations used in this study were up to 20 μmol N L^{-1}, well within the range of concentrations used in other studies where no such curves were reported (e.g. Cochlan and Bronk, 2001). The urea atom % enrichments in this study were made up of 100% stock solution to accommodate the background levels, and a 10% spike solution, which was used to get a range of increasing concentrations (see Table 3.2). This was

done to circumvent the problem of widely varying aqueous enrichments that result from spiking with 100% stock solutions. Therefore, final aqueous enrichments were always close to 10% of ambient concentrations, with some small departures depending on how close the 100% spike was to achieving a 10% enrichment of ambient concentration. In this case, the explanation suggested by Bronk et al (2004) does not apply. The suggestion by Tamminen and Irmisch (1996) is more feasible, where the concentrations measured by the diacetyl monoxime method overestimates the biologically available urea. Chen et al. (2015) assessed the different methods of analysing urea and still recommended the diacetyl monoxime method over the enzymatic (urease) method, but argue sample preparation and timing need to be controlled very precisely. It is thus suggested that the seemingly erroneous urea curves are due to potential overestimations of biologically available urea. Further tests are recommended to incorporate suggestions made by Chen et al. (2015) to assess if any differences are observed. It is also recognised that metabolic enzymes and mechanisms of regulation that are involved in the assimilation of urea are diverse and not well understood; genome sequencing holds potential for further insight (Solomon et al., 2010).

Effective diameter in low biomass systems

The effective diameter is a useful metric to quantify the net bio-optical properties of phytoplankton assemblages (Bernard et al., 2009; Evers-King et al., 2014). In a high biomass scenario, >100 μmol N L^{-1} of particulate nitrogen (see Chapter 2), it was shown that D_{eff} could quantify the mass-specific uptake rates of regenerated nitrogen according to allometric size scaling. In this data set, although qualitatively a negative trend is apparent between vNH_4^+/vurea and D_{eff}, there is no significant relationship. No relationship was found between vNO_3^- and D_{eff} either. This is suggested to be due to the nature of the community structure: relating the shape and range of the size spectra. On average, the biomass, as measured by particulate nitrogen, was 4 times smaller in this data set than in Chapter 2.

It appears that the efficacy of using D_{eff} to represent the whole assemblage is sensitive to the shape of the distribution, and complex size distributions are poorly represented by effective

diameters. The narrow spread in calculated effective diameter used in this study (mean= 19.92 μm, mean absolute deviation = 4.41 μm) may also explain the statistically poor relationships between effective diameters and the other nitrogen sources. Equally, the particle size distributions used assume finite limits at both ends of the size spectrum but, with inherently open ended particle size distributions, there will be some inevitable error in this assumption (Sheldon and Parsons, 1967; Bryan et al., 2012). Furthermore, as the communities were predominantly made up of chain forming diatom species, the effects of chain formation need to be understood, because these can alter the interpretations of size spectra measured. Future work is recommended to address the quantification of a bulk size metric in low biomass waters.

Conclusions

The hydrodynamics in Saldanha Bay are driven by density differences between the bay and the inner shelf where warm, nutrient-deplete surface waters exit the bay, and cold, nutrient-rich waters enter the bay at depth. During the upwelling season, Saldanha maintains strong thermal stratification and injections of NO_3^- rich waters into the bay rarely penetrate through the thermocline. Sub-surface Chl-*a* maxima, sitting around 4m, could also act as a 'nutrient trap', whereby nutrients are taken up before they are brought to the surface. The summer is characterised by nutrient-deplete surface waters and NO_3^- rich water at depth. During the winter, downwelling-favourable winds (north-westerlies) allow for mixing and a homogeneous distributions of nutrients within the water column. The uptake of nitrogen reflects this seasonal dynamic in the water column. Light limitation occurs at depth during both seasons, but nutrient limitation at the surface is prominent during the summer months. Nutrient availability, or the ability to access it, was considered to be the strongest limiting factor in phytoplankton growth and biomass accumulation.

The phytoplankton assemblages were predominantly composed of diatom species, with a presence of dinoflagellates in many samples, but most notably at the end of the upwelling season. Community structure was particular to each sampling period, with high diversity within

diatoms observed throughout the year, and highest diversities observed during winter. This falls in line with the commonly accepted notion that species diversity will increase in response to greater competition for resources (Tilman, 1986), in the case of Saldanha Bay, nutrient availability and light. The nutrient acquisition strategies of the assemblages, as measured by K_s and V_{max}, varied according to the availability of ambient nutrient concentrations.

This case study was used to assess how well D_{eff} could quantify the size structure and the nitrogen utilisation of the measured communities, which showed a predominantly strong presence of many species of diatoms. In chapter 2, D_{eff} could adequately represent the size dependencies of the uptake of regenerated nitrogen, but not NO_3^-. This was considered to be due to some bi-modality in the size spectra, as well as the presence of diatoms. In this data set, no relationship was found between the uptake of any of the nitrogen species and D_{eff}. This was surprising for NH_4^+ and urea, given the strong relationships found in the previous chapter. The reason for such poor relationships are considered to be due to the nature of the size spectra measured, the small range in size distributions and the much lower biomass observed in Saldanha Bay. It is concluded that D_{eff} could not represent the nitrogen dynamics of the low biomass communities observed in this dataset.

Chapter 4

Estimating nitrogen uptake from ambient concentrations and cell size

Abstract

Bulk measurements can be made of phytoplankton standing stocks on a quasi-synoptic scale but it is more difficult to measure rates of production and nutrient uptake. This chapter presents a method to estimate nitrogen uptake rates in productive coastal environments. Observed phytoplankton cell size distributions and ambient nitrogen concentrations are used to calculate uptake rates of nitrate, ammonium and total nitrogen by different size fractions of diverse phytoplankton communities in a coastal upwelling system. The data are disaggregated into size categories, uptake rates are calculated and these uptake rates are re-aggregated to obtain bulk estimates. The calculations are applied to 72 natural assemblages for which nitrogen uptake rates and particle size distributions were measured *in situ*. The calculated values of total N uptake integrated across all size classes are similar to those of *in situ* bulk measurements (N slope=0.90), (NH_4^+ slope=0.96) indicating dependence of NH_4^+ and total N uptake on ambient N concentrations and cell size distributions of the phytoplankton assemblages. NO_3^- uptake was less well explained by cell size and ambient concentrations, but regressions between measured and estimated rates were still significant. The results suggest that net nitrogen dynamics can

be quantified at an assemblage scale using size dependencies of Michaelis-Menten uptake parameters. These methods can be applied to particle size distributions that have been routinely measured in eutrophic systems to estimate and subsequently analyse variability in nitrogen uptake.

Introduction

The diversity of phytoplankton communities influences the flows of carbon, nitrogen and other important elements through the marine environment. Marine ecosystem models that aim to capture this relationship represent phytoplankton diversity either by different functional groups (Follows and Dutkiewicz, 2011), cell size (e.g. Moloney et al., 1991; Baird and Suthers, 2007; Banas, 2011; Ward et al., 2012) or by both (Le Quéré et al., 2005; Aumont et al., 2015). Our understanding of the consequences of this diversity on global biogeochemistry is still limited (Lomas et al., 2014). In a broad ecological context, in addition to taxonomic distinction, the term diversity currently includes functionality within an environment (Tilman, 2001; McGill et al., 2006; Westoby and Wright, 2006; Litchman et al., 2007). A challenge in biogeochemical modeling is to try account for diversity among organisms and its role in nutrient flux (Follows and Dutkiewicz, 2011), plasticity in organism traits (Pahlow and Oschlies, 2009), trade-offs in energy expenditure and the relationships between physiological traits and environmental forcing (Aksnes and Cao, 2011). The most commonly used function to model nutrient uptake is the Michaelis-Menten equation and parameter values for maximum uptake rates (V_{max}) and half saturation constants (K_s) are widely available in the literature (see Litchman et al., 2015), often resolved at the species level in batch/continuous cultures (e.g. Eppley et al., 1969 and see Edwards et al., 2015) and typically at a genus level from natural populations (see Collos et al., 2005). The variation in V_{max} and K_s within phytoplankton groups and in relation to cell size were extensively reviewed by Litchman et al. (2007) and Edwards et al. (2012), where large variation was evident between and within phylogenetic groups. K_s values, for example, were found to vary over two orders of magnitude for a given group (Collos et al., 2005; Aksnes and Cao,

2011; Franks, 2009; Seeyave et al., 2009). Collos et al. (2005) found strong genus-specific differences in K_s between *Thalassiosira* spp. and *Chaetoceros* spp., both diatoms, under similar nutrient levels. Absolute values of V_{max} and their range are highest in diatoms, whereas K_s values are highest in dinoflagellates (Litchman et al., 2007; Edwards et al., 2012). The paucity of K_s values to account for all genotypic diversity in natural assemblages, under variable environmental conditions, as well as computational costs, has meant that K_s is often regarded a constant. The assumption that these parameter values are invariant within phylogenetic groups has been highlighted as a potential source of error when parameterising nutrient uptake by Michaelis-Menten kinetics (Franks, 2009).

Several studies have aimed to quantify the dynamic physiological response of phytoplankton cells to changing environmental conditions (e.g. Smith and Yamanaka, 2007; Pahlow et al., 2008; Bonachela et al., 2011; Smith et al., 2011) and have improved our conceptual understanding of cellular constraints on nutrient uptake and growth. Such dynamic trait-based approaches have been incorporated into large-scale modeling studies (Arteaga et al., 2014), with improved agreement between *in situ* values and model output (Smith et al., 2015). In many situations, the necessary *in situ* data are not available to constrain the dynamic response of a diverse, natural assemblage within a realistic, local context. Relatively simple size-based models can adequately replicate large scale dynamics of nitrogen in the marine environment (Ward et al., 2012; Acevedo-Trejos et al., 2014) with the advantage of reducing the number of free parameters, and thus model uncertainty, by using size-scaling exponents (Baird and Suthers, 2007; Banas, 2011; Ward et al., 2012). The size structure of plankton assemblages and the dominant size fraction will dictate, to some degree, the pathways of nutrients and how they are transferred to higher trophic levels (Probyn et al., 1990; Moloney et al., 1991; Chisholm, 1992; van der Lingen et al., 2006). Litchman et al. (2007) found strong empirical relationships between organism size and physiological rates (V_{max} and K_s) and considered cell size to be a master trait. Our understanding of the variability in uptake kinetic parameters in relation to community composition and environmental variability is poor, and there is a need for field-based and laboratory studies of physiological processes of phytoplankton groups (Gregg et al., 2003; Litchman et al., 2007;

Allen and Fulton, 2010).

This study hypothesised that some of the variance in Michaelis-Menten parameter values can be accounted for by considering the size spectra of the phytoplankton populations. To test such an hypothesis, measured particle size distributions (from Beckman Coulter Counter data) were used to calculate sets of theoretical, size-based biomass and Michaelis-Menten parameters for different field samples. Ambient nitrogen concentrations from each sample were applied to Michaelis-Menten models to estimate size-based nitrogen uptake rates and these were integrated across all sizes for the sample. These calculated rates were subsequently compared to measured *in situ* bulk uptake rates to estimated uptake rates of NO_{3^-} and total N (total N=NO_{3^-} +NO_4^+). This research offers a tool to extend the application of pre-existing particle cell size distributions, relying on robust assumptions of the size dependence of nitrogen metabolism.

Methods

Uptake rates were calculated from measured *in situ* particle size distributions (PSDs) and ambient nutrient concentrations. Figure 4.1 illustrates the steps that were taken and details of each step are discussed further below. In brief,

1) Measured PSDs were converted to a biomass per size bin by assuming a volume to nitrogen ratio (Moloney and Field, 1989; Menden-Deuer and Lessard, 2000). The sum of the estimated biomasses per size bin was compared to a corresponding *in situ* measurement of particulate nitrogen (PN).

2) Uptake parameters (V_{max} and K_s) were calculated per size bin, using published relationships in Ward et al. (2012).

3) A Michaelis-Menten model was used to estimate absolute uptake rates (ρ) of NO_3^- and NH_4^+ in μmol L^{-1} h^{-1} for each size bin, using ambient nutrient concentrations. The sums of the estimated uptake rates per size bin (ρNO_3^- and ρNH_4^+) were compared to corresponding *in situ* uptake measurements.

The implications of the assumptions of each step are evaluated in the discussion.

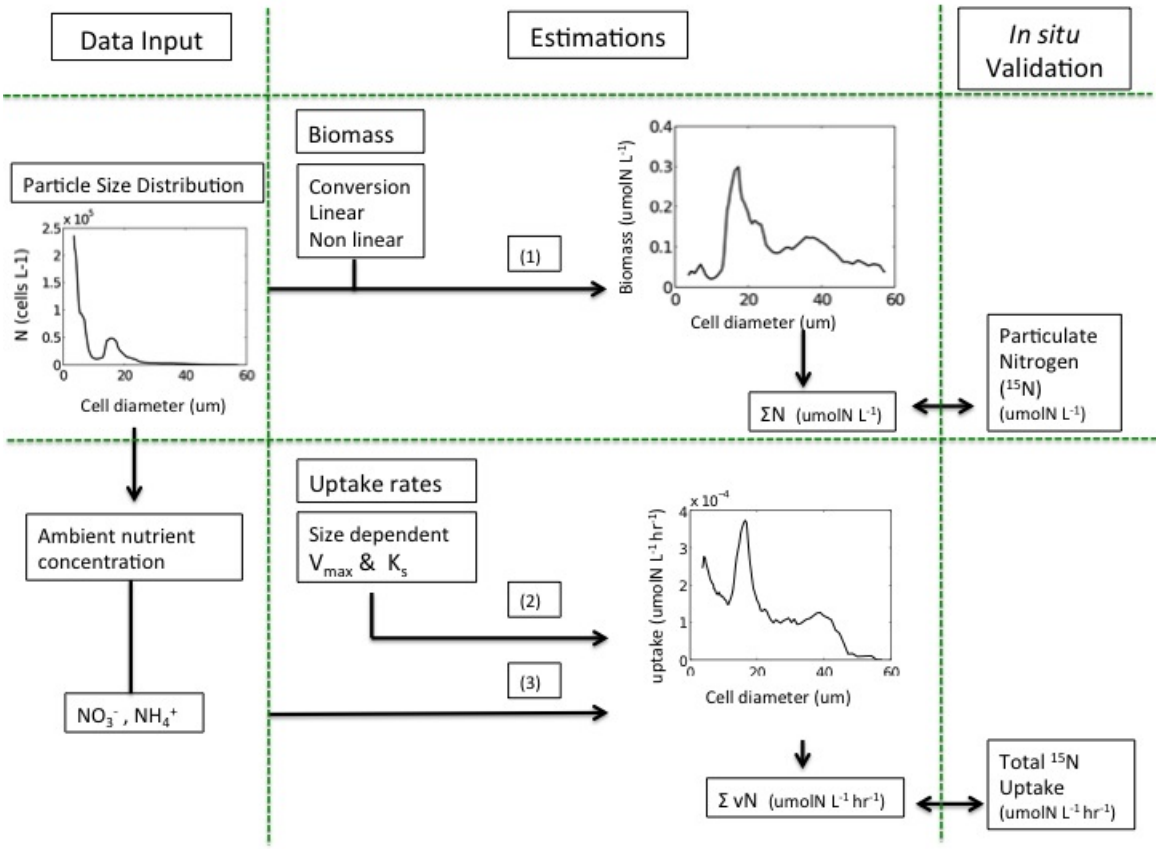

Figure 4.1: The steps taken to estimate biomass and uptake rates of NH_4^+ and NO_3^- from two data sources: Coulter Counter derived particle size distributions (PSD) and ambient nutrient concentrations.

In situ

Data from three separate case studies (Chapters 2 and 3) were used in this analysis. Data from Lamberts Bay came from sampling periods 25 February - 11 March 2004 and 15 March - 6 April 2005. In Saldanha Bay, sampling took place every 2 months for a period of 3 days from January 2012 to January 2013. Chapter 2 provides comprehensive descriptions of all ancillary data collected during these periods. Data used in this study include: particle size distributions (PSDs), biomass measured as particulate nitrogen, nitrogen concentrations (NO_3^-, NH_4^+) and the uptake of each. For the determinations of particle size distributions, nutrient concentrations, ^{15}N uptake and particulate nitrogen calculations, water samples were collected using a 5 L Niskin water sampler and stored in 20 L black buckets, which were then transported

to the laboratory within 1-2 hours of collection. Details of all methods of determination of nutrient concentration, nitrogen uptake and particulate biomass (PN) are described in Chapter 2. It must be noted that incubation lengths differ between Lamberts Bay and Saldanha Bay. Lamberts Bay incubations were for up to 4 hours, during midday light, whereas Saldanha Bay data were incubated for 24 hours. The differences between the two incubation times has been accounted for by scaling the 4 hour incubations to 24 hours. The assumption was made that daylight was 14 hours and that uptake during the night was 55% less for NH_4^+ and 12% less for NO_3^-, as measured at in-shore locations in Probyn et al. (1996). The effects of isotope dilution are not accounted for.

(1) Converting particle size distributions (PSDs) to nitrogen biomass

Particle size measurements were made using a Beckman Coulter Counter as described in previous chapters. PSDs were used to calculate total biomass of the assemblage in μmolN L^{-1} (Fig. 4.2) to compare to *in situ* measurements of particulate nitrogen. Measured biomass of particulate nitrogen (μmol N L^{-1}) includes all particulate matter down to a cut-off nominal size of 0.7 μm (GF filter), whereas Coulter Counter measurements have a lower limit of 3 μm. Two separate methods were used to estimate cellular nitrogen from cell volume for each size bin.

Non-Linear conversion of cell volume to biomass

Menden-Deuer and Lessard (2000) collated published relationships between cell volume (μm^3) and cellular nitrogen for dinoflagellates. Their resulting equation 4.1 was applied to each size bin to derive a biomass per cell in the size class (Fig 4.2). Total biomass per size bin was calculated by multiplying by cell abundance (N) within each size bin. The equation and values follow Menden-Deuer and Lessard (2000) and are hereafter referred to as the non-linear conversion:

$$log\, pg\, N\, cell^{-1} = -0.928 + 0.849 * logVol\, (\mu m^3) \tag{4.1}$$

Linear conversion of cell volume to biomass

Moloney and Field (1989), following Fenchel and Finlay (1983), assumed a linear relationship between cell volume (μm^3) and nitrogen content (μmolN), hereafter referred to as the linear conversion (see Fig. 4.2). Fenchel and Findlay (1983) used separate conversions for carbon and nitrogen (Table 4.1) based on values published in Finlay and Uhlig (1981). Carbon biomass was also calculated using this method, as a carbon biomass is required in addition to nitrogen biomass to solve for size-dependent uptake parameters, detailed below.

Table 4.1: Conversions used by Moloney and Field (1989) to estimate biomass (pgC, pgN) via a linear relationship between cellular volume and carbon/nitrogen content. Values from Fenchel & Findlay (1983)

Conversion
1μm^3= 0.071 pgC (dry)
1μm^3= 0.0185 pgN (dry)

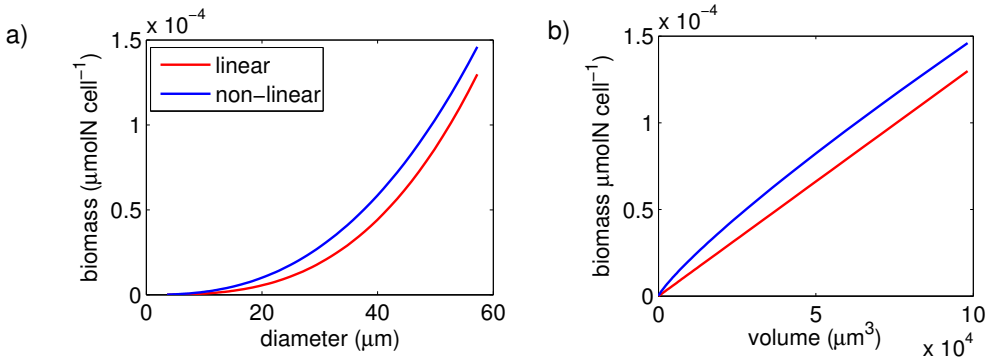

Figure 4.2: The linear (Moloney and Field,1989) and non-linear conversion (Menden-Deuer and Lessard, 2000) techniques employed to estimate biomass from particle size distributions. a) biomass along the equivalent spherical diameter distribution b) the relationship between cell volume and biomass.

(2) Uptake parameters

Allometric

Size-dependent uptake parameters, V_{max} (μmol N μmol C^{-1} h^{-1}) and K_s (μmol N L^{-1}), were calculated per size bin (Fig. 4.3) using general allometric equations (aVol^b) with values a and

b from Ward et al. (2012) (Table 4.2). Conversions of units were carried out by normalising to carbon, calculated using the linear conversion to carbon (Table 4.1). Using formulations from Ward et al. (2012), NH_4^+ uptake is faster per cell than NO_3^- and small cells take up nitrogen at faster rates and with smaller K_s values than large cells (Fig. 4.3c).

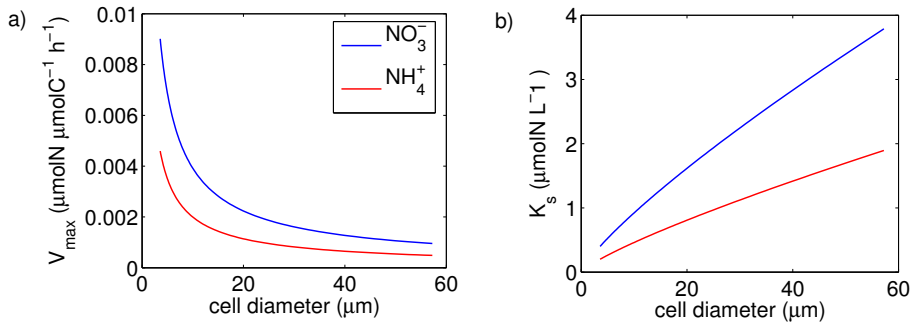

Figure 4.3: Values of Michaelis-Menten uptake parameters as a function of size, calculated using the formulations of Ward et al. (2012). a) mass specific maximum uptake rate (V_{max}) and b) half saturation constant (K_s) per cell in each size bin for NO_3^- (blue line) and NH_4+ (red line) (from Ward et al., 2012)..

Non-allometric

The non-allometric rates were calculated using a fixed V_{max} and K_s value for all bins along the size spectrum. Sensitivity of the parameter values was tested by comparing the outcome of 9 combinations of realistic values for NO_3^- : V_{max} = [0.1, 0.5, 1] , K_s = [0.5, 2, 15]; and NH_4^+: V_{max} = [0.1, 0.5, 1] and K_s = [0.1, 1, 10].

(3) Estimating uptake rates

The size-dependent parameters (Table 4.2) were applied to the Michaelis-Menten equation to calculate nitrogen uptake rate for each size bin, using nitrogen biomass per size bin and ambient nitrogen concentrations. The NO_3^- taken up by the assemblage was calculated by summing across all size bins:

$$\rho NO_3^- = \sum_{i=1} \frac{(V_{max_i} * PN_i * NO_{3_i}^-)}{(NO_3^- + Ks_i)} \tag{4.2}$$

where *PN* is the nitrogen biomass of the cells per size bin. The same equation was used to calculate NH_4^+. Estimated uptake rates (h^{-1}) were compared to the relative measured *in situ* N uptake.

Assessments were made between measured and estimated values of uptake rates of NO_3^-, NH_4^+ and total N by using an absolute percentage difference and bias estimates (Zibordi et al., 2004).

Re-examining the effects of ammonium repression

The inhibition, or more accurately, repression of nitrate uptake by ammonium was calculated using the exponential parameter function (Wroblewski, 1977; Dutkiewicz et al., 2009; Ward et al., 2012). The ammonium repression term (ψ) was estimated using the measured *in situ* data and was solved using a three variable (V_{max}, K_s, ψ) equation:

$$\rho NO_3^- = V_{max_{no_3}} \left(\frac{NO_3^-}{NO_3^- + Ks_{no_3}} \cdot e^{-\psi NH_4^+} \right) \tag{4.3}$$

For total nitrogen uptake (ρN) the uptake of NH_4^+ was incorporated:

$$\rho N = V_{max_{no_3}} \left(\frac{NO_3^-}{NO_3^- + Ks_{no_3}} \cdot e^{-\psi NH_4^+} \right) + V_{max_{nh_4}} \left(\frac{NH_4^+}{NH_4^+ + Ks_{nh4}} \right) \tag{4.4}$$

Table 4.2: Parameters and their units used to estimate biomass and uptake rates from measured particle size distributions. Where appropriate, daily rates were divided by 24 to get hourly rates. Size-dependent uptake parameters, V_{max} and K_s, are calculated as $a\text{Vol}^b$

Parameter	symbol	unit	a	b	value	Reference
cell volume	Vol	μm^3				
cell abundance per size class	N	cells L^{-1}				
mass cell $^{-1}$ per size class		μmolN cell^{-1}				
$\sum$ assemblage biomass		μmolN L^{-1}				
maximum uptake rate	$V_{max_{no3}}$	mmolN mmolC^{-1} h^{-1}	0.51	-0.27		Ward et al. (2012)
	$V_{max_{nh4}}$	mmolN mmolC^{-1} h^{-1}	0.26	-0.27		Ward et al. (2012)
half saturation constant	$K_{s_{no3}}$	mmolN m^{-3}	0.17	0.27		Ward et al. (2012)
	$K_{s_{nh4}}$	mmolN m^{-3}	0.085	0.27		Ward et al. (2012)
$\sum$ assemblage uptake rate of total N	ρN	μmolN L^{-1} h^{-1}				
$\sum$ assemblage uptake rate of NO_3^-	ρNO_3^-	μmolN L^{-1} h^{-1}				
$\sum$ assemblage uptake rate of NH_4^+	ρNH_4^+	μmolN L^{-1} h^{-1}				
ambient nutrient concentration	NO_3^-, NH_4+	μmolN L^{-1}				
NH_4^+ repression parameter	ψ	μmol N^{-1}			1.99	

Results

In situ

The range of values for measured particulate nitrogen, ambient nitrogen concentrations and uptake rates vary among the three case studies (Fig. 4.4). This variability reflects distinct assemblages observed in each case study. Highest values of particulate nitrogen (PN) were observed in Lamberts Bay (LB04 and LB05) relative to Saldanha Bay. LB05 was dominated by a dinoflagellate *Prorocentrum triestinum* with maximum particulate nitrogen reaching 146 μmol N L^{-1}, in association with lowest ambient nitrogen concentrations. SB samples had relatively low biomass (average 10.3 μmol N L^{-1}), almost completely dominated by diatoms. Highest field-measured uptake rates of total nitrogen (Fig. 4.5 a) and NO_3^- (Fig. 4.5 b) were seen in LB04, corresponding to an assemblage dominated by a ciliate *Myrionecta rubra* and a diatom (*Skeletonema* spp.) with a maximum of 0.67 μmol N L^{-1} h^{-1}. Rates of NH_4^+ uptake were lower on average than NO_3^- uptake in all case studies (Fig. 4.5 c). The size spectra measured were highly variable per sample. Figures 4.6 a, c and e show typical size distributions of a low biomass range, and Figures 4.6 b,d, and f show samples of high biomass, illustrating distributions of multi-modality.

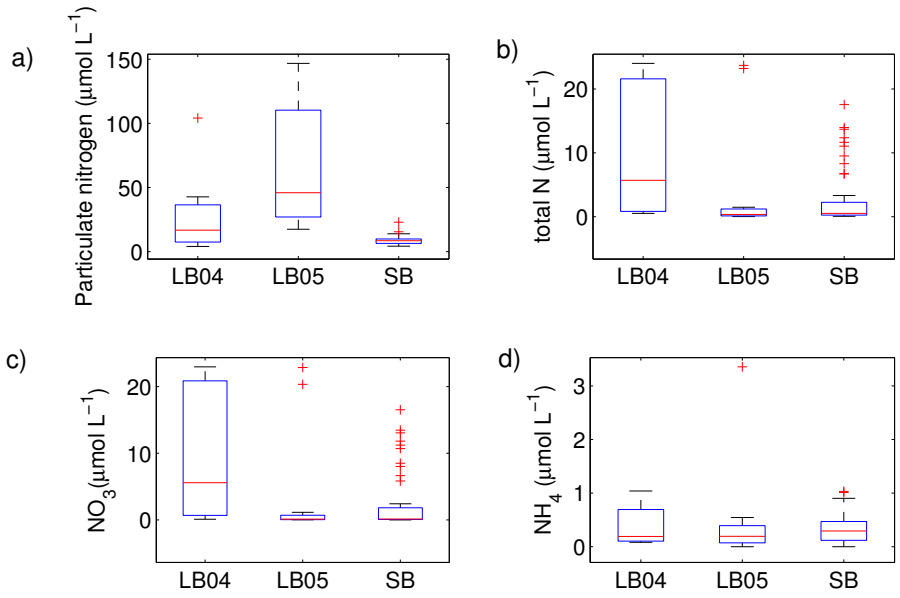

Figure 4.4: Summary box plots of the *in situ* data from Lamberts Bay 2004 and 2005 (LB04, LB05) and Saldanha Bay (SB) for a) particulate nitrogen, b) total N ($NO_3^- + NH_4^+$), c) NO_3^- and d) NH_4^+ concentrations. Boxes are medians, 25th and 75th quartiles and whiskers are extreme values not considered outliers, which are shown as crosses. SB (n=52), LB04 (n=9), LB05(n=13)

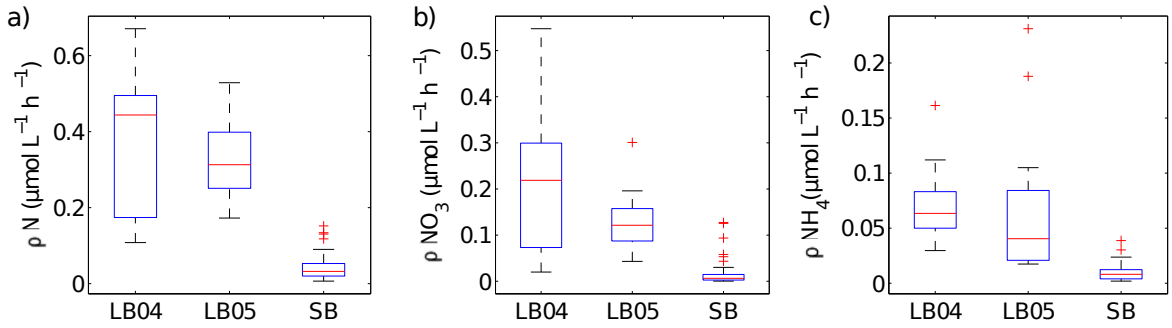

Figure 4.5: Summary box plots of *in situ* measured uptake rates for a) total nitrogen, b) NO_3^- and c) NH_4^+ for the different case studies (LB04, LB05, SB). Boxes are medians, 25th and 75th quartiles and whiskers are extreme values not considered outliers, which are shown as crosses. SB (n=52), LB04 (n=9), LB05 (n=13)

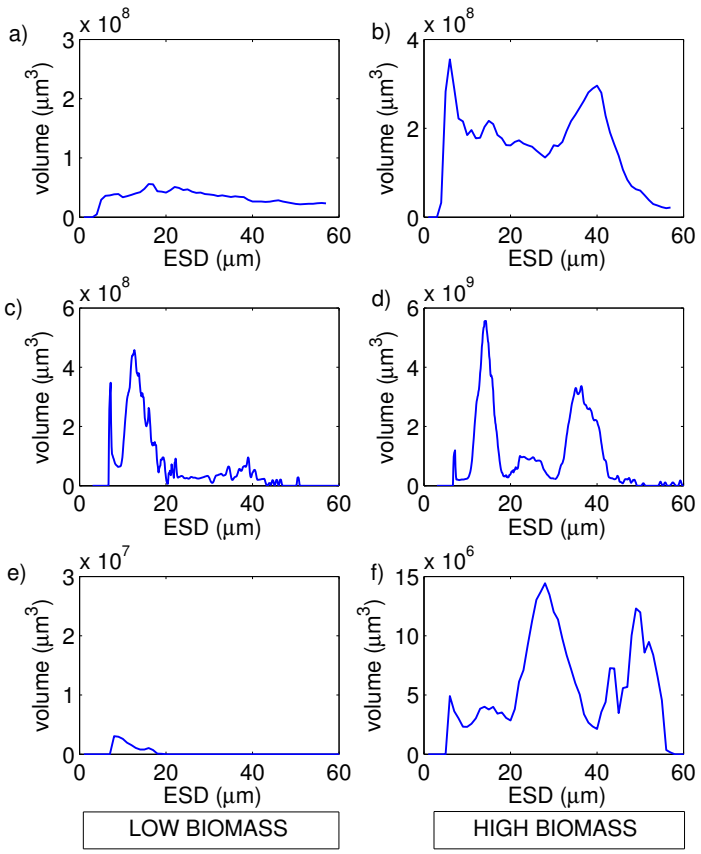

Figure 4.6: Example size spectra from the Coulter Counter for low biomass (left panels) and high biomass (right panels) for (a,b) LB04, (c,d) LB05, and (e,f) SB sample periods.

Conversions to biomass

The two methods of conversion from cell volume to mass gave estimates of particulate nitrogen that were significantly correlated with measured *in situ* values (Fig. 4.7). For the combined data set (SB and LB), the strongest correlation resulted from the non-linear conversion (r=0.78, p=1.01 x10^{-8}), although the linear conversion was almost as strong (r= 0.76, p=1.68 x10^{-8}). The two regressions comparing measured *in situ* and estimated particulate nitrogen using the linear and non-linear conversion methods, were assessed by testing H_0: slope = 1 (Table 4.4). The regression slopes for the linear and non-linear conversions were greater than one, but were not significantly different; linear ($t_{0.05,72}$=3.65,p=0.99) and non-linear ($t_{0.05,72}$=3.33,p=0.99). Both slopes provided surprisingly good predictions of biomass from particle size distributions and both conversion methods. The non-linear conversion of Menden-Deuer and Lessard (2000)

was used in further estimates of uptake rates.

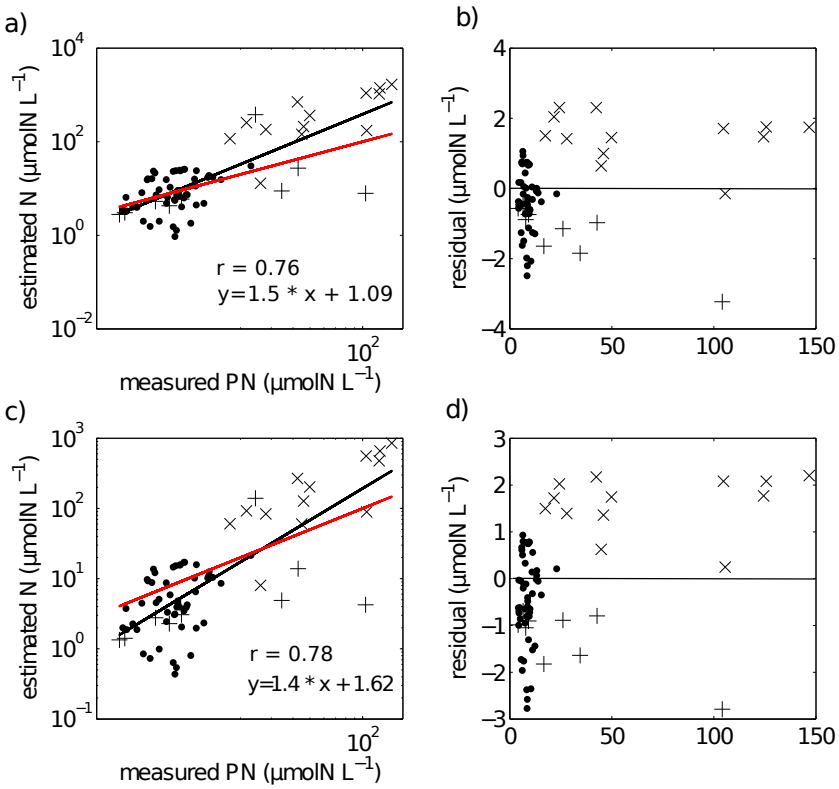

Figure 4.7: Regression analysis showing the relationships between measured and estimated particulate nitrogen using a) non-linear conversion, with b) corresponding log residuals, c) linear conversion with d) corresponding log residuals. Black line refers to fitted regression line, red line has a hypothetical slope of 1:1 such that measured=estimated values. (• SB),(+ LB04), (x LB05)

Estimating nitrogen uptake

The ranges of estimated N uptake rates were similar to those measured *in situ* (Fig. 4.8). Predictions of nitrogen uptake rates were significantly correlated with respective measured uptake rates: NO_3^- (r=0.60, p<0.05); NH_4^+ (r=0.61, p<0.05) and total N (r=0.67, p<0.05). The slopes of the relationship between measured and estimated uptake rate values were also assessed testing H_0: slope=1 (Table 4.3). The regression slopes were not statistically different from 1 for NH_4^+ ($t_{0.05,67}$=-0.26=, p=0.30) and total N ($t_{0.05,67}$=-0.26, p=0.40); this was not the case for NO_3^- ($t_{0.05,72}$=-3.06, p<0.01). An inhibition term (ψ) of 1.99 µmol N^{-1} was estimated for NO_3^- uptake. The resulting predictions for ρNO_3^- were similar to those of ρNO_3^- with no inhibition,

with an increase in bias when inhibition is included (bias ρNO_3^-= 0.03, bias $\rho NO_3^{-\psi}$= -0.72). Predictions of total N uptake do not differ greatly when an inhibition term is applied; ρN (slope= 0.97), ρN^{ψ}(slope=1.05) (Table 4.3) but more bias is introduced with an inhibition term (ρN^{ψ}=-0.89, bias ρN= -1.10). Estimations of ρNO_3^- (both with and without an inhibition term) did not match those measured *in situ* (Table 4.3). The comparisons between measured and calculated mass-specific rates also showed poor agreement, and no statistical similarity was observed between the two data sets (Table 4.3). The relationships between estimated and measured ρNH_4^+, ρN and ρN^{ψ} were not statistically different (Table 4.3) and are thus considered good predictions of the uptake of NH_4^+ and total N. The non-allometric rates were also compared with each other and an hypothetical 1:1 slope (Fig. 4.9). Of the 9 different combinations of uptake parameters tested (H_0 slope =1), one set was close to 1 but significantly different from 1 (slope = 0.96, p<0.005) for NO_3^-, and 2 sets for NH_4^+, the closest being not significantly different from 1 (slope = 1.2, p=0.78) (Table 4.4)

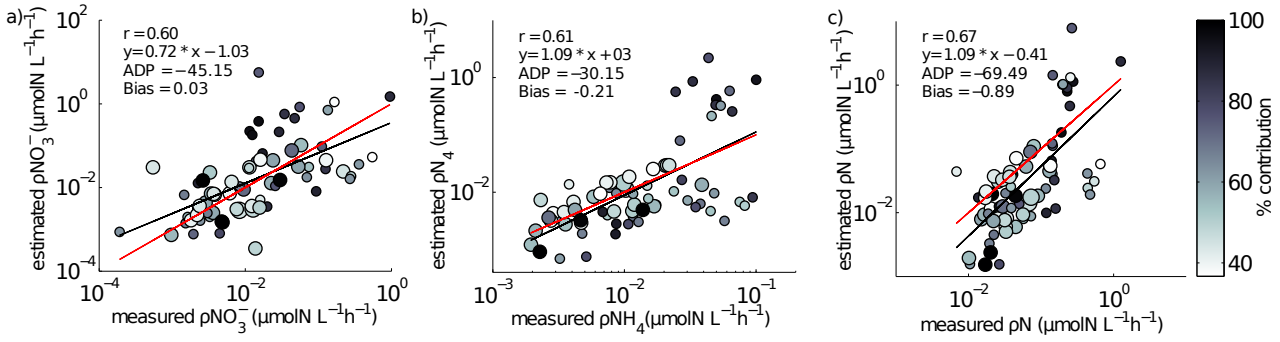

Figure 4.8: Comparisons between *in situ* measured and model estimated uptake rates using size dependent V_{max} and K_s from Ward et al. (2012). a) ρNO_3^- b) ρNH_4^+, c) ρN. Symbol size is representative of two size groups: small circle is <15 μm; large circle is 15–30 μm . The third, largest size group of 30–60 μm did not dominate uptake rates in any of the samples. Colour bar represents the percentage contribution to the bulk uptake rate by the dominant size group. Red line is a hypothetical 1:1 slope, black line is the regression between measured and model uptake rates.

Table 4.3: Comparison of regressions and t test values between *in situ* measured and calculated uptake rates of NO_3^-, NH_4^+ and total N. t= a-1/Standard Error (SE) where H_0: slope =1. DF = 72, critical value of t (1.66) and alpha (α=0.05).

	a (slope)	SE	b (intercept)	r^2	t(df=72)	p value
Particulate nitrogen						
measured v non linear estimate	1.5	0.141	-1.09	0.61	3.33	0.99
measured v linear estimate	1.4	0.144	-1.62	0.59	3.65	0.99
Absolute uptake rates						
measured v estimated ρNO_3^-	0.68	0.10	-1.36	0.37	-3.06	<0.01
measured v estimated ρNO_3^- (ψ= 1.99)	0.65	0.11	-2.25	0.32	-3.20	<0.01
measured v estimated ρNH_4^+	0.92	0.15	-0.60	0.36	$-0.51_{df=67}$	0.30
measured v estimated ρN	0.97	0.13	-0.90	0.42	-0.26	0.40
measured v estimated ρN (ψ= 1.99)	1.05	0.14	-0.88	0.44	-0.34	0.63
Mass-specific uptake rates						
measured v estimated vNO_3^-	-0.26	0.11	-2.44	0.07	-11.13	<0.01
measured v estimated vNH_4^+	0.44	0.09	0.27	0.28	-6.48	<0.01
measured v estimated vN	0.38	0.26	-3.85	0.03	-2.33	0.01

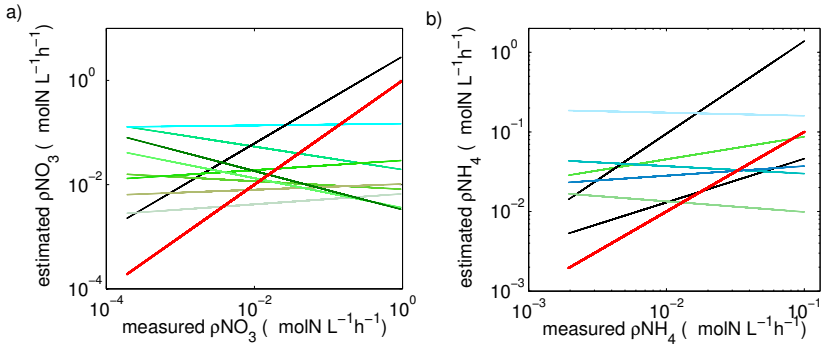

Figure 4.9: Trend lines for each combination of V_{max} and K_s for a) NO_3^- and b) NH_4^+. Red line is the hypothetical 1:1 slope, black lines represent slopes that are closest to 1 (see Table 4.4).

Table 4.4: The combination of uptake parameters (V_{max} and K_s) that resulted in the regression slope closest to 1.

	K_s	$Vmax$	a(slope)	t(df_{NO3}= 72, df_{NH4}=69)	*p*-value
NO_3^-	0.5	1	0.96	-3.72	<0.01
NH_4^+	0.01	1	1.2	0.79	0.78
NH_4^+	0.5	1	0.4	-2.30	0.01

Re-examining the effect of ammonium repression on NO_3^- uptake.

Using a three parameter (V_{max}, K_s and ψ) equation to predict mass specific vNO_3^- (h^{-1}) explains a larger portion of the observed variability in measured vNO_3^- values (r^2 = 0.4) than when using just two predictors (r^2 = 0.35) (Fig. 4.10). The solution results in an ammonium repression parameter (ψ) value of 1.99 μmol N^{-1}.

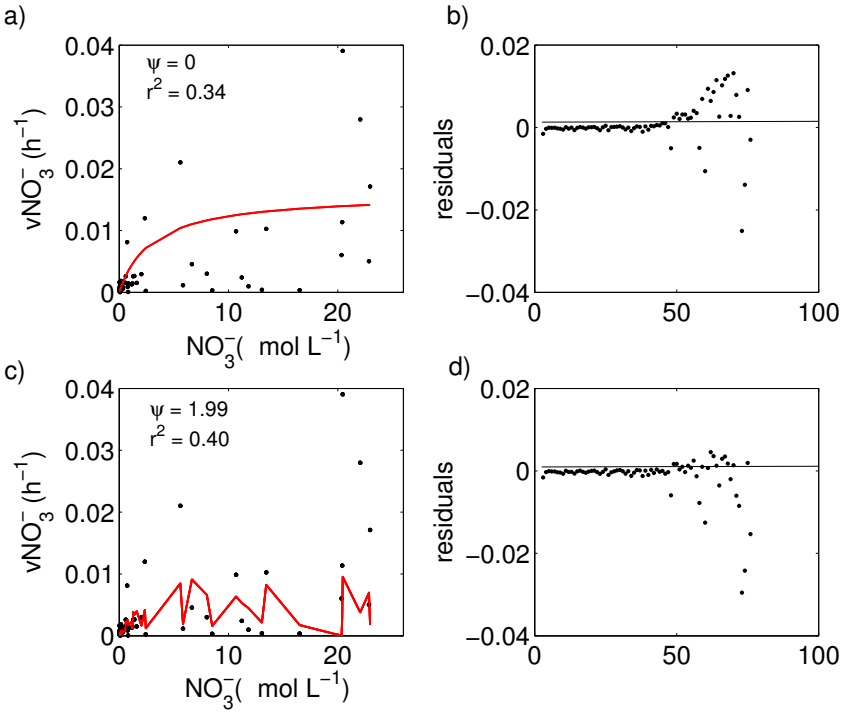

Figure 4.10: Best model fit (red line) to explain variability in observed vNO_3^- as a function of a) NO_3^- concentration and c) NO_3^- concentration and NH_4^+ repression and their respective residuals b), d).

When using the repression term (ψ=1.99), as estimated using best model fit (Fig 4.10), the predictions for ρNO_3^- are similar to those of ρNO_3^- with no inhibition, although bias is reduced (bias $\rho NO_3^{-\psi}$= 0.05, bias ρNO_3^-= 0.16). The difference in statistical significance between measured and estimated uptake values, between incorporating a repression term and not, is evident, although marginal. Predictions of total N uptake better match those measured *in situ* when an inhibition term is applied; ρN (slope= 1.07), ρN^{ψ} (slope=1.05) (Table 4.3) and much less bias (bias ρN^{ψ}= 0.06, bias ρN= 0.14). Estimations for ρNO_3^- (both with and without repression term) did not statistically match those measured *in situ* (Table 4.3). The relationships

between estimated and measured ρNH_4^+, ρN and ρN^ψ are not statistically different (Table 4.3) and are thus considered good predictions of NH_4^+ and total N uptake.

Discussion

Predictions of biomass and nitrogen uptake rates were made using measured particle size distributions of natural assemblages, volume to biomass conversions (Menden-deuer et al., 2000) and size-dependent Michaelis-Menten uptake parameters (Ward et al., 2012). The *in situ* values used to validate the modeled values had a large range and thus a large spread existed in the data. There were good correlations between estimated and measured particulate N. This strong correlation gives necessary confidence in using particle size distributions derived from the Beckman Coulter Counter to predict the uptake rates of NH_4^+, total N and to a lesser extent NO_3^-. Significant correlations were found between modeled and *in situ* measured uptake rates and the values predicted for the uptake of NH_4^+ and total N were statistically similar to values measured *in situ*.

Conversions to biomass

Both conversion models used to derive particulate nitrogen from particle size distributions (via non-linear or linear functions) yield similar results, with a good correlation between estimated and measured values. The regression equations used to estimate biomass were applied to all assemblages, which were most often mixed assemblages, i.e. containing dinoflagellates (LB05), ciliates (LB04), and diatoms (SB). LB05 had a high percentage of the dinoflagellate *Prorocentrum triestinum* at very high biomass (max. 146 μmol N L^{-1}, and the correlation coefficients for this particular data set are strongest. Even so, when applied to assemblages containing different taxa (ciliates or diatoms), overall the conversion factors performed well and the regression fit is close to a 1:1 relationship between measured and estimated nitrogen biomass. An even better fit may have resulted if group-specific conversion factors were used, but such empirical relationships for volume:nitrogen of the groups measured in this study were not found

in the literature. It is noted that diatoms, for example, contain less carbon per unit volume than other groups, attributed to their significantly higher vacuole volume (Strathmann, 1967; Sicko-Goad et al., 1984). Cellular nitrogen content or nitrogen stores have also been observed to vary considerably between different species of phytoplankton (Parsons et al., 1961; Dortch and Conway, 1984).

Further errors could have been introduced by the assumptions made in deriving particle size distributions via a Coulter Counter, which assumes sphericity of cells. This could lead to underlying bias because of non-spherical groups (e.g. dinoflagellates) or particles of elongate shape, e.g. chain-forming diatoms, which are known to introduce error and can lead to an under/overestimation of total volume (Boyd and Johnson, 1995). Furthermore, the Coulter Counter measures down to 2 μm diameter (with confidence from 5 μm) and thus omits the sub-micron range due to limitations in technical capabilities. Nevertheless, the Coulter Counter has been used in several studies to successfully derive volume to carbon ratios (Mullin et al., 1966; Strathmann, 1967; Montagnes et al., 1994) and the presented results provide confidence that such data can adequately represent the particulate biomass of the nitrogen inventory in natural, diverse assemblages in eutrophic systems, characterised by large cells and high biomass.

The data presented here show that particle size distributions convert well to a measure of biomass, despite the broad scale application of a dinoflagellate volume:nitrogen conversion to mixed assemblages, the exclusion of sub-micron size ranges, and the assumptions of sphericity when using the Coulter counter. It has been noted that quantitative measurements of particulate carbon/nitrogen are in general lacking (Behrenfeld et al., 2006), and it is suggested that Coulter Counter derived PSDs can provide adequate measures of nitrogen biomass, most notably, when examining communities in eutrophic systems. Such conversions may not be as successful in oligotrophic areas, where cell size distributions are characteristically dominated by pico/nano-plankton (<2 μm), but would need further investigation.

Estimating uptake rates

A significant correlation exists between the estimated and measured uptake rates of NO_3^-, NH_4^+ and total N, for natural assemblages. The slopes of the regressions for the estimated versus measured values of NH_4^+ and total N uptake were close to 1, indicating statistical similarity to what was measured in situ. The size-dependence of the Michaelis-Menten uptake parameters, V_{max} and K_s, used by Ward et al. (2012), proved to be adequate values and yielded comparable results of nitrogen uptake to what had been measured *in situ*. Several studies have called into question the adequacy of the Michaelis-Menten kinetics equation to describe nutrient uptake in phytoplankton (Droop, 1974; Pasciak, 1974; Aksnes and Egge, 1991). These criticisms are based on the premise that the equation does not account for differences in uptake rates in limiting or non-limiting conditions (Rhee, 1974; Grover, 1991), or that internal stores of nutrients can dictate uptake based on simple diffusion limitation (Droop, 1974). Both Michaelis-Menten uptake parameters are subject to variability, not only in different species but due to differences in nutrient availability and varying environmental conditions (Lomas and Glibert, 1999; Collos et al., 2005 and references therein). Smith et al. (2009) suggest that optimal uptake kinetics, which accounts for physiological acclimation to fluctuating environmental conditions, is a superior alternative to standard Michaelis-Menten descriptions of V_{max} and K_s. A flexible phytoplankton functional type (FlexPFT) model (Smith et al., 2015), which resolves the dynamic response of phytoplankton communities, was able to reproduce productivity and Chl-*a* values of two contrasting time series better than when no flexible response was included. Thus, the limitations of Michaelis-Menten are recognised, more particularly in its assumption that parameter values are constant during environmental fluctuations. However, its use will most likely remain popular due its simplicity and the availability of parameter values in the literature. The variability of *in situ* measured uptake rates of NH_4^+ and total N is statistically matched by the variability in what was estimated using size-scaled parameters, which implies that much of the variability in Michaelis-Menten parameters, when applied at an assemblage scale, can be accounted for by simple size scaling of V_{max} and K_s. The results also imply that net community rates of NH_4^+ and total nitrogen uptake are driven by ambient concentrations and cell size.

As expected, the case for NO_3^- was more complex. Although the slope of the estimated ρNO_3^- was positive and close to 1, statistically it was significantly different from 1, and reveals the potential importance of other influencing factors, in addition to cell size and ambient concentration. The repression of NO_3^- uptake by NH_4^+ may explain some of the variability observed in *in situ* measured values that is not accounted for in the model estimates. Numerous studies have shown an interaction between NH_4^+ and NO_3^- uptake (e.g. McCarthy et al., 1975; Muggli and Smith, 1993; Harrison et al., 1996). NH_4^+ is generally considered to repress the uptake of NO_3^- (Dortch, 1990) but this is observed to be a highly variable process, where NH_4^+ can have little to no effect on NO_3^- uptake (Kokkinakis and Wheeler, 1987) or can enhance rather than inhibit NO_3^- uptake (Dortch, 1990). The extent to which NH_4^+ will affect NO_3^- uptake is not just species-dependent, but is also affected by physiological state and the preconditioning nutrient concentrations (Varela and Harrison, 1999; L'Helguen et al., 2008). Equally, the concentration of NH_4^+ at which repression of NO_3^- uptake occurs varies between systems (Dortch, 1990; Dugdale et al., 2006, 2007; Probyn et al., 2015). The effect of incorporating a repression/inhibition term, in this case, made little difference to the estimates of ρNO_3^- and ρN. A range of inhibition parameter values used in other studies were also investigated, ranging from 1.5 (Kishi et al., 2007) to 4.6 (Dutkiewicz et al., 2009), with little significant change in statistical comparisons. The value of 1.99, the outcome of a best fit model to the NO_3^- uptake values for this study, was deemed optimal for the range of values measured. Another suggestion to explain the deviations from Michaelis-Menten kinetics for NO_3^- uptake, is the potential for 'shift-up' kinetics described in Dugdale et al (1990; 2006). It was observed that NO_3^- uptake may not follow Michaelis-Menten kinetics consistently along the upwelling timeframe, where initial (highest) concentrations of NO_3^- will not equate to highest uptake rates, as communities take time to respond to new injections of NO_3^-.

The predictions did not work when measured and calculated biomass-specific rates (h^{-1}) were compared (Table 4.3). This is not surprising. The measured uptake rates result from an interplay between ambient nitrogen concentrations, total particulate nitrogen and the structure (size and taxa) of the phytoplankton assemblage, which will affect mass-specific rates as well

as affinity for nitrogen. Mass-specific values influence physiological efficiency, with small cells having faster mass-specific rates and greater affinity for nitrogen at low concentrations than large cells. These influences of assemblage structure cannot be accounted for when dividing uptake rates by measured particulate nitrogen. Much of the uptake signal is dominated by the small fractions (<15 μm) of the size spectra (Fig. 4.8) and highest uptake rates are observed when the small size fractions dominate and thus biomass is low, illustrating that the successful predictions of uptake rates is not driven by high biomass. Absolute uptake rates can be considered an 'ecosystem' metric of nitrogen dynamics, and this study shows that, in a eutrophic environment, size-scaled MM parameters can be used to predict NH_4^+ and total N uptake, keeping the numbers of parameters to a minimum and thus minimising uncertainty associated with each parameter. Data to constrain added parameters are not available from the *in situ* experiments. The non-allometric predictions, which use constant V_{max} and K_s values across the entire spectrum resulted in a variety of regression slopes, with few matching a 1:1 relationship. The kinetic parameter values used all fall within a realistic range observed in the region, and of the nine combinations tested (Fig. 4.9), no significant prediction was made for NO_3^- (although the slope was close to 1) and one successful prediction was made for NH_4^+. However, it would be difficult to know in advance which parameter values to use, whereas the allometric calculations produced good matches to the observations.

Conclusions

The Michaelis-Menten uptake equation was applied to particle size distributions to calculate the size-dependent uptake of NO_3^- and NH_4^+. A size dependence of uptake kinetic parameters was included so as to make cell size intrinsically constrained in the Michaelis-Menten uptake equation. A large proportion of the variability observed in uptake rates of nitrogen measured *in situ*, in various assemblages, was explained by ambient nutrient concentrations and cell size, in spite of several simplifications and sources of error. The case for NO_3^- uptake was not as strong as NH_4^+ and is suggested to be due to the complex suppressive behaviour of NH_4^+ on NO_3^- uptake

as well potential 'shift-up' effects observed in upwelling systems. In addition, accounting for the internal storage of NO_3^- may have improved estimations of ρNO_3^-, but are beyond the scope of these data. Nevertheless, realistic approximations of nitrogen uptake, and thus new production (Dugdale and Goering, 1967), are achieved when using size-scaled Michaelis-Menten uptake parameters and particle size distributions. The strength of this study lies in its application to *in situ* measurements of cell size distributions and ambient nutrient concentration, to derive approximations of nitrogen uptake. Further research is recommended to include Dissolved Organic Nitrogen uptake rates into approximations of total N uptake, given its significant contribution to total production (Harrison et al., 1985; Probyn, 1988). This is no menial task however, given its complex kinetic behaviour (Eppley et al., 1971; Bronk et al., 2004; Solomon et al., 2010) and current lack of size-scaling relationships in the literature. New production, considered to be the portion of primary production with the highest implications for carbon export or the flow of energy to higher trophic levels (Probyn, 1992; Hutchings, 1992; Dugdale et al., 2006), is a useful measurement in studies of ecosystem dynamics. In the absence of laborious and expensive ^{15}N data, the use of particle size distributions to estimate nitrogen uptake can be a useful tool in assemblage scale studies of nitrogen dynamics in productive coastal upwelling systems.

Chapter 5

Summary and conclusions

Chapter Summary

Chapter 2: Can effective diameter capture the nitrogen utilisation by high biomass blooms at upwelling/downwelling timescales?

The presence of large cell sizes, in high biomass, is often associated with harmful algal blooms in the southern Benguela. In some instances, a single value phytoplankton size proxy, effective diameter (D_{eff}), representative of the gross optical characteristics of the assemblage, can indicate the presence of large celled, high biomass blooms using remote sensing data (Evers-King, 2014). The biogeochemical relevance of such a metric, which is closely related to the proliferation of high biomass blooms, was evaluated in this chapter. The nitrogen utilisation of two separate blooms in 2004 and 2005 in Lamberts Bay, dominated by harmful algal species (*Myrionecta rubra* and *Prorocentrum triestinum),* set the necessary scene to be able to evaluate the usefulness of such a metric. The nitrogen uptake was assessed in relation to environmental conditions and community structure. Relationships between D_{eff} and the uptake rates of nitrogen were quantified.

The main findings of this chapter were:

- In 2004, *Myrionecta rubra* were present in both upwelling and downwelling conditions and proliferated to high biomass (104 μmol N L^{-1}) with high rates of primary productivity (303 mgC m^{-3} h^{-1}). They showed a wide range in nitrogen use during their proliferation, as evidenced by the wide range in *f*-ratios (0.1 and 0.74) in samples in which they dominated the biomass.
- In 2005, *Prorocentrum triestinum* reached even higher biomass (147 μmol N L^{-1}) and primary productivity (340 mgC m^{-3} h^{-1}). Their proliferation was associated with conditions characteristic of harmful algal blooms: stratified and NO_3^- depleted waters.
- Urea appeared to be an important source of nitrogen during both harmful algal blooms.
- Significant regressions showed that D_{eff} proved to be useful in quantifying the uptake of NH_4^+ (r=-0.54, p<0.005) and urea (r=-0.59, p<0.005).
- No significant relationship between vNO_3^- and D_{eff} was found. However, a positive correlation was evident between *f*-ratio (vNO_3^-/ [vNO_3^- + vNH_4^+ + urea]) and D_{eff}, implying that D_{eff} can represent the bulk nitrogen dynamics in high biomass algal assemblages.
- The lack of a significant relationship between vNO_3^- and D_{eff} was suggested to be due to multi-modality in the size distributions of several samples as well as the presence of diatoms, which might have obscured the relationship due to genus/species-specific nutrient utilisation strategies.

Several limitations to this study are acknowledged. Firstly, this research does not consider the effect of top-down influences in structuring the phytoplankton assemblages, and subsequently the rates of nutrient uptake. Secondly, the nutrient pre-history of assemblages can play an important role in influencing the rates of nutrient uptake (Harrison et al., 1996), most notably NO_3^-, and were not considered in the analyses. Finally, quantitative insight might have been gained into the relationship (or lack thereof) between vNO_3^- and D_{eff} had the microscopy samples been sized. A comparative approach between microscopy and the Coulter Counter size distributions would have been useful. As a result, several questions arose that merit further consideration.

- How well does the effective diameter (derived from Coulter Counter derived size distributions) compare to other metrics of assemblage size? e.g. mean trait, trait variance, mean assemblage volume as derived from microscopy counts.

- How do the different methods to derive size distributions (e.g. Coulter Counter and flow cytometry) compare in their output of an effective diameter? The use of a flow cytometer would facilitate a broader range in cell sizes (pico to micro plankton).

Chapter 3: What are the strongest factors influencing nitrogen uptake in diatom-dominated assemblages? Can effective diameter represent the bulk nitrogen dynamics in such assemblages?

In the previous chapter, the variable presence of diatoms was suggested to be one factor reducing the strength of the relationship between vNO_3^- and D_{eff}. Diatoms are observed to display strong species-specific strategies of nutrient uptake. Phytoplankton assemblages measured in a year-long case study in Saldanha Bay were diatom-dominated throughout the sample year, consequently providing a good record of the variability in nitrogen nutrition of diatoms as a group, under varying environmental conditions. Variability in the uptake rates of NO_3^-, NH_4^+ and urea was assessed in relation to environmental conditions and community structure. Concurrent kinetic experiments were also carried out to provide a deeper physiological basis to potentially explain observed patterns in N uptake. And finally the relationships between nitrogen uptake rates and D_{eff} were assessed. The main findings of chapter 3 were:

- The variability in uptake rates of all nitrogen forms was mostly accounted for by ambient concentrations, and in many deeper samples (>6m), both in winter and summer, light limitation. Nutrient limitation at the surface was a prominent feature during summer months as injections of NO_3^--rich bottom waters rarely protruded the strong thermocline.

- Concurrent uptake kinetic experiments revealed high variability in Michaelis-Menten uptake parameters for NO_3^- and NH_4^+. It is suggested that ambient nitrogen concentrations

as well as taxon-specific uptake strategies were strong factors influencing the variability in the uptake parameters.

- Urea did not conform, in any instance, to the saturating nature of Michaelis-Menten, suggested to be potentially due to over-estimations of 'biologically available' urea as a result of the method of analysing urea.

- Qualitative relationships were observed between the mass-specific uptake rates of regenerated nitrogen and D_{eff}, but no significant relationship was observed for NO_3^-. This was suggested to be potentially due to the presence of chain forming diatoms and comparatively lower biomass and a smaller range in size distributions than observed in the previous chapter.

In addition to such findings, several limitations were recognised in this study: First, the effects of diatom chain-formation on the size distributions measured via a Beckman Coulter Counter were assumed to be negligible. The approximations of biovolume did not consider all of the species observed in the microscopy samples. But the most numerous and largest cell sizes were considered to contribute a large enough signal to assemblage dynamics to assess their influences. Further, the incubation times to estimate the nutrient uptake rates were longer than the 2-6hrs usually advised for such experiments. Several questions arose that merit deeper investigation.

- How could multi-modality in size distributions be accounted for?

- How does the presence of chain-forming diatoms affect a) the accurate measurement of particle cell size distributions and b) the calculations of effective diameter from the Coulter Counter? How do they compare to measurements from flow cytometry?

Chapter 4: Can a size-based approach to phytoplankton diversity and nitrogen dynamics account for the variability observed in measured *in situ* nitrogen uptake rates by natural populations?

Quantifying the nitrogen dynamics in a way that reflects the diversity in phytoplankton assemblages is an exciting area of current research. This chapter took a size-based approach to estimating nitrogen uptake, by applying the Michaelis-Menten uptake equation to measured particle size distributions, and calculating the size-dependent uptake rates of NO_3^-, NH_4^+ and total nitrogen (NO_3^- + NH_4^+). The main findings of chapter 4 are:

- Size distributions from the Beckman Coulter Counter were adequate means of quantifying the particulate biomass (μmol N L^{-1}) of measured assemblages via linear (Moloney and Field, 1989) or non-linear relationships (Menden-Deuer and Lessard, 2000).
- The calculated values of NH_4^+ and total N uptake integrated across all size classes were similar to those of *in situ* bulk measurements (N slope=0.90), (NH_4^+ slope=0.96), indicating dependence of NH_4^+ and total N uptake on ambient N concentrations and cell size distributions of the phytoplankton assemblages.
- NO_3^- uptake was less well explained by cell size and ambient concentrations, but correlation coefficients between measured and estimated NO_3^- uptake rates were still significant.
- Cell size distributions, ambient nutrient concentrations and size-dependent Michaelis-Menten uptake parameters are sufficient to derive accurate approximations of nitrogen uptake rates.

Several limitations to this study are acknowledged. First, this chapter did not include Droop formulations of NO_3^- uptake to account for internal storage of NO_3^-. Many of the samples used in this study displayed high abundance of diatoms, whose physiology is dependent upon the capacity to store nutrients. It became evident that accounting for the cellular storage of NO_3^- might have improved model predictions. Second, further recognised is what Dugdale et al.

(2006) pointed out regarding the need for formulations of NO_3^- uptake that are specific to upwelling systems. Suggestion made in their study were not addressed, but the results of the behaviour of NO_3^- in all three chapters lead to consideration of further possible formulations of the uptake model. Subsequently, several questions arose that merit further consideration in future studies, also addressed in 'Future Directions'.

- Would the inclusion of multi-phasic kinetic parameters (Collos et al., 2005) improve estimates of NO_3^- uptake? This would involve setting thresholds of ambient NO_3^- concentrations for when different transport systems would be activated.
- How would Droop formulations (size-dependent nitrogen storage) compare with Michaelis-Menten formulations? Assumptions could be made on the size-dependence of internally stored N.
- Could simulations of size distributions using effective diameter and effective variance *(sensu* Arduini et al., 2005) be used to estimate nitrogen uptake rates? This could potentially extend the EAP algorithm to produce an approximated N flux value for observed algal assemblages using remote sensing data.

Conclusions

Functional diversity in natural assemblages: the case for nitrogen

One underlying theme throughout this thesis was the representation of functional diversity in algal assemblages by the means of a measurable trait, cell size. The collation of available trait data in the literature (see Edwards et al. 2015) will undoubtedly spur on many further studies (e.g. Lindemann et al., 2016) regarding the variability in the many measured traits, most of which come from culture experiments. This research considered cell size and simplified size distribution proxies in natural assemblages, exposed to the fluctuating dynamics of a natural system. Thus, disentangling the concomitant factors on how cell size influences nitrogen dynamics in a natural system will have some inevitable assumptions. Moreover, the use of a

single value to represent the bulk properties of the assemblage will sometimes introduce some error. Nevertheless, on the whole, cell size was strongly correlated to the uptake of regenerated forms of nitrogen. This was evidenced when cell size was considered as D_{eff} (Chapter 2) and as entire size distributions (Chapter 4). In cases of no quantitative relationship (Chapter 3), the usefulness of D_{eff} was questionable in samples of low biomass, smaller size range and dominated by many chain-forming diatoms. The uptake of NO_3^- appeared less constrained by cell size when quantified as D_{eff} (Chapter 2 and 3), but the relationship is very promising when the entire size distribution is considered (Chapter 4). This reveals some differences between small and large cells and their capacity to utilise NO_3^-. The metabolic pathways involved in the assimilation of NH_4^+ and to a lesser extent, urea, are simpler and turnover rates shorter than for NO_3^- assimilation. Thus, it is suggested that the uptake of regenerated forms of nitrogen is consistent within the constraints of allometric scaling across the size spectrum, but NO_3^- may not be. Trait-based approaches to nitrogen dynamics, more specifically in upwelling systems, require the size spectrum as a whole to adequately quantify NO_3^- fluxes.

The effective diameter as a single value size proxy.

The effective diameter, D_{eff}, is a product of the equivalent algal population (EAP) algorithm that has been shown to be a quantitative, representative, size metric for the bulk bio-optical properties of algal assemblages (Bernard et al., 2009; Evers-King et al., 2014). Given the high frequency of harmful algal blooms in the region that are associated with large cells, and by proxy high biomass, the single-value size metric provides a useful platform in detecting the presence of certain harmful algal blooms (Evers-King, 2014). Furthermore, as D_{eff} is considered a representative of the dominant size class of an assemblage, it is also possible, and theoretically plausible, that further inferences from satellite data could be made of the biogeochemistry. This would involve regression relationships between phytoplankton cell size and nutrient fluxes. In this thesis, the assessments made of D_{eff} in relation to nitrogen uptake revealed some promising results. In blooms of potentially harmful algal species at high biomass, the relationships between D_{eff} and mass-specific uptake rates of regenerated nitrogen were significant, but for

NO_3^- the situation was more complex. But, in samples of comparatively lower biomass, quantitatively useful relationships between the uptake rates for all nitrogen sources and D_{eff} were not evident. Given that regenerated nitrogen is often an important nutritional component of some HABs in the southern Benguela (Seeyave et al., 2009) and HABs are often observed in high biomass (Pitcher et al., 1998a), D_{eff} can be considered a useful metric in describing regenerated nitrogen dynamics in HABs. The conclusion from the previous section can also be affirmed; regenerated nitrogen appears to be constrained by allometric dependencies, but the uptake of NO_3^- is affected to a significantly lesser extent. Further work is needed to understand when the departures from allometric scaling laws are significant in quantifications of NO_3^- uptake.

Future directions

- ***In situ* observations:** Robust evidence from observational data shows that upwelling-favourable winds have intensified, most notably at higher latitudes (Rykaczewski et al., 2015; García-Reyes et al., 2015). The potential effects of this on the functioning of the Benguela upwelling ecosystem are yet to be mechanistically understood, opening many avenues for future research. Our current understanding is that differences between periods of upwelling-favourable winds and downwelling-favourable winds mark bottom-up selective criteria for anchovy and sardine respectively (van der Lingen et al., 2006), large diatoms favouring anchovies and small dinoflagellates favouring sardines. The St Helena Bay monitoring line offers a time series (from 2000-2007) of *in situ* particle size distributions that may provide some insight into the patterns of cell size and environmental conditions at longer time scales than what is currently published. Can the dynamics in phytoplankton cell size distributions shed any light on long-term trends in the shifts between dinoflagellate and diatom dominance in response to changes in physical forcing? Routine measurements of more extensive information on the phytoplankton assemblages using an imaging FlowCytoBot would greatly enhance studies of phytoplankton diversity.

Relationships between phytoplankton diversity, dominant cell size and the nature of the physical forcing at longer time scales would be informative.

- **The EAP algorithm to infer approximate products of biogeochemistry:** One of the major findings of this thesis was that the shape of particle size spectra can provide valuable information on the rates and dynamics of nitrogen (see chapter 4). In the absence of *in situ* measurements of particle size distributions, it is suggested that satellite-derived products, such as D_{eff}, can provide some information on the bulk properties of natural assemblages. In the context of nitrogen, D_{eff}, in itself, was only adequate under certain circumstances and thus further information is needed to quantify biogeochemistry. The generation of particle size distributions (sensu Arduini et al., 2005) by combining D_{eff} with other parameters, such as an effective variance (the width of the distribution), is hypothesised to be a potential method that can provide greater detail from satellite-derived ocean color products. Figure 5.1 illustrates a framework that depicts the guiding steps to inferring nitrogen dynamics from remote sensing data. The framework opens up several key avenues of future work which relate to testing the assumptions and sensitivities associated with 1) generating the size spectra and 2) improving the size-dependent nutrient uptake model. A preliminary/exploratory discussion of each, in the context of the suggested framework (Fig. 5.1) as well as in their own right, is provided below. Preliminary results (Fig 5.2) suggest that in the absence of *in situ* measurements, D_{eff} can be used (either as a single value or in concert with effective variance) to approximate the nitrogen utilisation rates of natural assemblages in a eutrophic system, such as the southern Benguela. Appendix I details the methods used in the preliminary assessments made in figure 5.2.

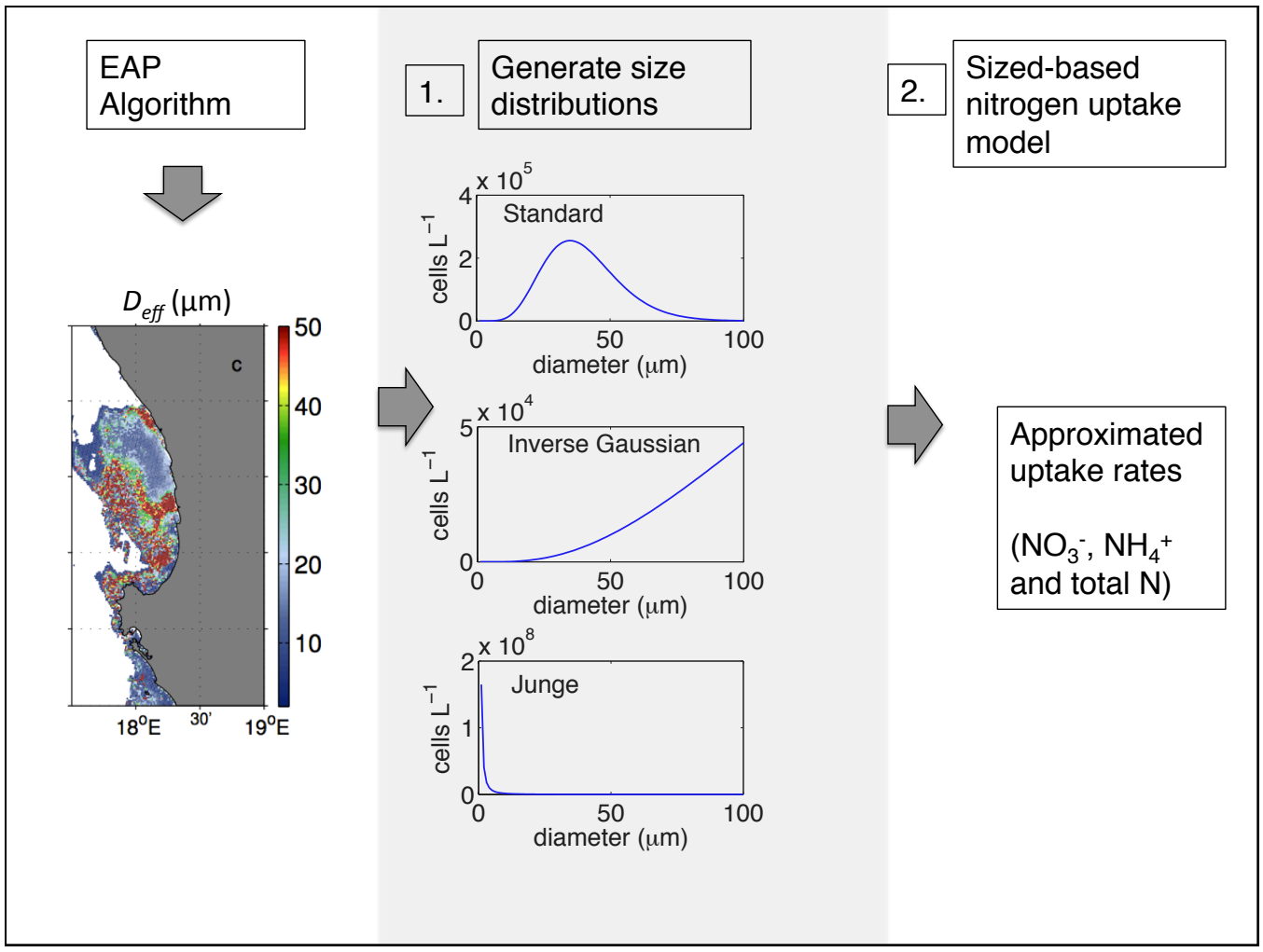

Figure 5.1: Simplified schematic depicting the broad themes of future research, relating to the generation of size spectra from satellite derived products such as effective diameter (D_{eff}) and the improvement and extension of the nitrogen uptake model described in Atkins et al. (2016).

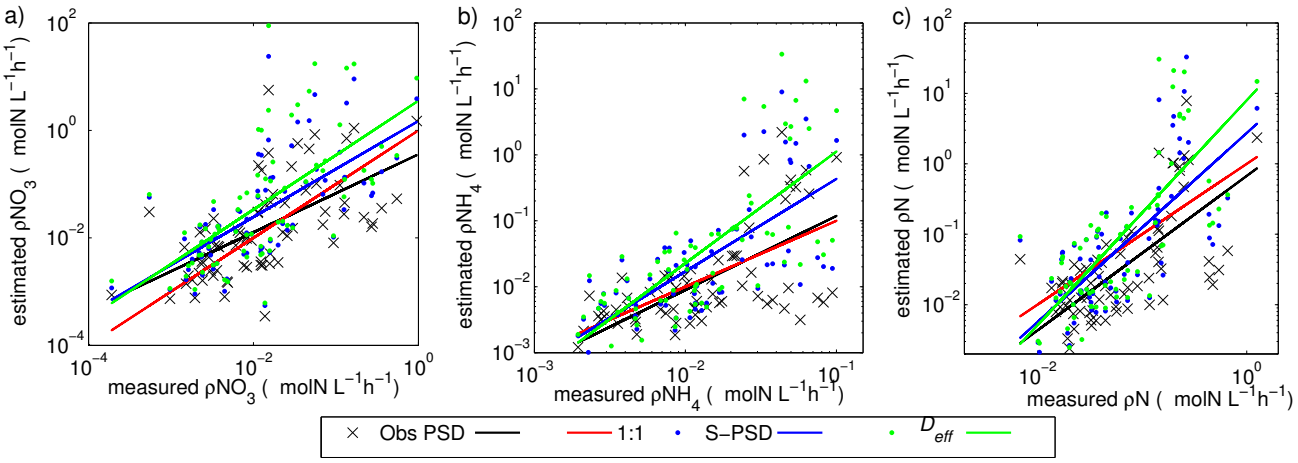

Figure 5.2: Preliminary results of the comparison between the different representations of the size distributions in the calculations of uptake rates for a) NO_3^-, b) NH_4^+ and c) total N . The 'obs PSD' (in black) uses the measured size distributions as described in chapter 4. 'S-PSD' (in blue) is a standard distribution generated using the calculated effective diameter and effective variance (as outlined in Fig. 5.1 and described in Bernard et al., 2007). The 'D_{eff}' (in green) uses simply the D_{eff} value and assumes total volume (as a proxy of biomass) is found within the single size class. See Appendix I for methods used and Table A1 for resultant values .

1. **The size spectra:** Quantifying the size spectra is of use in studying the flow of energy in ecological systems. Many studies use the slope and intercept of size spectra (e.g. Canales et al., 2015) but the effective diameter (derived from satellite data) and effective variance are attractive alternatives (e.g. Arduini et al., 2005). Beyond simply feeding into what is depicted in Figure. 5.1, satellite-derived size spectra may be used to explore ecological patterns in phytoplankton dynamics at scales not available from *in situ* measurements. It was recognised in this thesis and in other studies (e.g. Acevedo-Trejos et al., 2016) that describing multi-modality in size distributions is a challenge in size-based quantifications of biomass and biogeochemistry. How can we effectively account for multi-modality? Further work is required to estimate the errors associated with using the generated size spectra in an ecological context.

2. **Extension of the size-dependent nutrient uptake model:** The adequate representations of nutrient uptake remains a popular theme in the literature (e.g. Edwards et al., 2015; Lindemann et al., 2016). The model presented in this thesis showed a high degree of reproducibility of the observed nitrogen uptake rates, but there remains much scope to

improve estimations of NO_3^- uptake. Accounting for an internal quota (Droop, 1973), applying multi-phasic kinetic parameters (Collos et al., 2005) and the non-linearity in uptake affinities (Lindemann et al., 2016) may all potentially improve on the model proposed in this thesis and in Atkins et al. (2016).

2465

References

Acevedo-Trejos, E., Brandt, G., and Merico, A. (2015). Mechanisms shaping phytoplankton community structure and diversity in the ocean. *Nature*, 5:17–20.

Acevedo-Trejos, E., Brandt, G., Merico, A., and Smith, S. L. (2013). Biogeographical patterns of phytoplankton community size structure in the oceans. *Global Ecology and Biogeography*, 22(9):1060–1070.

Acevedo-Trejos, E., Brandt, G., Smith, S. L., and Merico, A. (2016). PhytoSFDM version 1.0.0: Phytoplankton Size and Functional Diversity Model. *Geoscientific Model Development Discussions*, (May):1–22.

Acevedo-Trejos, E., Brandt, G., Steinacher, M., and Merico, A. (2014). A glimpse into the future composition of marine phytoplankton communities. *Frontiers in Marine Science*, 1(July):1–12.

Agawin, N. S. R., Duarte, C. M., and Agusti, S. (2000). Nutrient and temperature control of the contribution of picoplankton to phytoplankton biomass and production. 45(3):591–600.

Aksnes, D. and Egge, J. (1991). A theoretical model for nutrient uptake in phytoplankton. *Marine Ecology Progress Series*, 70:65–72.

Aksnes, D. L. and Cao, F. J. (2011). Inherent and apparent traits in microbial nutrient uptake. *Marine Ecology Progress Series*, 440:41–51.

Alexandrov, M. D. and Lacis, A. A. (2000). A new three-parameter cloud / aerosol particle size distribution based on the generalized inverse Gaussian density function. 116:153–165.

2485 Allen, J. I. and Fulton, E. (2010). Top-down, bottom-up or middle-out? Avoiding extraneous
2486 detail and over-generality in marine ecosystem models. *Progress in Oceanography*, 84(1-
2487 2):129–133.

2488 Alvain, S., Loisel, H., and Dessailly, D. (2012). Theoretical analysis of ocean color radiances
2489 anomalies and implications for phytoplankton groups detection in case 1 waters. *Optics Ex-*
2490 *press*, 20(2):1070–1083.

2491 Alvain, S., Moulin, C., Dandonneau, Y., and Breon, F. (2005). Remote sensing of phytoplankton
2492 groups in case 1 waters from global SeaWiFS imagery. *Deep Sea Research*, 52:1989–2004.

2493 Alvain, S., Moulin, C., Dandonneau, Y., and Loisel, H. (2008). Seasonal distribution and suc-
2494 cession of dominant phytoplankton groups in the global ocean: A satellite view. *Global Bio-*
2495 *geochemical Cycles*, 22(3):1–6.

2496 Andersen, K. and Beyer, J. (2006). Asymptotic size determines species abundance in the
2497 marine size spectrum. *The American Naturalist*, 168(1):54–61.

2498 Anderson, D. M., Cembella, A. D., and Hallegraeff, G. M. (2012). Progress in Understanding
2499 Harmful Algal Blooms: Paradigm Shifts and New Technologies for Research, Monitoring, and
2500 Management. *Annual Review of Marine Science*, 4(1):143–176.

2501 Anderson, D. M., Glibert, P. M., and Burkholder, J. M. (2002). Harmful algal blooms and eu-
2502 trophication: nutrient sources, compositions, and consequences. *Estuaries*, 25(4):704–726.

2503 Anderson, T. R. (2005). Plankton functional type modelling: running before we can walk?
2504 *Journal of Plankton Research*, 27(3).

2505 Arduini, R., Minnis, P., Smith Jnr, W., Ayers, J., Khaiyer, M., and Heck, P. (2005). Sensitivity of
2506 satellite-retrieved cloud properties to the effective variance of cloud droplet size distribution.
2507 In *Fifteenth ARM Science Team Meeting Proceedings*, pages 1–13, Daytona Beach, Florida.

2508 Armstrong, R. (2006). Optimality-based modeling of nitrogen allocation and photoacclimation in

2509 photosynthesis. *Deep-Sea Research Part II: Topical Studies in Oceanography*, 53(5-7):513–
2510 531.

2511 Arteaga, L., Pahlow, M., and Oschlies, A. (2014). Global patterns of phytoplankton nutrient and
2512 light colimitation inferred from an optimality-based model. *Global Biogeochemical Cycles*,
2513 28(7):648–661.

2514 Atkins, J. F., Moloney, C. L., Probyn, T. A., and Bernard, S. (2016). *In situ* measurements
2515 and model estimates of NO3 and NH4 uptake by different phytoplankton size fractions in the
2516 Southern Benguela upwelling system. *Frontiers in Marine Science*, 3(3):1–11.

2517 Ault, T. (2000). Vertical migration by the marine dinoflagellate *Prorocentrum triestinum* max-
2518 imises photosynthetic yield. *Oecologia*, 125(4):466–475.

2519 Aumont, O., Ethé, C., Tagliabue, A., Bopp, L., and Gehlen, M. (2015). PISCES v2: an ocean
2520 biogeochemical model for carbon and ecosystem studies. *Geoscientific Model Development*
2521 *Discussions*, 8(2):1375–1509.

2522 Azam, F. and Malfatti, F. (2007). Microbial structuring of marine ecosystems. *Nature reviews.*
2523 *Microbiology*, 5(10):782–791.

2524 Baird, M. E. and Suthers, I. M. (2007). A size-resolved pelagic ecosystem model. *Ecological*
2525 *Modelling*, 203(3-4):185–203.

2526 Bakun, A. (1990). Global climate change and intensification of coastal ocean upwelling. *Science*
2527 *(New York, N.Y.)*, 247(4939):198–201.

2528 Bakun, A., Black, B., Bograd, S. J., García-Reyes, M., Miller, A. J., Rykaczewski, R. R., and
2529 Sydeman, W. J. (2015). Anticipated Effects of Climate Change on Coastal Upwelling Ecosys-
2530 tems. *Current Climate Change Reports*, 1:85–93.

2531 Banas, N. S. (2011). Adding complex trophic interactions to a size-spectral plankton model:
2532 Emergent diversity patterns and limits on predictability. *Ecological Modelling*, 222(15):2663–
2533 2675.

Banse, K. (1975). Rates of growth, respiration and photosynthesis as related to cell size. A review. *Journal of Phycology*, pages 135–141.

Barnes, C., Irigoien, X., De Oliveira, J., Maxwell, D., and Jennings, S. (2011). Predicting marine phytoplankton community size structure from empirical relationships with remotely sensed variables. *Journal of Plankton Research*, 33(1):13–24.

Barton, A. D., Dutkiewicz, S., Flierl, G., Bragg, J., and Follows, M. J. (2010). Patterns of diversity in marine phytoplankton. *Science (New York, N.Y.)*, 327(5972):1509–11.

Barton, A. D., Pershing, A. J., Litchman, E., Record, N. R., Edwards, K. F., Finkel, Z. V., Kiø rboe, T., and Ward, B. a. (2013). The biogeography of marine plankton traits. *Ecology Letters*, 16(4):522–534.

Behrenfeld, M. J., Westberry, T. K., Boss, E. S., O'Malley, R. T., Siegel, D. A., Wiggert, J. D., Franz, B. a., McClain, C. R., Feldman, G. C., Doney, S. C., Moore, J. K., Dall'Olmo, G., Milligan, a. J., Lima, I., and Mahowald, N. (2009). Satellite-detected fluorescence reveals global physiology of ocean phytoplankton. *Biogeosciences*, 6(5):779–794.

Behrenfeld, M. J., Worthington, K., Sherrell, R. M., Chavez, F. P., Strutton, P., McPhaden, M., and Shea, D. M. (2006). Controls on tropical Pacific Ocean productivity revealed through nutrient stress diagnostics. *Nature*, 442(7106):1025–8.

Berg, G. M., Balode, M., Purina, I., Bekere, S., Béchemin, C., and Maestrini, S. Y. (2003). Plankton community composition in relation to availability and uptake of oxidized and reduced nitrogen. *Aquatic Microbial Ecology*, 30(3):263–274.

Berg, G. M., Glibert, P. M., Lomas, M. W., and Burford, M. A. (1997). Organic nitrogen uptake and growth by the chrysophyte *Aureococcus anophagefferens* during a brown tide event. *Marine Biology*, 129(2):377–387.

Bernard, S. (2005). The Bio-Optical Detection of Harmful Algal Blooms in the Department of Oceanography. (August).

2559 Bernard, S., Kudela, R. M., Franks, P., Fennel, W., Kemp, A., Fawcett, A., and Pitcher, G. C.
2560 (2006). The requirements for forecasting harmful algal blooms in the Benguela. In *Large*
2561 *Marine Ecosystems*, volume 14, chapter 14, pages 273–294.

2562 Bernard, S., Probyn, T. A., and Quirantes, A. (2009). Simulating the optical properties of
2563 phytoplankton cells using a two-layered spherical geometry. *Biogeosciences Discussions*,
2564 6(1):1497–1563.

2565 Bernard, S., Shillington, F., and Probyn, T. A. (2007). The use of equivalent size distributions of
2566 natural phytoplankton assemblages for optical modeling. *Optics express*, 15(5):1995–2007.

2567 Bonachela, J. A., Raghib, M., and Levin, S. A. (2011). Dynamic model of flexible phytoplankton
2568 nutrient uptake. *Proceedings of the National Academy of Sciences*, 108(51):20633–20638.

2569 Bopp, L., Aumont, O., Cadule, P., Alvain, S., and Gehlen, M. (2005). Response of diatoms
2570 distribution to global warming and potential implications: A global model study. *Geophysical*
2571 *Research Letters*, 32(May):L19606.

2572 Boyd, C. M. and Johnson, G. (1995). Precision of size determination of resistive electronic
2573 counters. *Journal of Plankton Research*, 17:41–58.

2574 Brewin, R. J., Hardman-Mountford, N. J., Lavender, S. J., Raitsos, D. E., Hirata, T., Uitz, J.,
2575 Devred, E., Bricaud, A., Ciotti, A., and Gentili, B. (2011). An intercomparison of bio-optical
2576 techniques for detecting dominant phytoplankton size class from satellite remote sensing.
2577 *Remote Sensing of Environment*, 115(2):325–339.

2578 Brewin, R. J. W., Lavender, S. J., and Hardman-Mountford, N. J. (2010). Mapping size specific
2579 phytoplankton primary production on a global scale. *Journal of Maps*, 6(1):448–462.

2580 Bronk, D. A. and Glibert, P. M. (1993). Application of l5N tracer method to the study of dissolved
2581 organic nitrogen uptake during spring and summer in Chesapeake Bay. *Marine Biology*,
2582 115:501–508.

Bronk, D. A., Sanderson, M. P., Mulholland, M. R., Heil, C. A., and Neil, J. M. (2004). Organic and inorganic nitrogen uptake kinetics in field populations dominated by Karenia brevis. In Steidinger, K.A., Landsberg, J.J., Tomas, C.R. and Vargo, G., editor, *Harmful Algae*, volume 1, pages 3–5. Florida Fish and Wildlife Conservation Commission, Florida Institute of Oceanography, and Intergovernmental Oceanographic Commission of UNESCO.

Brown, C. W. and Podestá, G. P. (1997). Remote sensing of coccolithophore blooms in the Western South atlantic ocean. *Remote Sensing of Environment*, 60(1):83–91.

Brown, J. H., Gillooly, J. F., Allen, A. P., Savage, V. M., and West, G. B. (2004). Toward a metabolic theory of ecology. *Ecology*, 85(7):1771–1789.

Brown, P. and Hutchings, L. (1987). The development and decline of phytoplankton blooms in the southern Benguela upwelling system. 2. Nutrient relationships. *South African Journal of Science*, 5(1):393–409.

Bruggeman, J. and Kooijman, S. A. L. M. (2007). A biodiversity-inspired approach to aquatic ecosystem modeling. *Limnology and Oceanography*, 52(4):1533–1544.

Bryan, A. K., Engler, A., Gulati, A., and Manalis, S. R. (2012). Continuous and long-term volume measurements with a commercial coulter counter. *PLoS ONE*, 7(1):1–8.

Bulit, C., Díaz-Ávalos, C., and Montagnes, D. J. S. (2004). Assessing spatial and temporal patchiness of the autotrophic ciliate *Myrionecta rubra*: A case study in a coastal lagoon. *Marine Ecology Progress Series*, 268:55–67.

Burkholder, J. M., Glibert, P. M., and Skelton, H. M. (2008). Mixotrophy , a major mode of nutrition for harmful algal species in eutrophic waters. 8:77–93.

Bury, S. J., Boyd, P. W., Preston, T., Savidge, G., and Owens, N. J. (2001). Size fractionated primary production and nitrogen uptake during a North Atlantic phytoplankton bloom. Implications for carbon export estimates. *Deep-Sea Research*, 48:680–720.

Canales, T. M., Law, R., and Blanchard, J. L. (2015). Shifts in plankton size-spectra modulate growth and coexistence of anchovy and sardine in upwelling systems. *Canadian Journal of Fisheries and Aquatic Sciences*, 621(October 2015):611–621.

Carvalho, G., Minnet, P., Fleming, L., Banzon, V. T., and Baringer, W. (2010). Satellite remote sensing of harmful algal blooms: A new multi-algorithm method for detecting the Florida Red Tide (*Karenia brevis*). *Harmful Algae*, 9(5):440–448.

Cavagna, A. J., Elskens, M., Griffiths, F. B., Fripiat, F., Jacquet, S. H. M., Westwood, K. J., and Dehairs, F. (2011). Contrasting regimes of production and potential for carbon export in the Sub-Antarctic and Polar Frontal Zones south of Tasmania. *Deep-Sea Research Part II: Topical Studies in Oceanography*, 58(21-22):2235–2247.

Cermeño, P., Marañón, E., Harbour, D., and Harris, R. P. (2006). Invariant scaling of phytoplankton abundance and cell size in contrasting marine environments. *Ecology Letters*, 9(11):1210–1215.

Cerucci, M., Jaligama, G. K., and Ambrose, R. B. (2010). Comparison of the Monod and Droop Methods for Dynamic Water Quality Simulations. *Journal of Environmental Engineering*, 136(10):1009–1019.

Chakraborty, S. and Feudel, U. (2014). Harmful algal blooms: Combining excitability and competition. *Theoretical Ecology*, 7(3):221–237.

Chapin, F. (1997). Biotic control over the functioning of ecosystems. *Science*, 277:500–504.

Chen, L., Ma, J., Huang, Y., Dai, M., and Li, X. (2015). Optimization of a colorimetric method to determine trace urea in seawater. *Limnology and Oceanography: Methods*, 13(6):303–311.

Chisholm, S. W. (1992). Phytoplankton Size. In *Primary Productivity and Biogeochemical Cycles in the Sea*, pages 213–237.

Ciotti, A. M. and Bricaud, A. (2006). Retrievals of a size parameter for phytoplankton and spectral light absorption by colored detrital matter from water-leaving radiances at SeaWiFS

channels in a continental shelf region off Brazil. *Limnology and Oceanography: Methods*, 4:237–253.

Ciotti, A. M., Lewis, M. R., and Cullen, J. J. (2002). Assessment of the relationships between dominant cell size in natural phytoplankton communities and the spectral shape of the absorption coefficient. *Limnology and Oceanography*, 47(2):404–417.

Cloern, J. E., Cole, B. E., and Hager, W. (1994). Notes on a *Mesodinium rubrum* red tide in San Francisco Bay (California, USA). *Journal of Plankton Research*, 16:1269–1276.

Cochlan, W. P. and Bronk, D. A. (2001). Nitrogen uptake kinetics in the Ross Sea, Antarctica. *Deep-Sea Research Part II-Topical Studies in Oceanography*, 48(19-20):4127–4153.

Cochlan, W. P., Herndon, J., and Kudela, R. M. (2008). Inorganic and organic nitrogen uptake by the toxigenic diatom *Pseudo-nitzschia australis* (Bacillariophyceae). *Harmful Algae*, 8(1):111–118.

Cockcroft, A., Schoeman, D. S., Pitcher, G. C., Bailey, G. C., and Van Zyl, D. L. (1998). A mass stranding, or walkout, of West Coast Rock Lobster *Jasus lalandii* in Elands Bay, South Africa. Causes, results and implications. In Von Kaupel Klein, J. C. and Schram, F. R., editor, *Crustacean Issues*, volume 12, pages 673–688.

Collos, Y. (1980). Transient situations in nitrate assimilation by marine diatoms. 1. Changes in uptake parameters during nitrogen starvation. *Limnology and Oceanography*, 25(6):1075–1081.

Collos, Y. (1992). Nitrogen budgets and dissolved organic matter cycling. *Marine Ecology Progress Series*, 90(2):201–206.

Collos, Y., Gagne, C., Laabir, M., Vaquer, A., Cecchi, P., and Souchu, P. (2004). Nitrogenous nutrition of *Alexandrium Catenella* (Dinophyceae) in cultures and in Thau Lagoon, Southern France. *Journal of Phycology*, 40(1):96–103.

Collos, Y., Siddiqi, M., Wang, M., Glass, D., and Harrison, P. (1992). Nitrate uptake kinetics by two marine diatoms using the radioactive tracer 13N. *Journal of Experimental Marine Biology and Ecology*, 163(2):251–260.

Collos, Y. and Slawyk, G. (1976). Significance of cellular nitrate content in natural populations of marine phytoplankton growing in shipboard cultures. *Marine Biology*, 34(1):27–32.

Collos, Y., Vaquer, a., Bibent, B., Slawyk, G., Garcia, N., and Souchu, P. (1997). Variability in Nitrate Uptake Kinetics of Phytoplankton Communities in a Mediterranean Coastal Lagoon. *Estuarine, Coastal and Shelf Science*, 44(3):369–375.

Collos, Y., Vaquer, A., Bibent, B., Souchu, P., Slawyk, G., and Garcia, N. (2003). Response of coastal phytoplankton to ammonium and nitrate pulses: Seasonal variations of nitrogen uptake and regeneration. *Aquatic Ecology*, 37(3):227–236.

Collos, Y., Vaquer, A., Laabir, M., Abadie, E., Laugier, T., Pastoureaud, A., and Souchu, P. (2007). Contribution of several nitrogen sources to growth of *Alexandrium catenella* during blooms in Thau lagoon, southern France. *Harmful Algae*, 6(6):781–789.

Collos, Y., Vaquer, A., and Souchu, P. (2005). Acclimation of nitrate uptake by phytoplankton to high substrate levels. *Journal of Phycology*, 41(3):466–478.

Crawford, D. (1989). *Mesodinium rubrum*: the phytoplankter that wasn't . *Marine Ecology Progress Series*, 58(1988):161–174.

Crichton, M., Hutchings, L., Lamont, T., and Jarre, a. (2013). From physics to phytoplankton: prediction of dominant cell size in St Helena Bay in the Southern Benguela. *Journal of Plankton Research*, 35(3):526–541.

Cullen, J., Doolittle, W. F., Levin, S., and Li, W. (2007). Patterns and Prediction in Microbial Oceanography. *Oceanography*, 20(2):34–46.

Cury, P., Bakun, A., Crawford, R., Jarre, A., Quiñones, R., Shannon, L., and Verheye, H. (2000).

Small pelagics in upwelling systems: patterns of interaction and structural changes in wasp waist ecosystems. *ICES Journal of Marine Science*, 57(3):603–618.

Dauchez, S., Legendre, L., Fortier, L., Levasseur, M., De, D., and Laval, U. (1996). Nitrate uptake by size-fractionated phytoplankton on the Scotian Shelf (Northwest Atlantic). Spatial and temporal variability. *Journal of Plankton Research*, 18(4):577–595.

Demarcq, H., Barlow, R., and Hutchings, L. (2007). Application of a chlorophyll index derived from satellite data to investigate the variability of phytoplankton in the Benguela ecosystem. *African Journal of Marine Science*, 29(2):271–282.

Diaz, H. F. and Bradley, R. S. (2005). *The Hadley Circulations: Present, Past and Future*. Kluwer Academic Publishers.

Doney, S., Lima, I., Moore, J., Lindsay, K., Behrenfeld, M., Westberry, T., Mahowald, N., Glover, D., and Takahashi, T. (2009). Skill metrics for confronting global upper ocean ecosystem-biogeochemistry models against field and remote sensing data. *Journal of Marine Systems*, 76:95–112.

Dortch, Q. (1990). The interaction between ammonium and nitrate uptake in phytoplankton. *Marine Ecology Progress Series*.

Dortch, Q., Clayton, J. R., Thoresen, S. S., and Ahmed, S. I. (1984). Species differences in accumulation of nitrogen pools in phytoplankton. *Marine Biology*, 81(3):237–250.

Dortch, Q. and Conway, H. (1984). Interactions between nitrate and ammonium uptake: variation with growth rate, nitrogen source and species. *Marine Biology*, 79:151–164.

Douding, L. and Goebel, J. (2001). Five Red Tide Species in Genus Prorocentrum Including the Description of *Prorocentrum Donghaiense*. *Chinese Journal of Oceanology and Limnology*, 19(4):337–344.

Droop, M. R. (1973). Some Thoughts on Nutrient Limitation in Algae. *Journal of Phycology*, 9(3):264–272.

Droop, M. R. (1974). The Nutrient Status of Algal Cells in Continuous Culture. *Journal of the Marine Biological Association of the UK*, 54:825–855.

Dugdale, R. (1967). Limitation in the Sea: Dynamics, identification, and significance. *Limnology and Oceanography*, 12(4):685–695.

Dugdale, R. and Goering, J. (1967). Uptake of new and regenerated forms of nitrogen in primary productivity. *Limnology and Oceanography*, 12:196–206.

Dugdale, R. C. and Wilkerson, F. P. (1986). The use of 15N to measure nitrogen uptake in eutrophic ocean. Experimental considerations. *Limnology and Oceanography*, 31(4):673–689.

Dugdale, R. C., Wilkerson, F. P., Hogue, V. E., and Marchi, A. (2006). Nutrient controls on new production in the Bodega Bay, California, coastal upwelling plume. *Deep-Sea Research Part II: Topical Studies in Oceanography*, 53(25-26):3049–3062.

Dugdale, R. C., Wilkerson, F. P., Hogue, V. E., and Marchi, A. (2007). The role of ammonium and nitrate in spring bloom development in San Francisco Bay. *Estuarine, Coastal and Shelf Science*, 73(1-2):17–29.

Dugdale, R. C., Wilkerson, F. P., Morel, A., and Physique, L. D. (1990). Realization of new production in coastal upwelling: A means to compare relative performance areas. 35(4):822–829.

Dutkiewicz, S., Follows, M. J., and Bragg, J. G. (2009). Modeling the coupling of ocean ecology and biogeochemistry. *Global Biogeochemical Cycles*, 23(4):1–15.

Dutkiewicz, S., Jahn, O., Ward, B., Follows, M., Hickman, A., Follet, C., and Taniguchi, D. (2016). Modeling diverse phytoplankton communities. In *Colour and Light in the Ocean from Earth Observation (CLEO) Relevance and Applications Products from Space and Perspectives from Models*, page Presentation.

Edwards, K., Klausmeier, C., and Litchman, E. (2015). Nutrient utilization traits of phytoplankton. *Ecology*, 96(8):2311–2311.

Edwards, K. F., Litchman, E., and Klausmeier, C. (2013). Functional traits explain phytoplankton community structure and seasonal dynamics in a marine ecosystem. *Ecology Letters*, 16(1):56–63.

Edwards, K. F., Thomas, M. K., Klausmeier, C. A., and Litchman, E. (2012). Allometric scaling and taxonomic variation in nutrient utilization traits and maximum growth rate of phytoplankton. *Limnology and Oceanography*, 57(2):554–566.

Egge, J. K. and Aksnes, D. L. (1992). Silicate as regulating nutrient in phytoplankton competition. *Marine Ecology Progress Series*, 83(2-3):281–289.

Eppley, R. and Peterson, B. J. (1979). Particulate organic matter flux and planktonic new production in the deep ocean. *Nature*, 282:677–680.

Eppley, R. W., Carlucci, A. F., Kiefer, D., McCarthy, J. J., Venrick, E., and Williams, P. M. (1971). Phytoplankton growth and composition in shipboard cultures supplied with nitrate, ammonium, or urea as the nitrogen source. *Limnology and Oceanography*, 16(5):741–751.

Eppley, R. W. and Rogers, J. N. (1970). Inorganic nitrogen assimilation of *Ditylum brightwelli*, a marine plankton diatom. *J. Phycol.*, 6(4):344–351.

Eppley, R. W., Rogers, J. N., and McCarthy, J. J. (1969). Half-saturation constants for uptake of nitrate and ammonium by marine phytoplankton. *Limnology and Oceanography*, 14(6):912–920.

Evers-King, H. (2014). *Phytoplankton community structure determined through remote sensing and in situ optical measurements*. PhD thesis, University of Cape Town.

Evers-King, H., Bernard, S., Robertson Lain, L., and Probyn, T. A. (2014). Sensitivity in reflectance attributed to phytoplankton cell size: forward and inverse modelling approaches. *Optics Express*, 22(10):11536–11551.

Falkowski, P. G., Katz, M. E., Knoll, A. H., Quigg, A., Raven, J. A., Schofield, O., and Taylor, F. J. R. (2004). The evolution of modern eukaryotic phytoplankton. *Science (New York, N.Y.)*, 305(5682):354–360.

Falkowski, P. G. and Owens, T. G. (1978). Effects of light-intensity on photosynthesis and dark respiration in six species of marine phytoplankton. *Marine Biology*, 45(4):289–295.

Fasham, M., Ducklow, H., and McKelvie, S. (1990). A nitrogen-based model of plankton dynamics in the oceanic mixed layer. *Journal of Marine Research*, 48(3):491–639.

Fawcett, A., Pitcher, G. C., Bernard, S., Cembella, A. D., and Kudela, R. M. (2007). Contrasting wind patterns and toxigenic phytoplankton in the southern Benguela upwelling system. *Marine Ecology Progress Series*, 348:19–31.

Fenchel, T. and Finlay, B. J. (1983). Respiration rates in heterotrophic, free living protozoa. *Microbial Ecology*, 9(2):99–122.

Field, Beherenfeld, M., Randerson, J., and Falkowski, P. (1998). Primary Production of the Biosphere: Integrating Terrestrial and Oceanic Components. *Science*, 281(5374):237–240.

Finkel, Z. V., Beardall, J., Flynn, K. J., Quigg, A., Rees, T. A. V., and Raven, J. (2010). Phytoplankton in a changing world: Cell size and elemental stoichiometry. *Journal of Plankton Research*, 32(1):119–137.

Finkel, Z. V., Falkowski, P. G., and Knoll, A. (2007). Does phytoplankton cell size matter? The evolution of modern marine food webs. In *Evolution of Aquatic Photoautotrophs*, pages 333–350. Academic press, San Diego.

Finlay, B. and Uhlig, G. (1981). Calorific and carbon values of marine and freshwater protozoa. *Helgolander meeresuntersuchungen*, 34:401–412.

Follows, M., Dutkiewicz, S., Grant, S., and Chisholm, S. (2007). Emergent biogeography of microbial communities in a model ocean. *Science*, 315(5820):1843–1846.

2778 Follows, M. J. and Dutkiewicz, S. (2011). Modeling diverse communities of marine microbes.
2779 *Annual review of marine science*, 3:427–451.

2780 Franks, P. J. S. (2009). Planktonic ecosystem models: Perplexing parameterizations and a
2781 failure to fail. *Journal of Plankton Research*, 31(11):1299–1306.

2782 Furnas, M. J. (1983). Nitrogen dynamics in lower Narragansett Bay, Rhode Island. I. Up-
2783 take by size-fractioned phytoplankton populations. *Journal of Plankton Research 5:677-692*,
2784 5(5):657–676.

2785 Gandhi, N., Ramesh, R., Srivastava, R., Sheshshayee, M. S., Dwivedi, R. M., and Raman, M.
2786 (2010). Nitrogen Uptake Rates during Spring in the NE Arabian Sea. *International Journal of*
2787 *Oceanography*, 2010:1–10.

2788 García-Reyes, M., Sydeman, W. J., Schoeman, D. S., Rykaczewski, R. R., Black, B. A., Smit,
2789 A. J., and Bograd, S. J. (2015). Under Pressure: Climate Change, Upwelling, and Eastern
2790 Boundary Upwelling Ecosystems. *Frontiers in Marine Science*, 2(December):1–10.

2791 Geider, R. and La Roche, J. (2002). Redfield revisited: variability of C:N:P in marine microalgae
2792 and its biochemical basis. *European Journal of Phycology*, 37(1):1–17.

2793 GEOHAB (2001). Global Ecology and Oceanography of Harmful Algal Blooms, Science Plan.
2794 In G. Pitcher, T. Moita, V. Trainer, R. Kudela, F. Figueras and T.A. Probyn, editor, *GEOHAB*
2795 *Core Research Project: HABs in Upwelling Systems,*, page 87. IOC and SCOR, Paris and
2796 Baltimore.

2797 Gilpin, L. C., Davidson, K., and Roberts, E. (2004). The influence of changes in nitrogen: Silicon
2798 ratios on diatom growth dynamics. *Journal of Sea Research*, 51(1):21–35.

2799 Glibert, P. (2012). Ecological stoichiometry and its implications for aquatic ecosystem sustain-
2800 ability. *Current Opinion in Environmental Sustainability*, 4(3):272–277.

2801 Glibert, P., Anderson, D., Gentien, P., Granéli, E., and Sellner, K. (2005). The Global, Complex
2802 Phenomena of Harmful Algal Blooms. *Oceanography*, 18(2):136–147.

Glibert, P. and Garside, C. (1992). Diel variability in nitrogenous nutrient uptake by phytoplankton in the Chesapeake Bay plume. *Journal of Plankton Research*, 14(2):271–288.

Glibert, P., Kana, T., and Brown, K. (2013). From limitation to excess: the consequences of substrate excess and stoichiometry for phytoplankton physiology, trophodynamics and biogeochemistry, and the implications for modeling. *Journal of Marine Systems*, 125:14–28.

Glibert, P. M. (2016). Margalef revisited: A new phytoplankton mandala incorporating twelve dimensions, including nutritional physiology. *Harmful Algae*, 55(May):25–30.

Glibert, P. M., Garside, C., Fuhrman, J. A., and Roman, M. R. (1991). Dependent coupling of inorganic and organic nitrogen uptake and regeneration in the plume of the Chesapeake Bay estuary and its regulation by large heterotrophs. *Limnology and Oceanography*, 36(5):895–909.

Glibert, P. M. and Goldman, J. C. (1981). Rapid ammonium uptake by marine phytoplankton. *marine Biology letters*, 2:25–31.

Glibert, P. M., Harrison, J., Heil, C., and Seitzinger, S. (2006). Escalating worldwide use of urea - A global change contributing to coastal eutrophication. *Biogeochemistry*, 77(3):441–463.

Glibert, P. M., Lipschultz, F., McCarthy, J. J., and Altabet, M. A. (1982). Isotope dilution models of uptake and remineralization of ammonium by marine plankton. *Limnology and Oceanography*, 27(4):639–650.

Glibert, P. M. and McCarthy, J. J. (1984). Uptake and assimilation of ammonium and nitrate by phytoplankton: Indices of nutritional status for natural assemblages. *Journal of Plankton Research*, 6(4):677–697.

Glibert, P. M., Wilkerson, F. P., Dugdale, R. C., Parker, A. E., Alexander, J., Blaser, S., and Murasko, S. (2014). Phytoplankton communities from San Francisco Bay Delta respond differently to oxidized and reduced nitrogen substrates even under conditions that would otherwise suggest nitrogen sufficiency. *Frontiers in Marine Science*, 1(July):1–16.

Glibert, P. M., Wilkerson, F. P., Dugdale, R. C., Raven, J. A., Dupont, C. L., Leavitt, P. R., Parker, A. E., Burkholder, J. M., and Kana, T. M. (2016). Pluses and minuses of ammonium and nitrate uptake and assimilation by phytoplankton and implications for productivity and community composition, with emphasis on nitrogen-enriched conditions. *Limnology and Oceanography*, 61(1):165–197.

Gocke, K., Dawson, R., and Liebezit, G. (1981). Availability of dissolved free glucose to heterotrophic micro-organisms. *Marine Biology*, 62:209–216.

Grasshoff, K., Ehrardt, M. and Kremling, K. (1983). *Methods of seawater analysis*. John Wiley and Sons.

Gregg, W. W., Ginoux, P., Schopf, P. S., and Casey, N. W. (2003). Phytoplankton and iron: Validation of a global three-dimensional ocean biogeochemical model. *Deep-Sea Research Part II: Topical Studies in Oceanography*, 50(22-26):3143–3169.

Grover, J. P. (1991). Resource Competition in a Variable Environment: Phytoplankton Growing According to the Variable-Internal-Stores Model. *The American Naturalist*, 138(4):811.

Gruber, N. (2008). The marine nitrogen cycle: Overview and Challenges. In Capone, Douglas G., Bronk, D.A., Mulholland, M., and Carpenter, E., editors, *Nitrogen in the Marine Environment.*, chapter 1, pages 1–43. Elsevier, Burlington.

Hallegraeff, G. M. (1993). A review of harmful algal blooms and their apparent global increase. *Phycologia*, 32(2):79–99.

Hansen, P. J. and Fenchel, T. (2006). The bloom forming symbiont *Mesodinium rubrum* harbours a single permanent endosymbiont. *Marine Biology Research*, 2:169–177.

Harris, G. P. (1980). Temporal and Spatial Scales in Phytoplankton Ecology. Mechanisms, Methods, Models, and Management. *Canadian Journal of Fisheries and Aquatic Sciences*, 37(5):877–900.

Harrison, W. (1990). Nitrogen utilization in chlorophyll and primary productivity maximum layers: an analysis based on the f-ratio . *Marine Ecology Progress Series*, 60(1):85–90.

Harrison, W., Head, E.J.H., Conover, R., Longhurst, A., and Sameoto, D. (1985). The distribution and metabolism of urea in the eastern Canadian Arctic. *Deep Sea Research Part A. Oceanographic Research Papers*, 32:23–42.

Harrison, W. G., Harris, L. R., and Irwin, B. D. (1996). The kinetics of nitrogen utilization in the oceanic mixed layer: Nitrate and ammonium interactions at nanomolar concentrations. *Limnology and Oceanography*, 41(1):16–32.

Healey, F. (1980). Slope of the monod equation as an indicator of advantage in nutrient competition. *Microbial Ecology*, 5(4):281–286.

Hecky, R., Campbell, P., and Hendzell, L. (1993). The stoichiometry of carbon, nitrogen and phosphorous in particular matter of lakes and oceans. *Limnology and Oceanography*, 38:709–724.

Hein, M., Pedersen, M. F., and Sand Jensen, K. (1995). Size-dependent nitrogen uptake in micro- and macroalgae. *Marine Ecology Progress Series*, 118(1-3):247–254.

Herfort, L., Peterson, T. D., Campbell, V., Futrell, S., and Zuber, P. (2011). *Myrionecta rubra* (*Mesodinium rubrum*) bloom initiation in the Columbia River estuary. *Estuarine, Coastal and Shelf Science*, 95(4):440–446.

Hibbing, M. E., Fuqua, C., Parsek, M. R., and Peterson, S. B. (2010). Bacterial competition: surviving and thriving in the microbial jungle. *Nature reviews. Microbiology*, 8(1):15–25.

Hirata, T., Aiken, J., Hardman-Mountford, N., Smyth, T., and Barlow, R. (2008). An absorption model to determine phytoplankton size classes from satellite ocean colour. *Remote Sensing of Environment*, 112(6):3153–3159.

Hirata, T., Hardman-Mountford, N. J., Brewin, R. J. W., Aiken, J., Barlow, R., Suzuki, K., Isada, T., Howell, E., Hashioka, T., Noguchi-Aita, M., and Yamanaka, Y. (2011). Synoptic rela-

tionships between surface Chlorophyll-*a* and diagnostic pigments specific to phytoplankton functional types. *Biogeosciences*, 8(2):311–327.

Hoagland, P., Jin, D., Polansky, L., Kirkpatrick, B., Kikpatrick, G., Fleming, L., Reich, A., Watkins, S., Ullmann, S., and Backer, L. (2009). The costs of respiratory illnesses arising from Florida Gulf Coast *Karenia brevis* blooms. *Environmental Health Perspective*, 117(8):1239–1243.

Horstman, D. (1981). Reported red-water outbreaks and their effects on fauna of the west and south coasts of South Africa 1959-1980. *Fish.Bull.S.Afr.*, 15:71–88.

Howard, M. D. A., Cochlan, W. P., Ladizinsky, N., and Kudela, R. M. (2007). Nitrogenous preference of toxigenic Pseudo-nitzschia australis̊(Bacillariophyceae) from field and laboratory experiments. *Harmful Algae*, 6:206–217.

Hu, Y. X. and Stamnes, K. (1993). An accurate parameterization of the radiative properties of water clouds suitable for use in climate models.

Hunt, G. L. and McKinnell, S. (2006). Interplay between top-down, bottom-up, and wasp-waist control in marine ecosystems. *Progress in Oceanography*, 68(2-4):115–124.

Hunter, M. D. and Price, P. W. (2012). Playing chutes and ladders: Heterogeneity and the relative roles of bottom up and top down forces in natural communities. *Ecology*, 73(3):724–732.

Hutchings, L. (1992). Fish harvesting in a variable, productive environment. Searching for rules or searching for exceptions? *South African Journal of Marine Science*, 12(1):297–318.

Hutchings, L., Augustyn, C. J., Cockcroft, A., Van Der Lingen, C., Coetzee, J., Leslie, R. W., Tarr, R. J., Oosthuizen, H., Lipinski, M. R., Roberts, M. R., Wilke, C., Crawford, R., Shannon, L. J., and Mayekiso, M. (2009). Marine fisheries monitoring programmes in South Africa. *South African Journal of Science*, 105(5-6):182–192.

Irigoien, X., Flynn, K. J., and Harris, R. P. (2005). Phytoplankton blooms: A 'loophole' in microzooplankton grazing impact? *Journal of Plankton Research*, 27(4):313–321.

Joint, I. and Groom, S. (2000). Estimation of phytoplankton production from space: current status and future potential of satellite remote sensing. *Journal of Experimental Marine Biology and Ecology*, 250(1-2):233–255.

Jonsson, P. and Tiselius, P. (1990). Feeding behaviour, prey detection and capture efficiency of the copepod Acartia tonsa feeding on planktonic ciliates . *Marine Ecology Progress Series*, 60:35–44.

Junge, C. (1963). *Air chemistry and radioactivity*. Academic Press, London.

Kerr, S. (1974). Theory of size distribution in ecological communities. *Journal of the Fisheries Board of Canada*, 31(12):1859–1862.

Kim, H. (1986). Ecological study of Dinoflagellates responsible for Red Tide 2. The population growth of *Prorocentum minimun* (Pav.) Schiller. *The Korean Journal of Phycology*, 1(1):103–106.

Kiørboe, T. (1993). Turbulence, phytoplankton cell size, and the structure of pelagic food webs. *Adavances in Marine Biology*, 29:1–72.

Kiørboe, T. (2008). *A mechanistic approach to plankton ecology*, volume 10. Princeton University Press, Princeton.

Kishi, M., Kashiwai, M., Ware, M., Megrey, B. A., Eslinger, D. L., Werner, F. E., Noguchi-Aita, M., Azumaya, T., Fuji, M., Hashimoto, S., Huang, D., Lizumi, H., Ishida, Y., Kang, S., Kantakov, G. A., Kimo, H., Komatsu, K., Navrotsky, V. V., Smith, S. L., Tadokoro, K., Tsuda, A., Yamamura O., Yamanaka Y., Yokouchi K., Yoshiei N., Zhang J., Zuenko Y. I., and Zvalinsky, I. (2007). NEMURO a lower trophic level model for the North Pacific marine ecosystem. *Ecological Modelling*, 202:12–25.

Kokkinakis, S. and Wheeler, P. (1987). Nitrogen uptake and phytoplankton growth in coastal upwelling regions. *Limnology and Oceanography*, 32(5):1112–1123.

Koroleff, F. (1983). Determination of urea. In Grasshoff, K., Ehrhardt, E., Kremling, K., editor, *Methods of seawater analysis*, pages 158–162. Verlag Chemie, Weinheim.

Kostadinov, T. S., Siegel, D. a., and Maritorena, S. (2009). Retrieval of the particle size distribution from satellite ocean color observations. *Journal of Geophysical Research*, 114(C9):1–22.

Kostadinov, T. S., Siegel, D. a., and Maritorena, S. (2010). Global variability of phytoplankton functional types from space: Assessment via the particle size distribution. *Biogeosciences*, 7(10):3239–3257.

Kristiansen, S. and Lund, B. A. (1989). Nitrogen cycling in the Barents Sea. Uptake of nitrogen in the water column. *Deep Sea Research Part A. Oceanographic Research Papers*, 36(2):255–268.

Kudela, R., Pitcher, G., Probyn, T., Figueiras, F., Moita, T., and Trainer, V. (2005). Harmful Algal Blooms in Coastal Upwelling Systems. *Oceanography*, 18(2):184–197.

Kudela, R. M., Seeyave, S., and Cochlan, W. P. (2010). The role of nutrients in regulation and promotion of harmful algal blooms in upwelling systems. *Progress in Oceanography*, 85(1-2):122–135.

Kutser, T., Metsamaa, L., Strömbeck, N., and Vahtmäe, E. (2006). Monitoring cyanobacterial blooms by satellite remote sensing. *Estuarine, Coastal and Shelf Science*, 67(1-2):303–312.

Labib, W. (1996). Water Discoloration in Alexandria, Egypt, April 1993. I. Occurrence of *Prorocentrum Triestinum Schiffer* (Red Tide) Bloom and Associated Physical and Chemical Conditions. *Chemistry and Ecology*, 12(3):163–170.

Laws, E., Falkowski, P. G., Smith, W. O., Ducklow, H., and McCarthy, J. J. (2000). Temperature effects on export production in the open ocean. *Global Biogeochemical Cycles*, 14(4):1231–1246.

Lawton, J. (1999). Are there general laws in ecology? *OIKOS*, 84(2):177–192.

Le Quéré, C. L., Harrison, S. P., Colin Prentice, I., Buitenhuis, E. T., Aumont, O., Bopp, L., Claustre, H., Cotrim Da Cunha, L., Geider, R., Giraud, X., Klaas, C., Kohfeld, K. E., Legendre, L., Manizza, M., Platt, T., Rivkin, R. B., Sathyendranath, S., Uitz, J., Watson, A. J., and Wolf-Gladrow, D. (2005). Ecosystem dynamics based on plankton functional types for global ocean biogeochemistry models. *Global Change Biology*, 11:2016–2040.

Levin, S. A. (1992). The problem of pattern and scale in ecology. *Ecology*, 73(6):1943–1967.

Levy, M., Jahn, O., Dutkiewicz, S., Follows, M. J., and D'Ovidio, F. (2015). The dynamical landscape of marine phytoplankton diversity. *Journal of the Royal Society Interface*, 12:20150481.

L'Helguen, S., Maguer, J. F., and Caradec, J. (2008). Inhibition kinetics of nitrate uptake by ammonium in size-fractionated oceanic phytoplankton communities: Implications for new production and f-ratio estimates. *Journal of Plankton Research*, 30(10):1179–1188.

Li, J., Glibert, P. M., and Zhou, M. (2010). Temporal and spatial variability in nitrogen uptake kinetics during harmful dinoflagellate blooms in the East China Sea. *Harmful Algae*, 9(6):531–539.

Lind, P. and Jeyasingh, P. (2015). Genotypic differences in phosphorous use physiology in producers (*Chlamydomonas reinhardtii*) and consumers (*Daphnia pulex*) interact to alter primary and secondary production. *Evolutionary Ecology*, 29:551–563.

Lindemann, C., Fiksen, O., Andersen, K., and Aksnes, D. (2016). Scaling laws in phytoplankton nutrient uptake affinity. *Frontiers in Marine Science*, 3(March):1–6.

Lindholm, T. (1985). *Mesodinium rubrum* - a unique photosynthetic ciliate. *Adv. Aquatic Microbiol.*, 3:1–48.

Litchman, E., Edwards, K. F., and Klausmeier, C. A. (2015). Microbial resource utilization traits and trade-offs: implications for community structure, functioning, and biogeochemical impacts at present and in the future. *Frontiers in Microbiology*, 06(April):1–10.

Litchman, E., Edwards, K. F., Klausmeier, C. A., and Thomas, M. K. (2012). Phytoplankton niches, traits and eco-evolutionary responses to global environmental change. *Marine Ecology Progress Series*, 470:235–248.

Litchman, E. and Klausmeier, C. A. (2008). Trait-Based Community Ecology of Phytoplankton. *Annual Review of Ecology, Evolution, and Systematics*, 39(1):615–639.

Litchman, E., Klausmeier, C. a., Schofield, O. M., and Falkowski, P. G. (2007). The role of functional traits and trade-offs in structuring phytoplankton communities: scaling from cellular to ecosystem level. *Ecology letters*, 10(12):1170–81.

Lomas, M. W., Bonachela, J. A., Levin, S. A., and Martiny, A. C. (2014). Impact of ocean phytoplankton diversity on phosphate uptake. *In review*, 111(49):17540–5.

Lomas, M. W. and Glibert, P. M. (1999). Temperature regulation of nitrate uptake: A novel hypothesis about nitrate uptake and reduction in cool-water diatoms. *Limnology and Oceanography*, 44(3):556–572.

Lomas, M. W. and Glibert, P. M. (2000). Comparisons of nitrate uptake, storage, and reduction in marine diatoms and flagellates. *Journal of Phycology*, 36(5):903–913.

Losada, M., Guerrero, M. G., and Vega, J. M. (1981). The assimilatory reduction of nitrate. In *Biology of Inorganic Nitrogen and Sulfur*, pages 30–63. Spinger, Berlin Heidelberg.

MacIsaac, J. and Dugdale, R. (1972). Interactions of light and inorganic nitrogen in controlling nitrogen uptake in the sea. *Deep Sea Research and Oceanographic Abstracts*, 19(3):209–232.

Maguer, J., L'Huelgen, S., Caradec, J., and Klein, C. (2011). Size-dependent uptake of nitrate and ammonium as a function of light in well-mixed temperate coastal waters. *Continental Shelf Research*, 31(15):1620–1631.

Malone, T. (1980a). Algal size. In Morris, I., editor, *The physiological ecology of phytoplankton*, pages 433–464. Blackwell, London.

Malone, T. C. (1980b). Size-fractionated primary productivity of marine phytoplankton. In Falkowski, P., editor, *Primary Productivity in the Sea*, pages 301–320. Plenum, New York.

Margalef, R., Estrada, M., and Blasco, D. (1979). Functional morphology of organisms involved in red tides, as adapted to decaying turbulence. In Seliger, D. L. T. and H., H., editors, *Toxic Dinoflagellate Blooms*, pages 89–94. Elsevier.

Matson, P. A. (1992). Special Feature: The Relative Contributions to Top Down and Bottom Up Forces in Population and Community Ecology. *Ecology*, 73(3):723.

McCann, K. S. (2000). The diversity-stability debate. *Nature*, 405(6783):228–233.

McCarthy, J., Taylor, W., and Taft, J. (1975). The dynamics of nitrogen and phosphorous cycling in the open waters of the chesapeake bay. *Marine Chemistry in Coastal Environment*, pages 664–681.

McCarthy, J. J. and Goldman, J. C. (1979). Nitrogenous nutrition of marine phytoplankton in nutrient-depleted waters. *Science*, 203(4381):670–672.

McCarthy, J. J., Taylor, W. R., and Taft, J. L. (1977). Nitrogenous nutrition of the plankton in the Chesapeake Bay:1. Nutrient availability and phytoplankton preferences. *Limnology and Oceanography*, 22(6):996–1011.

McClain, C. R. (2009). A decade of satellite ocean color observations. *Annual review of marine science*, 1:19–42.

McGill, B. J., Enquist, B. J., Weiher, E., and Westoby, M. (2006). Rebuilding community ecology from functional traits. *Trends in Ecology and Evolution*, 21(4):178–185.

Menden-Deuer, S. and Lessard, E. J. (2000). Carbon to volume relationships for dinoflagellates, diatoms, and other protist plankton. *Limnology and Oceanography*, 45(3):569–579.

Merico, A., Bruggeman, J., and Wirtz, K. (2009). A trait-based approach for downscaling complexity in plankton ecosystem models. *Ecological Modelling*, 220(21):3001–3010.

Michaels, A., Karl, D., and Capone, D. (2001). Element Stoichiometry, New Production and Nitrogen Fixation. *Oceanography*, 14(4):68–77.

Miller, P. I., Shutler, J. D., Moore, G. F., and Groom, S. B. (2006). SeaWiFS discrimination of harmful algal bloom evolution. *International Journal of Remote Sensing*, 27(11):2287–2301.

Mitchell-Innes, B. A. and Pitcher, G. C. (1992). Hydrographic parameters as indicators of the suitability of phytoplankton populations as food for herbivorous copepods. *South African Journal of Marine Science*, 12(1):355–365.

Mitra, A. and Flynn, K. J. (2010). Modelling mixotrophy in harmful algal blooms: More or less the sum of the parts? *Journal of Marine Systems*, 83(3-4):158–169.

Moloney, C. L., Fennessy, S. T., Gibbons, M. J., Roychoudhury, A., Shillington, F. A., von der Heyden, B. P., and Watermeyer, K. (2013). Reviewing evidence of marine ecosystem change off South Africa. *African Journal of Marine Science*, 35(3):427–448.

Moloney, C. L., Field, J., and Lucas, M. (1991). The size-based dynamics of plankton food webs. II. Simulations of three contrasting southern Benguela food webs. *Journal of Plankton Research*, 13(5):1039–1092.

Moloney, C. L. and Field, J. G. (1989). General allometric equations for rates of nutrient uptake, ingestion, and respiration in plankton organisms. *Limnology and Oceanography*, 34(7):1290–1299.

Monod, J. (1949). The Growth of Bacterial Cultures. *Annual Review of Microbiology*, 3(1):371–394.

Montagnes, D., Berges, J., Harrison, P., and Taylor, F. (1994). Estimating carbon, nitrogen, protein and chlorophyll a from volume in marine phytoplankton. *Limnology and Oceanography*, 39:1044–1060.

Montagnes, D. J. S. and Lynn, D. H. (1989). The annual cycle of *Mesodinium rubrum* in the wa-

ters surrounding the Isles of Shoals, Gulf of Maine. *Journal of Plankton Research*, 11(2):193–201.

Monteiro, P. M. S. and Largier, J. L. (1999). Thermal Stratification in Saldanha Bay (South Africa) and Subtidal, Density-driven Exchange with the Coastal Waters of the Benguela Upwelling System. *Estuarine, Coastal and Shelf Science*, 49:877–890.

Monteiro, P. M. S., Spolander, B., and Brundrit, G. B. (1998). Shellfish mariculture in the Benguela system. Estimates of nitrogen driven new production in Saldanha Bay using two physical models. *Journal of Shellfish Research*, 17(1):3–13.

Moore, K., Doney, S., and Lindsay, K. (2002). An intermediate complexity marine ecosystem model for the global domain. *Deep Sea Research Part II*, 49:403–462.

Mouw, C. and Yoder, J. (2005). Primary production calculations in the Mid-Atlantic Bight, including effects of phytoplankton community size structure. *Limnology and Oceanography*, 50(4):1232–1243.

Muggli, D. and Smith, W. J. (1993). Regulation of nitrate and ammonium uptake in the Greenland Sea. *Marine Biology*, 208:199–208.

Mulholland, M. R. and Lomas, M. W. (2008). Nitrogen Uptake and Assimilation. In Capone D.G., Bronk, D.A., Mulholland, M.R. and Carpenter, E., editor, *Nitrogen in the Marine Environment.*, pages 303–359. Academic Press.

Mullin, M., Sloan, P., and Eppley, R. (1966). Relationship between carbon content, cell volume and area in phytoplankton. *Limnology and Oceanography*, 11:307–311.

Nair, A., Sathyendranath, S., Platt, T., Morales, J., Stuart, V., Forget, M. H., Devred, E., and Bouman, H. (2008). Remote sensing of phytoplankton functional types. *Remote Sensing of Environment*, 112(8):3366–3375.

Nelson, G. and Hutchings, L. (1983). The Benguela upwelling area. *Progress in Oceanography*, 12(3):333–356.

Nydahl, F. (1976). On the optimum conditions for the reduction of nitrate to nitrite by cadmium. *Talanta*, 23(5):349–357.

Packard, T., Blasco, D., and Barber, R. (1978). *Mesodinium rubrum* in the Baja California Upwelling system. In Boje, R. B. and Tomczak, M., editors, *Upwelling Ecosytems*, pages 72–74. Springer Berlin Heidelberg.

Paerl, H. W. (1991). Ecophysiological and trophic implications of light-stimulated amino acid utilization in marine picoplankton. *Applied and Environmental Microbiology*, 57(2):473–479.

Pahlow, M. (2005). Linking chlorophyll nutrient dynamics to the Redfield NC ratio with a model of optimal phytoplankton growth. *Marine Ecology Progress Series*, 287:33–43.

Pahlow, M., Dietz, H., and Oschlies, A. (2013). Optimality-based model of phytoplankton growth and diazotrophy. *Marine Ecology Progress Series*, 489:1–16.

Pahlow, M. and Oschlies, A. (2009). Chain model of phytoplankton P, N and light colimitation. *Marine Ecology Progress Series*, 376(2):69–83.

Pahlow, M., Vézina, A. F., Casault, B., Maass, H., Malloch, L., Wright, D. G., and Lu, Y. (2008). Adaptive model of plankton dynamics for the North Atlantic. *Progress in Oceanography*, 76(2):151–191.

Parsons, T., Maita, Y., and Lalli, C. (1984). *A manual chemical and biological methods for seawater analysis.* Pergamon, New York.

Parsons, T. R., Stephens, K., and Strickland, J. D. H. (1961). On the Chemical Composition of Eleven Species of Marine Phytoplankters. *Journal of the Fisheries Research Board of Canada*, 18(6):1001–1016.

Pasciak, W. J. G. (1974). Transport limitation of nutrient uptake in phytoplankton. *Limnology and Oceanography*, 19(6):881–888.

Pitcher, G., Agenbag, J., Calder, D., Horstman, D., Jury, M., and Taunton-Clark, J. (1995). Red tides in relation to the meteorology of the southern Benguela upwelling system. In Lassus,

P., Arzul, G., Erard, E., Gentien, P., and Marcaillou, C., editors, *Harmful Marine Algal Blooms*, pages 657–662. Intercept Ltd.

Pitcher, G., Boyd, A., Horstman, D., and Mitchell-Innes, B. (1998a). Subsurface dinoflagellate populations, frontal blooms and the formation of red tide in the southern Benguela upwelling system. *Marine Ecology Progress Series*, 172:253–264.

Pitcher, G., Walker, D., Mitchell-Innes, B., and Moloney, C. L. (1991). Short term variability during an anchor station study in the southern Benguela upwelling system: Phytoplankton dynamics. *Progress in Oceanography*, 28(1):39–64.

Pitcher, G. C. and Boyd, A. J. (1996). Across-shelf and alongshore dinoflagellate distributions and the mechanisms of red tide formation within the southern Benguela upwelling system. In Yasumoto, T., Oshima, Y., Fukuyo, Y., editor, *Harmful and Toxic Algal Blooms.*, pages 243–246. Intergovernemental Oceanographic Commission of UNESCO, Paris.

Pitcher, G. C., Boyd, A. J., Horstman, D. A., and Mitchell-Innes, B. A. (1998b). Subsurface dinoflagellate populations, frontal blooms and the formation of red tide in the southern Benguela upwelling system. *Marine Ecology Progress Series*, 172:253–264.

Pitcher, G. C. and Calder, D. (2000). Harmful algal blooms of the southern Benguela Current: a review and appraisal of monitoring from 1989 to 1997. *South African Journal of Marine Science*, 22(1):255–271.

Pitcher, G. C. and Cockcroft, A. C. (1998). Low oxygen, rock lobster strandings and PSP. In Intergovernmental Oceanographic Commission of UNESCO, editor, *Harmful Algal News*, volume 17, pages 1–3. Paris.

Pitcher, G. C. and Nelson, G. (2006). Characteristics of the surface boundary layer important to the development of red tide on the southern Namaqua shelf of the Benguela upwelling system. *Limnology and Oceanography*, 51(6):2660–2674.

Pitcher, G. C. and Probyn, T. A. (2011). Anoxia in southern Benguela during the autumn of 2009 and its linkage to a bloom of the dinoflagellate *Ceratium balechii*. *Harmful Algae*, 11:23–32.

Pitcher, G. C. and Weeks, S. J. (2006). 7 The variability and potential for prediction of harmful algal blooms in the southern Benguela ecosystem. In Shannon, V., Hempel, G., Malanotte-Rizzoli, P., Moloney, C. and Woods, J., editor, *Large Marine Ecosystems*, volume 14, chapter 14, pages 125–146. Elsevier B.V.

Platt, T. (1985). Structure of the marine ecosystem: its allometric basis. In Ulanowicz, R.E. and Platt, T., editor, *In: Ulanowicz, R.E. and Platt, T. (Eds.): Ecosystems theory for biological oceanography. Can. Bull. Fish. Aquat. Sciences*, volume 213, pages 55–64. Can. Bull. Fish. Aquat. Sci.

Platt, T., Gallegos, C. L., and Harrison, W. G. (1980). Photoinibition of photosynthesis in natural assemblages of marine phytoplankton. *Journal of Marine Research*, 38(4):687–701.

Probyn, T. A. (1985). Nitrogen uptake by size-fractionated phytoplankton populations in the southern Benguela upwelling system. *Marine Ecology Progress Series*, 22:249–258.

Probyn, T. A. (1987). Ammonium regeneration by microplankton in an upwelling environment. *Marine Ecology Progress Series*, 37(1965):53–64.

Probyn, T. A. (1988). Nitrogen utilization by phytoplankton in the Namibian upwelling region during an austral spring. *Deep Sea Research Part A. Oceanographic Research Papers*, 35(8):1387–1404.

Probyn, T. A. (1992). The inorganic nitrogen nutrition of phytoplankton in the southern Benguela: new production, phytoplankton size and implications for pelagic foodwebs. *South African Journal of Marine Science*, 12(1):411–420.

Probyn, T. A., Atkins, J. F., and Pitcher, G. C. (2015). Saldanha Bay, South Africa III: new production and carrying capacity for bivalve aquaculture. *South African Journal Of Marine Science*, 37(4):521–531.

Probyn, T. A. and Painting, S. J. (1985). Nitrogen uptake by size-fractionated phytoplankton populations in Antarctic surface waters. *Limnology and Oceanography*, 30(6):1327–1332.

Probyn, T. A., Pitcher, G. C., Monteiro, P. M. S., Boyd, A. J., and Nelson, G. (2000). Physical processes contributing to harmful algal blooms in Saldanha Bay , South Africa. *South African Journal of Marine Science*, 22(November):285–297.

Probyn, T. A., Waldron, H. N., and James, A. G. (1990). Size-fractionated measurements of nitrogen uptake in aged upwelled waters: Implications for pelagic food webs. *Limnology and Oceanography*, 35(1):202–210.

Probyn, T. A., Waldron, H. N., Searson, S., and Owens, N. J. P. (1996). Diel variability in nitrogenous nutrient uptake at photic and subphotic depths. *Journal of Plankton Research*, 18(11):2063–2079.

Prowe, A. E. F., Pahlow, M., Dutkiewicz, S., and Oschlies, A. (2014). How important is diversity for capturing environmental-change responses in ecosystem models? *Biogeosciences*, 11(12):3397–3407.

Ptacnik, R., Solimini, A. G., Andersen, T., Tamminen, T., Brettum, P. I., Lepistö, L., Willén, E., and Rekolainen, S. (2008). Diversity predicts stability and resource use efficiency in natural phytoplankton communities. *Proceedings of the National Academy of Sciences of the United States of America*, 105(13):5134–5138.

Raitsos, D., Lavender, S. J., and Maravelias, C. (2008). Identifying four phytoplankton functional types from space: An ecological approach. *Limnology and Oceanography*, 53(2):605–613.

Raven, J. (1997). The vacuole: a cost-benefit analysis. In Leigh, R. and Sanders, D., editors, *The plant vacuole. Advances in Botanical Research incorporating Advances in Plant Pathology*, pages 59–82. San Diego.

Raven, J. A. (1980). Nutrient transport in microalgae. *Advances in Microbiological Physiology*, 21:47–226.

Redfield, A. C. (1958). The biological control of chemical factors in the environment. *American Scientist*, 46(3).

Reynolds, C. S. (1989). Physical determinants of phytoplankton succession. In Sommer, U., editor, *Plankton Ecology*, pages 9–56. Brock-Springer, Madison.

Rhee, G.-Y. (1974). Phosphate uptake under nitrate limitation by *Scenedesmus* sp. and its ecological implications. *Journal of Phycology*, 10:470–475.

Rhee, G.-Y. (1978). Effects of N:P atomic ratios nitrate limitation on algal growth, cell composition, nitrate uptake. *Limnology and Oceanography*, 23(1):10–25.

Riegman, R., Flameling, I. A., and Noordeloos, A. M. (1998). Size-fractionated uptake of ammonium, nitrate and urea and phytoplankton growth in the North Sea during spring 1994. *Marine Ecology Progress Series*, 173:85–94.

Robertson Lain, L., Bernard, S., and Evers-King, H. (2014). Biophysical modelling of phytoplankton communities from first principles using two-layered spheres: Equivalent Algal Populations (EAP) model. *Optics Express*, 22(14):16745.

Rouault, M., Pohl, B., and Penven, P. (2010). Coastal oceanic climate change and variability from 1982 to 2009 around South Africa. *African Journal of Marine Science*, 32(2):237–246.

Ryan, J. P., Fischer, A. M., Kudela, R. M., Gower, J. F. R., King, S. A., Marin, R., and Chavez, F. P. (2009). Influences of upwelling and downwelling winds on red tide bloom dynamics in Monterey Bay, California. *Continental Shelf Research*, 29(5-6):785–795.

Rykaczewski, R. R., Dunne, J. P., Sydeman, W. J., García-Reyes, M., Black, B. A., and Bograd, S. J. (2015). Poleward displacement of coastal upwelling-favorable winds in the ocean's eastern boundary currents through the 21st century. *Geophysical Research Letters*, 42(15):6424–6431.

Ryther, J. H. (1969). Photosynthesis and fish production in the sea. *Science (New York, N.Y.)*, 166(901):72–76.

Ryther, J. H. and Dunstan, W. M. (1971). Nitrogen, phosphorus, and eutrophication in the coastal marine environment. *Science (New York, N.Y.)*, 171(975):1008–1013.

Sarthou, G., Timmermans, K. R., Blain, S., and Tréguer, P. (2005). Growth physiology and fate of diatoms in the ocean: A review. *Journal of Sea Research*, 53(1-2 SPEC. ISS.):25–42.

Sathyendranath, S., Lazzara, L., and Prieur, L. (1987). Variations in the spectral values of specific absorption of phytoplankton. *Limnology and Oceanography*, 32(2):403–415.

Sathyendranath, S., Stuart, V., Nair, A., Oka, K., Nakane, T., Bouman, H., Forget, M. H., Maass, H., and Platt, T. (2009). Carbon-to-chlorophyll ratio and growth rate of phytoplankton in the sea. *Marine Ecology Progress Series*, 383:73–84.

Sathyendranath, S., Watts, L., Devred, E., Platt, T., Caverhill, C., and Maass, H. (2004). Discrimination of diatoms from other phytoplankton using ocean-colour data. *Marine Ecology Progress Series*, 272:59–68.

Schaecter, M. (1968). Growth: cells and populations. In Mcquillen, J. and Mandlestam, K., editor, *Biochemistry of bacterial cell growth.*, pages 136–162. Wiley.

Seeyave, S., Probyn, T. A., Pitcher, G. C., Lucas, M. I., and Purdie, D. A. (2009). Nitrogen nutrition in assemblages dominated by *Pseudo-nitzschia* spp., *Alexandrium catenella* and *Dinophysis acuminata* off the west coast of South Africa. *Marine Ecology Progress Series*, 379(April 2005):91–107.

Serra, J. L., Llama, M. J., and Cadenas, E. (1978). Nitrate Utilization by the diatom *Skeletonema costatum*: II. Regulation of Nitrate Uptake. *Plant physiology*, 62(6):991–994.

Shannon, L. (2006). Benguela: Predicting a large marine ecosystem. A plan comes together. In Shannon, V., Hempel, G., Malanotte-Rizzoli, P., Moloney, C., and Woods, J., editors, *Large Marine Ecosystems*, pages 3–10. Elsevier, Amsterdam.

Shannon, L. J., Field, J. G., and Moloney, C. L. (2004). Simulating anchovy sardine regime shifts in the southern Benguela ecosystem. *Ecological modelling*, 172:269–281.

Sheldon, R. and Parsons, T. (1967). A continuous size spectrum for particulate matter in the sea. *Journal of Fisheries Research Board of Canada*, 24(5):909–915.

Sheldon, R. W., Prakash, A., and Sutcliffe, W. (1972). The size distribution of particles in the ocean. *Limnology and Oceanography*, 17(3):327–340.

Sicko-Goad, L. M., Schelske, C. L., and Stoermer, E. F. (1984). Estimation of intracellular carbon and silica content of diatoms from natural assemblages using morphometric techniques. *Limnology and Oceanography*, 29(6):1170–1178.

Sieburth, J. M., Smetacek, V., and Lenz, J. (1978). Pelagic ecosystem structure: Heterotrophic compartments of the plankton and their relatonship to plankton size fractions. *Limnology and Oceanography*, 23(6):1256–1263.

Smayda, T. J. (2000). *Ecological features of harmful algal blooms in coastal upwelling ecosystems*, volume 22.

Smayda, T. J. and Reynolds, C. S. (2001). Community Assembly in Marine Phytoplankton: Application of Recent Models to Harmful Dinoflagellate Blooms. *Journal of Plankton Research*, 23(5):447–461.

Smayda, T. J. and Reynolds, C. S. (2003). Strategies of marine dinoflagellate survival and some rules of assembly. *Journal of Sea Research*, 49(2):95–106.

Smetacek, V. (1999). Diatoms and the Ocean Carbon Cycle. *Protist*, 150:25–32.

Smith, A. R. C., Prezelin, B. B., Bidigare, R. R., Baker, K. S., and Smith, R. C. (2011). in coastal waters of photosynthetic modeling production biological parameters . 34(8):1524–1544.

Smith, S. D. (1988). Coefficients for sea surface wind stress, heat flux, and wind profiles as a function of wind speed and temperature. *Journal of Geophysical Research*, 95(C2):15467–15472.

Smith, S. L., Pahlow, M., Merico, a., Acevedo-Trejos, E., Sasai, Y., Yoshikawa, C., Sasaoka, K., Fujiki, T., Matsumoto, K., and Honda, M. C. (2015). Flexible phytoplankton functional type (FlexPFT) model: size-scaling of traits and optimal growth. *Journal of Plankton Research*, 0:1–16.

Smith, S. L. and Yamanaka, Y. (2007). Optimization-based model of multinutrient uptake kinetics. *Limnology and Oceanography*, 52(4):1545–1558.

Smith, S. L., Yamanaka, Y., Pahlow, M., and Oschlies, A. (2009). Optimal uptake kinetics: Physiological acclimation explains the pattern of nitrate uptake by phytoplankton in the ocean. *Marine Ecology Progress Series*, 384:1–12.

Smith, W. and Barber, R. (1979). A carbon budget for the autotrophic ciliate *Mesodinium rubrum*. *Journal of Phycology*, 15(1):27–33.

Solomon, C. M., Collier, J. L., Berg, G. M., and Glibert, P. M. (2010). Role of urea in microbial metabolism in aquatic systems: A biochemical and molecular review. *Aquatic Microbial Ecology*, 59(1):67–88.

Sommer, U. (1984). The paradox of the plankton: Fluctuations of phosphorus availability maintain diversity of phytoplankton in flow-through cultures. *Limnology and Oceanography*, 29(3):633–636.

Sommer, U. (1985). Comparison between steady state and non-steady state competition: Experiments with natural phytoplankton. *Limnology and Oceanography*, 30(2):335–346.

Sommer, U. (1989). The role of competition for resources in phytoplankton species succession. In Sommer, U., editor, *Plankton Ecology - succession in plankton communities*, pages 57–106. Spinger, Berlin.

Sordo, I., Barton, E., Cotos, J. M., and Pazos, Y. (2001). An inshore poleward current in the NW of the Iberian Peninsula detected from satellite images, and its relation with *G. catenatum* and *D. acuminata* blooms in the Galician Rias. *Estuarine, Coastal and Shelf Science*, 53:787–799.

Steele, J. (1954). Plant production in the northern North Sea. *Mar. Res. Ser. Scot. Home Dep.*, 7:1–36.

Steiner, C. F. (2003). Keystone predator effects and grazer control of planktonic primary production. 101(3):569–577.

Stoecker, D., Taniguchi, A., and Michaels, A. E. (1989). Abundance of autotrophic, mixotrophic and heterotrophic planktonic ciliates in shelf and slope waters. *Marine Ecology Progress Series*, 50(3):241–254.

Stolte, W. and Riegman, R. (1995). Effect of phytoplankton cell size on transient-state nitrate and ammonium uptake kinetics. *Microbiology*, 141(5):1221–1229.

Strathmann, R. R. (1967). Estimating the organic carbon content of phytoplankton from cell volume or plasma volume. *Limnology and Oceanography*, 12(3):411–418.

Strom, S. L. and Morello, T. A. (1998). Comparative growth rates and yelds of ciliates and heterotrophic dinoflagellates. *Journal of Plankton Research*, 20(3):571–584.

Stumpf, R. and Tomlinson, M. (2005). Remote sensing of harmful algal blooms. *Remote Sensing of Coastal Aquatic*, pages 277–296.

Stumpf, R. P., Culver, M. E., Tester, P. A., Tomlinson, M., Kirkpatrick, G. J., Pederson, B. A., Truby, E., Ransibrahmanakul, V., and Soracco, M. (2003). Monitoring *Karenia brevis* blooms in the Gulf of Mexico using satellite ocean color imagery and other data. 2:147–160.

Sun, J. and Liu, D. (2003). Geometric models for calculating cell biovolume and surface area for phytoplankton. *Journal of Plankton Research*, 25(11):1331–1346.

Sunda, W. G., Shertzer, K. W., and Hardison, D. R. (2009). Ammonium uptake and growth models in marine diatoms: Monod and Droop revisited. *Marine Ecology Progress Series*, 386:29–41.

Syrett, P. (1956). The assimilation of ammonia and nitrate by nitrogen starved cells of *Chlorella vulgaris* . *Physiologia Plantarum*, 9:19–28.

Syrett, P. (1981). Nitrogen metabolism in microalgae. *Canadian Bulletin Fisheries and Aquatic Science*, 210:182–210.

Tamminen, T. and Irmisch, A. (1996). Urea uptake kinetics of a midsummer planktonic community on the SW coast of Finland. *Marine Ecology Progress Series*, 130(1-3):201–211.

Tang, E. P. (1995). The allometry of algal growth rates. *Journal of Plankton Research*, 17(6):1325–1335.

Terseleer, N., Bruggeman, J., Lancelot, C., and Gypens, N. (2014). Trait-based representation of diatom functional diversity in a plankton functional type model of the eutrophied southern North Sea. *Limnology and Oceanography*, 59(6):1958–1972.

Thingstad, T. (1998). A theoretical approach to structuring mechanisms in the pelagic food web. *Hydrobiologia*, 363:59–72.

Thingstad, T., Strand, E., and Larsen, A. (2010). Stepwise building of plankton functional type (PFT) models: A feasible route to complex models? *Progress in Oceanography*, 84:6–15.

Tilman, D. (2001). Functional diversity. *Encyclopedia of Biodiversity*, 3(3):109–120.

Tilman, D., Kilham, S. S., and Kilham, P. (1982). Phytoplankton Community Ecology. The Role of Limiting Nutrients. *Annual Review of Ecology and Systematics*, 13(1):349–372.

Tilstone, G. H., Figueiras, F. G., and Fraga, F. (1994). Upwelling-downwelling sequences in the generation of red tides in a coastal upwelling system. *Marine Ecology Progress Series*, 112(3):241–254.

Trainer, V. L., Hickey, B. M., and Horner, R. a. (2002). Biological and physical dynamics of domoic acid production off the Washington coast. *Limnology and Oceanography*, 47(5):1438–1446.

Uitz, J., Claustre, H., Gentili, B., and Stramski, D. (2010). Phytoplankton class-specific primary production in the world's oceans: Seasonal and interannual variability from satellite observations. *Global Biogeochemical Cycles*, 24(3):1–6.

Uitz, J., Claustre, H., Morel, A., and Hooker, S. B. (2006). Vertical distribution of phytoplankton communities in open ocean: An assessment based on surface chlorophyll. *Journal of Geophysical Research*, 111:1–23.

Utermohl, H. (1958). Zur vervollkommnung der quantitativen Phytoplankton Methodik. *Mitt.Int.Ver.Theor.Angew.Limnol.*, 9:1–38.

Vallina, S. M., Follows, M. J., Dutkiewicz, S., Montoya, J. M., Cermeno, P., and Loreau, M. (2014). Global relationship between phytoplankton diversity and productivity in the ocean. *Nature communications*, 5:4299.

Vallina, S. M. and Le Quéré, C. (2011). Stability of complex food webs: Resilience, resistance and the average interaction strength. *Journal of Theoretical Biology*, 272(1):160–173.

van der Lingen, C., Hutchings, L., and Field, J. (2006). Comparative trophodynamics of anchovy *Engraulis encrasicolus* and sardine *Sardinops sagaxin* the southern Benguela: are species alternations between small pelagic fish trophodynamically mediated? *African Journal of Marine Science*, 28(3-4):465–477.

Varela, D. E. and Harrison, P. J. (1999). Effect of ammonium on nitrate utilization by *Emiliania huxley*, a coccolithophore from the oceanic northeastern Pacific. *Marine Ecology Progress Series*, 186:67–74.

Verheye, H. (2000). Decadal-scale trends across several marine trophic levels in the southern benguela upwelling system off South Africa. *Ambios*, 29(1):30–34.

Verity, P. G., Robertson, C. Y., Tronzo, C. R., Andrews, M. G., Nelson, J. R., and Sieracki, M. E. (1992). Relationships between cell volume and the carbon and nitrogen content of marine photosynthetic nanoplankton. *Limnology and Oceanography*, 37(7):1434–1446.

Ward, B., Friedrichs, M., Anderson, T., and Oschlies, A. (2010). Parameter optimisation techniques and the problem of underdetermination in marine biogeochemical models. *Journal of Marine Systems*, 81(1-2):34–43.

Ward, B. A. (2015). Temperature-correlated changes in phytoplankton community structure are restricted to polar waters. *PLoS ONE*, 10(8):1–15.

Ward, B. A., Dutkiewicz, S., Jahn, O., and Follows, M. J. (2012). A size-structured food-web model for the global ocean. *Limnology and Oceanography*, 57(6):1877–1891.

Watt, D. A., Amory, A. M., and Cresswell, C. F. (1992). Effect of nitrogen supply on the kinetics and regulation of nitrate assimilation in *Chlamydomonas reinhardtii Dangeard*. *J. Exp. Bot.*, 43:605–615.

West, G. B., Brown, J. H., and Enquist, B. J. (1997). A general model for the origin of allometric scaling laws in biology. *Science (New York, N.Y.)*, 276(5309):122–126.

Westoby, M. and Wright, I. J. (2006). Land-plant ecology on the basis of functional traits. *Trends in Ecology and Evolution*, 21(5):261–268.

Wilkerson, F. and Dugdale, R. C. (2008). Coastal Upwelling. In Capone, D. G., Bronk, D., Mulholland, M. R. and Carpenter, E. J., editor, *Nitrogen in the Marine Environment.*, pages 771–797. Elsevier, Oxford.

Wilkerson, F. P. and Dugdale, R. C. (1987). The use of large shipboard barrels and drifters to study the effects of coastal upwelling on phytoplankton dynamics. *Limnology and Oceanography*, 32(2):368–382.

Williams, C., Sharples, J., Mahaffey, C., and Rippeth, T. (2013). Wind-driven nutrient pulses to the subsurface chlorophyll maximum in seasonally stratified shelf seas. *Geophysical Research Letters*, 40(20):5467–5472.

Wirtz, K. and Pahlow, M. (2010). Dynamic chlorophyll and nitrogen:carbon regulation in algae optimizes instantaneous growth rate. *Marine Ecology Progress Series*, 402:81–96.

Wirtz, K. W. (2013). Mechanistic origins of variability in phytoplankton dynamics: Part I: Niche formation revealed by a size-based model. *Marine Biology*, 160(9):2319–2335.

Wirtz, K. W. and Eckhardt, B. (1996). Effective variables in ecosystem models with an application to phytoplankton succession. *Ecological Modelling*, 92(1):33–53.

Wright, R. T. and Hobbie, J. E. (1966). Use of glucose and acetate by bacteria and algae in aquatic ecosystems. *Ecology*, 47:447–464.

Wroblewski, J. (1977). A model of phytoplankton plume formation during variable Oregon upwelling. *Journal of Marine Research*, 35:357–394.

Wyatt, T. (2014). Margalef's mandala and phytoplankton bloom strategies. *Deep-Sea Research Part II: Topical Studies in Oceanography*, 101:32–49.

Yih, W., Hyung, S. K., Hae, J. J., Myung, G., and Young, G. K. (2004). Ingestion of cryptophyte cells by the marine photosynthetic ciliate *Mesodinium rubrum*. *Aquatic Microbial Ecology*, 36(2):165–170.

Zehr, J. P. and Ward, B. B. (2002). Nitrogen Cycling in the Ocean : New Perspectives on Processes and Paradigms MINIREVIEW Nitrogen Cycling in the Ocean : New Perspectives on Processes and Paradigms. *Applied and environmental microbiology*, 68(3):1015–1024.

Zibordi, G., Mélin, F., Hooker, S. B., D'Alimonte, D., and Holben, B. (2004). An Autonomous Above-Water System for the Validation of Ocean Color Radiance Data. *IEEE Transactions on Geoscience and Remote Sensing*, 42(2):401–415.

Zingone, A. and Enevoldsen, H. O. (2000). The diversity of harmful algal blooms: a challenge for science and management. *Ocean and Coastal Management*, 43(8):725–748.

3387

Appendix

- **Obs-PSD configuration:**

The observed particle size distribution (Obs-PSD) configuration used size distributions that were measured and is the same method as that used in chapter 4 (see Fig. 4.1)

- **S-PSD configuration:**

The standard-PSD configuration (S-PSD) follows closely equation 6 in Bernard et al. (2007) but scales to volume rather than surface area.

$$esd = VSF * r^{\left[\frac{(1-3V_{eff})}{V_{eff}}\right]} exp^{\left[\frac{-r}{(r_{eff}v_{eff})}\right]} \tag{5.1}$$

The VSF (volume scaling factor) term is introduced as the total projected volume scaling parameter, i.e. it is used to manipulate the magnitude of the equivalent size distribution (esd) by matching the total projected volume to that of the measured particle size distribution. The equivalent size distributions (esd) were calculated using the effective diameter (D_{eff}) and effective variance (V_{eff}) of the corresponding measured size distribution, where $r_{eff} = D_{eff}/2$. D_{eff} is calculated as in chapter 2 equation 2.2. Note: "ESD" is the equivalent spherical diameter, and "esd" is the equivalent size distribution.

$$D_{eff} = \frac{\int_1^{bins} \frac{\pi}{6} ESD^3}{\int_1^{bins} \frac{\pi}{4} ESD^2} \tag{5.2}$$

and

$$V_{eff} = \frac{\int_1^{bins} (r - r_{eff})^2 r^2 ESD}{r_{eff} \int_1^{bins} ESD} \tag{5.3}$$

In the absence of measured size distributions for volume scaling and for V_{eff}, satellite-derived Chl-*a* concentrations can be used to estimate total volume (e.g. Banse, 1977) and V_{eff} can be approximated as in Bernard et al. (2007).

- D_{eff} **configuration:**

Total volume is considered to be found only within the size class that corresponds to D_{eff}.

Table A1: Output values nitrogen uptake rates from the different representatives of size (Obs-PSD, S-PSD and D_{eff}) and *in situ* measured values. For total N uptake values as depicted in Fig. 5.2, total N= NO_3^- + NH_4^+.

ρ**NO$_3^-$**				ρ**NH$_4^+$**			
Obs PSD	S-PSD	D_{eff}	*in situ*	Obs PSD	S-PSD	D_{eff}	*in situ*
0.0035	0.0073	0.0197	0.0199	0.0081	0.0190	0.0506	0.0941
0.0955	0.3929	1.2680	0.1116	0.0164	0.0570	0.1848	0.0273
0.0309	0.1181	0.2718	0.0740	0.0096	0.0350	0.0800	0.0481
0.0176	0.0644	0.1788	0.0695	0.0063	0.0223	0.0618	0.0378
0.0243	0.1047	0.1800	0.2188	0.0068	0.0276	0.0481	0.0751
0.0358	0.1705	0.5033	0.3589	0.0055	0.0216	0.0651	0.0348
0.0186	0.0683	0.1034	0.2798	0.0058	0.0202	0.0306	0.0820
0.2220	0.3618	1.0424	0.0115	0.9158	1.6520	4.6732	0.1002
0.3817	0.6653	2.3739	0.0152	0.4174	0.7634	2.6835	0.0499
0.0421	0.0773	0.1253	0.0140	0.0784	0.1479	0.2402	0.0264
0.2134	0.5197	1.9349	0.0290	0.2566	0.6690	2.4953	0.0659
0.0650	0.1338	0.2581	0.0172	0.3335	0.8394	1.7530	0.0493
0.1810	0.3460	1.0089	0.0125	0.8568	2.2440	5.4181	0.0331
0.5725	1.4356	2.9977	0.0344	0.5654	1.9969	7.0269	0.0245
1.4945	3.8814	9.3840	0.9534	2.2024	9.0105	33.5860	0.0435
0.4537	1.5183	5.3554	0.0474	0.3240	1.4921	6.6852	0.0539
5.6179	23.8485	88.6595	0.0153	0.2132	1.5612	2.9482	0.0460

0.7060	3.2253	14.4427	0.1347	0.5863	3.4955	13.1517	0.0629
1.1046	9.0816	17.2499	0.1657	0.0047	0.0214	0.0237	0.0452
0.8387	4.6362	17.4355	0.0554	0.0031	0.0108	0.0217	0.0576
0.0534	0.3053	0.3410	0.5475	0.0037	0.0046	0.0055	0.0116
0.0161	0.0609	0.1224	0.2703	0.0072	0.0094	0.0104	0.0302
0.0008	0.0009	0.0011	0.0020	0.0060	0.0083	0.0098	0.0174
0.0016	0.0020	0.0023	0.0024	0.0019	0.0023	0.0026	0.0048
0.0020	0.0026	0.0031	0.0033	0.0040	0.0052	0.0062	0.0074
0.0014	0.0017	0.0019	0.0015	0.0028	0.0037	0.0041	0.0036
0.0020	0.0026	0.0030	0.0016	0.0057	0.0082	0.0091	0.0168
0.0032	0.0044	0.0048	0.0023	0.0007	0.0009	0.0013	0.0032
0.0127	0.0184	0.0204	0.0226	0.0007	0.0010	0.0016	0.0051
0.0009	0.0012	0.0016	0.0002	0.0083	0.0131	0.0152	0.0058
0.0008	0.0010	0.0017	0.0045	0.0078	0.0113	0.0161	0.0152
0.0446	0.0733	0.0845	0.0239	0.0012	0.0018	0.0019	0.0019
0.0229	0.0335	0.0474	0.0033	0.0035	0.0052	0.0056	0.0029
0.0007	0.0011	0.0011	0.0010	0.0021	0.0032	0.0035	0.0021
0.0044	0.0064	0.0069	0.0029	0.0073	0.0123	0.0147	0.0023
0.0072	0.0109	0.0118	0.0034	0.0029	0.0053	0.0046	0.0047
0.1029	0.1878	0.2257	0.0579	0.0113	0.0217	0.0184	0.0102
0.0031	0.0055	0.0048	0.0123	0.0144	0.0330	0.0254	0.0098
0.0028	0.0052	0.0044	0.0083	0.0043	0.0078	0.0077	0.0029
0.0031	0.0066	0.0051	0.0128	0.0019	0.0022	0.0025	0.0086
0.0073	0.0132	0.0130	0.0061	0.0028	0.0034	0.0042	0.0107
0.0081	0.0103	0.0110	0.0934	0.0028	0.0034	0.0033	0.0087
0.0110	0.0140	0.0170	0.0257	0.0045	0.0054	0.0062	0.0068
0.0097	0.0124	0.0114	0.0083	0.0048	0.0056	0.0101	0.0116
0.0127	0.0160	0.0174	0.0022	0.0032	0.0056	0.0060	0.0028

0.0277	0.0336	0.0581	0.1253	0.0045	0.0080	0.0088	0.0035
0.0051	0.0088	0.0095	0.0160	0.0068	0.0123	0.0132	0.0041
0.0036	0.0064	0.0070	0.0123	0.0137	0.0255	0.0287	0.0038
0.0303	0.0573	0.0611	0.0114	0.0047	0.0078	0.0088	0.0115
0.0304	0.0570	0.0641	0.0005	0.0060	0.0102	0.0108	0.0119
0.0003	0.0006	0.0006	0.0138	0.0046	0.0078	0.0088	0.0083
0.0033	0.0054	0.0057	0.0157	0.0030	0.0044	0.0057	0.0128
0.0030	0.0050	0.0057	0.0076	0.0049	0.0067	0.0067	0.0042
0.0066	0.0096	0.0125	0.0015	0.0036	0.0047	0.0047	0.0027
0.0025	0.0033	0.0033	0.0036	0.0129	0.0175	0.0182	0.0077
0.0090	0.0118	0.0118	0.0095	0.0009	0.0010	0.0009	0.0023
0.0768	0.1082	0.1116	0.0432	0.0032	0.0036	0.0033	0.0047
0.0015	0.0017	0.0016	0.0048	0.0049	0.0057	0.0049	0.0138
0.0015	0.0016	0.0015	0.0049	0.0096	0.0211	0.0650	0.0087
0.0152	0.0173	0.0155	0.0299	0.0094	0.0201	0.0392	0.0116
0.0147	0.0178	0.0148	0.0026	0.0130	0.0342	0.0622	0.0149
0.0106	0.0223	0.0688	0.0083	0.0103	0.0257	0.0514	0.0238
0.0025	0.0048	0.0093	0.0030	0.0185	0.0497	0.0418	0.0109
0.0125	0.0309	0.0562	0.0069	0.0148	0.0387	0.0345	0.0078
0.0292	0.0743	0.1472	0.0113	0.0147	0.0389	0.0336	0.0073
0.0016	0.0040	0.0034	0.0018	0.0094	0.0262	0.0240	0.0066
0.0022	0.0053	0.0048	0.0022	0.0292	0.0751	0.0755	0.0204
0.0067	0.0168	0.0145	0.0038	0.0296	0.0772	0.0800	0.0211
0.0450	0.1342	0.1222	0.1273	0.0295	0.0746	0.0774	0.0219
0.0036	0.0083	0.0084	0.0024	0.0254	0.0716	0.0632	0.0165
0.0136	0.0325	0.0337	0.0065				
0.0070	0.0160	0.0166	0.0037				
0.0462	0.1298	0.1145	0.0161				